PROCESSING OF TEXTURED ZnO BASED MATERIALS AND CHARACTERIZATION OF THEIR ANISOTROPIC PROPERTIES

Kahraman Keskinbora
Master of Science Thesis

Advanced Technologies Program – Program in Nanotechnology
Aralık - 2010

Bu tez çalışması Türkiye Bilimsel ve Teknolojik Araştırma Kurumu tarafından desteklenmiştir. Proje No: 110M021

JÜRİ VE ENSTİTÜ ONAYI

Kahraman KESKİNBORA'nın "Processing of textured ZnO based materials and characterization of their anisotropic properties" başlıklı İleri Teknolojiler Anabilim Dalı, Nanoteknoloji Bilim Dalındaki, Yüksek Lisans Tezi 9 Aralık 2010 tarihinde, aşağıdaki jüri tarafından Anadolu Üniversitesi Lisansüstü Eğitim-Öğretim ve Sınav Yönetmeliğinin ilgili maddeleri uyarınca değerlendirilerek kabul edilmiştir.

	Adı Soyadı	**İmza**
Üye (Tez Danışmanı)	**: Prof. Dr. ENDER SUVACI**	**…….**
Üye	**: Prof. Dr. SERVET TURAN**	**……..**
Üye	**: Doç. Dr. BÜLENT ASLAN**	**……..**

Anadolu Üniversitesi Fen Bilimleri Enstitsü Yönetim Kurulu'nun ……. tarih ve …….. sayılı kararıyla onaylanmıştır.

ÖZET

Yüksek Lisans Tezi

YÖNLENMİŞ MİKROYAPIYA SAHİP ZnO TABANLI MALZEMELERİN ÜRETİM SÜREÇLERİ VE ANİZOTROPİK ÖZELLİKLERİNİN KARAKTERİZASYONU

Kahraman KESKİNBORA

Anadolu Üniversitesi
Fen Bilimleri Enstitüsü
İleri Teknolojiler Ana Bilim Dalı - Nanoteknoloji Bilim Dalı

Danışman: Prof. Dr. Ender SUVACI
2010, 101 sayfa

Çok kristalli malzemeleri oluşturan tanelerin kristallografik yönlerinin birbirlerine göre rastgele olmayan dağılımına *yönlenme* denir. Bu yönlenme, tek kristallere özgü anizotropik özelliklerin çok kristalli malzemelerde de oluşturulmasına olanak verir. Yönlenme farklı üretim yöntemleri ile elde edilebilir. Yönlenmeyi kontrol ederek, malzeme özelliklerini kontrol etmek mümkündür. Bu çalışmada, kuvvetli bir manyetik alan (12 Tesla) kullanılarak yüksek yönlenmeye sahip, saf ZnO malzemeler elde edilmiş ve mikroyapısal ve yönlenme karakteristikleri, x-ışını ve elektron kırınımı yöntemleri ile belirlenmiştir. Önce manyetik alan altında yönlenme süreci optimize edilmiş, daha sonra yüksek yönlenmeye bağlı olarak ortaya çıkan anizotropik sinterleme küçülmesi sorunu üzerinde durulmuştur. Daha sonra, manyetik alanın uygulanış biçimi değiştirilerek malzemenin yönlenmesi (% 96, 75, 27 ve 0 Lotgering faktörü gibi) kontrol edilebilmiştir. Bu malzemelerin elektriksel dirençleri (3 – 0,5 Ohm.cm), sertlik (200 - 150 kgf/mm^2) ve ısıl difüziviteleri (16,5 – 18,5 mm^2/s) yöne ve yönlenmeye bağlı olarak ölçülmüştür. Bu ölçümler sonucunda uygulanan manyetik alanın simetrisinin, çok kristalli malzemenin yönlenme karakteristiğine ve dolayısıyla özellik simetrisine taşındığı görülmüştür. Son olarak, en yüksek yönlenme derecesine ve kalitesine sahip olan çok kristalli ZnO örnekler, ZnO nano-yapıların büyütülmesinde altlık olarak kullanılmıştır. Bazal ve bazı piramidal yüzeyler, tek tek büyümüş ve yönlenmiş nano çubukların elde edilmesine izin verirken, prizmatik yüzeyler üzerinde yoğun film oluşumu gözlenmiştir.

Anahtar Kelimeler: ZnO, Manyetik Alan, Yönlenme, Anizotropi, Nano-Yapılar

ABSTRACT

Master of Science Thesis

PROCESSING OF TEXTURED ZnO BASED MATERIALS AND CHARATERIZATON THEIR ANISOTROPIC PROPERTIES

Kahraman KESKINBORA

Anadolu University
Graduate School of Sciences
Advanced Technologies Program - Program in Nanotechnology

Supervisor: Prof. Dr. Ender SUVACI

2010, 101 pages

Non-random distribution of orientations of the grains, which make up the polycrystalline materials, with respect to each other is called *texture*. This texture makes it possible to have the anisotropic properties of single crystals in the polycrystalline materials. Texture can be obtained by different processes. It is possible to control the material properties by controlling the texture. In this study, highly oriented pure ZnO materials were obtained by utilizing a strong magnetic field (12 Tesla). Microtructure and texture characteristics of the samples were characterized by x-ray and electron diffraction methods. First the process of alignment, under a magnetic field, was optimized. Then the problem of anisotropic sintering shrinkage, which emerges due to high texture, was investigated. By varying the application type of the magnetic field, the texture of the material could be controlled (Like 96 %, 75 %, 27 % and 0 % Lotgering factor). Then, the electrical resistivity (3-0.5 Ohm.cm), hardness (200-150 kgf/mm^2), and thermal diffusivities (16.5-18.5 mm^2/s) were measured as a function of direction and texture. These measurements showed that the symmetry of the applied magnetic field is transferred to the texture characteristic and thus symmetry of the properties of the polycrystalline material. Finally, polycrystalline ZnO specimens with the highest texture degree and quality were utilized as substrates in growth of ZnO nano-structures. It was observed that the basal and some pyramidal planes, let fabrication of individually grown, aligned nano rods, while the dense films formed on prismatic surfaces.

Keywords: ZnO, Magnetic Field, Texture, Anisotropy, Nano-Structures

ACKNOWLEDGEMENTS

I would like to thank to my advisor Assoc. Prof. Dr. Ender Suvaci for his guidance since 2006 during my undergraduate and masters studies. His kindness and bona fide will always be remembered with pleasure.

Dr. Tohru S. Suzuki, is gratefully acknowledged for his patience, his hospitality and fruitful discussions. Prof. Dr. Yoshio Sakka is also sincerely acknowledged for his enthusiasm about our collaboration.

I would like to thank to Dr. İ. Özgür Özer for spending his time to teach me the ways of the lab and also for his kindness and friendship. I would like to thank to all my friends and colleagues from both groups in Turkey and in Japan, without whom it would be a very boring three years. In particular I would like to thank to Dr. Betül Yıldız for enduring me for more than three years as a next desk neighbor, to Dr. Neslihan Tamsü for her joyful friendship, to A. Murat Avcı for our discussions on almost about everything and Yasemin Çelik for her patience for the chaos we caused in the office. In addition I would like to thank to my dear friend Emre Tüfekçioğlu, for great coffee times.

Lots of thanks goes to Onur Eser, Güneş Alp Yakaboylu, Özcan Özmen, Tolun Uğuz and A. Gürkan Yılmazoğlu for being very good drinkers. It was them, who eased the challenges of the past three years by sharing the thoughts and insights.

I would like to thank to my family for supporting me on every issue without any expectations. They never gave up on me. Without them none of it would be possible.

Finally I would like to thank to my dear friend, valuable colleague and prospective wife Çiğdem Özsoy for her patience, wisdom, understanding, and endless help.

TABLE OF CONTENTS

FIGURES INDEX

1. INTRODUCTION AND THE STRUCTURE OF THE THESIS

Many of the physical properties depend on microstructure of the polycrystalline ceramic materials. Therefore, microstructure design is very important in the search for better materials. One of the ways to control microstructure, and thus, to control material properties, is the control of orientation of crystallites in the microstructure, i.e. texture engineering. In the context of materials science, definition of texture is the orientation distribution of crystallites in a polycrystalline material [1]. There are several methods for inducing texture and all of these methods utilize anisotropic behavior of the grains or powders under external influences. This influence is obtained by the application of some form of a gradient, including mechanical, thermal or electromagnetic gradients, to the material being processed [2].

Thermal gradients can cause strong textures in melt cast materials, especially in metals. Therefore, for instance, by creating a temperature gradient during, melt casting, can be used in engineering texture of appropriate materials. Application of thermal gradients during solidification is known to result in rapid growth of cubic crystals parallel to the direction of heat flow [3] causing <100> fiber texture in cubic crystals of some metals and alloys [4], [5]. Texture degree in thermally oriented microstructures can be controlled by parameters such as undercooling level, heat flow direction and composition. Unlike metals, ceramics are difficult to be textured via thermal gradients and there is only limited literature on this subject. For example; in a previous work, textured Al_2O_3 was produced via non-equilibrium solidification evoked by combination of a combustion synthesis and ultra-high gravity centrifugal force [6]. Although this texture was attributed to ultrahigh gravity field produced via centrifugation, by authors, it might as well be classified as a hybrid method since non-equilibrium solidification also played role in the formation of non-conventional, arrayed grain microstructure. Melt texturing is also applied to the high temperature superconductors for increasing the critical current density via engineering a textured microstructure [7]. Nevertheless, melt casting of ceramics is not an easy and convenient method for large scale production of textured ceramics because of the high temperatures required for the processes and this brings related difficulties along.

In the texture engineering of ceramic materials, mechanical methods include tape casting, extrusion, uni-axial pressing and similar forming techniques which can be used in conjunction with texture developing heat treatment processes such as oriented consolidation of anisometric particles (OCAP) [8-10], templated grain growth (TGG) [2], [11-13], reactive templated grain growth (RTGG) [14] and hetero-templated grain growth (HTGG) [15]. Recently, applications of OCAP, TGG, RTGG and HTGG for the production of textured piezoelectric materials have been reviewed by Kimura [16]. In these methods, a shear force is applied on powders composed of either completely anisometric particles (templates) to induce preferred orientation as in OCAP or small numbers of large template particles mixed with smaller matrix powder as in TGG, RTGG or HTGG. Former process is different from latter three methods in the sense that although highly textured materials can be produced with this method, a large number of anisometric particles are required, which can be rare or in some cases unavailable. Another problem is the low sinterability of such large and anisometric particles due to low radius of curvature of the well faceted surfaces of these particles. Latter three methods require less amount of anisometric particles with respect to OCAP, and one can achieve high degrees of texture upon sintering and grain growth but this still depends on morphological features of raw materials (i.e., anisotropic particles). These methods, where a mechanical force is used for alignment of particles, all employ industry standard shaping techniques at a relatively low cost but the need for considerable amount of anisometric particles is the main constrained in the large scale industrial application. Limited availability of templates might even make laboratory scale production of textured ceramics and subsequently research efforts in this field difficult. Another limitation related to such techniques is that they require liquid phase formers to enhance densification and reduce the constrained sintering effect induced by template particles. Therefore, obtaining single phase materials is difficult with such methods and sometimes requires pressure assisted sintering techniques.

Magnetic field based methods to induce texture in polycrystalline ceramics have gained much interest in the last decade due to their versatility in the processing of textured materials. Virtually all non-cubic ceramic crystals possess a very small anisotropy in their diamagnetic susceptibility and this anisotropy can

be utilized to align particles under a magnetic field. However, this anisotropy is very small [17], therefore, there is an inevitable need for a strong magnetic field for orientation of sub-micron/nano sized particles of weak diamagnetic materials [18]. This requirement was fulfilled by availability of commercial superconducting magnets which can create and sustain very high magnetic fields higher than 10 T. Magnetic field is usually applied while green parts are shaped via wet forming methods such as slip casting [19], [20], gel casting [21] or even electrophoretic deposition [22]. Main advantage of this method is the elimination of the necessity for template particles. Rather than morphological anisometry, a strong magnetic field exploits the anisotropic diamagnetic susceptibility of the weak diamagnetic crystals to orient them with respect to the applied magnetic field. When the magnetic field is applied to particles which are suspended in a liquid medium, the particles tend to align with respect to the magnetic field in a manner to reduce their energy. This energy reduction upon diamagnetic alignment is given by the following equations [23];

$$\Delta E = \frac{-\Delta\chi V B^2}{2\mu_0} \tag{1}$$

$$\Delta\chi = \chi_a - \chi_c \tag{2}$$

In the equation (1), ΔE , is the reduction of particle energy upon alignment of particle with respect to magnetic field. V is the volume of individual particle. B is the applied magnetic field. μ_0 is the permeability of vacuum. In the equation (2), χ_a and χ_c are diamagnetic susceptibilities of crystal along a and c axes, respectively. $\Delta\chi$ is the anisotropic diamagnetic susceptibility. Equation (1) defines, under which conditions, diamagnetic orientation can be achieved. Particles must have enough volume and/or have large enough diamagnetic anisotropic susceptibility to overcome thermal motion to orient under an applied magnetic field by satisfying the condition $\Delta E > k_B T$, where k_B is Boltzmann constant and T is absolute temperature . The equation (2) can be utilized to predict in which way individual particles of a particular material will orient themselves with respect to the magnetic field. For example, ZnO has the following kind of anisotropy in its diamagnetic susceptibilities; $\chi_c < \chi_a < 0$. Therefore, ZnO

crystallites try to minimize their energies by aligning their c-axis perpendicular to the direction of applied rotating magnetic field [20]. Particles aligned under magnetic field, creates a preferred orientation in the green part, which develops upon sintering. One disadvantage of this method is high initial investment required for establishment of the setup and one another is the difficulties related to scaling up of the production. Recently, magnetic field texturing of weak diamagnetic materials has been reviewed by Sakka and Suzuki [23].

Although there are several advantages of the texture engineering, there is still a lack of complete understanding on how the texture affects the processing and subsequently properties of materials. Texture affects both the processing stage and the final properties development. Therefore, in order to gain a better control over processing and properties of materials, a fundamental understanding about correlations between texture development and processing, and between texture development and properties must be established. Consequently, the research objective of this thesis was to reveal the effects of texture on processing, such as anisotropic sintering shrinkage or different growth types of ZnO nanostructures on textured substrates and properties such as hardness, electrical and thermal conductivity. Thesis is structured to reflect this basic objective; the first part is a general introduction, discussing the origins of anisotropy in materials and texture inducing processes, the second part of the thesis is concerned with the optimization of magnetic field processing parameters to obtain the ‘best’ texture in pure ZnO system via solid state sintering. The third part discusses the processing problems such as anisotropic sintering shrinkage behavior and subsequently the texture development. Furthermore, effects of magnetic field and template addition on texture development and anisotropic shrinkage are presented in this part. The fourth part is dedicated to the texture-microstructure-property relations and effects of texture and microstructure on hardness, electrical and thermal conductivity are discussed. The final part focusses on the utilization of textured ZnO ceramic substrates to grow ZnO nanostructures. Each chapter is written as self contained and can be read independently from the other parts of the thesis. So, some literature knowledge may reccur throughout the thesis.

2. OPTIMIZATION OF ZnO SLIP CASTING UNDER MAGNETIC FIELD

Effects of the processing parameters on microstructure and texture development during slip casting of ZnO under magnetic field had to be identified prior to the following research activities in this thesis. Accordingly, initial experiments were aimed at optimizing the procedures to achieve highly dense, and well textured ZnO polycrystalline ceramics.

Although previous studies [19], [21] on magnetic field alignment of ZnO showed that the highly oriented samples can be produced, none of those studies involved utilization of template particles (i.e. large anisometric particles) in the initial composition. Since template particles greatly affect magnetic alignment, sintering, and texture development optimum sintering conditions to achieve the targeted product should be determined. Therefore, the compositional parameters such as template content, binder content and their combined effects and effects of sintering temperature, duration as well as sintering regime, on texture and microstructure development were investigated to reach the optimum processing conditions.

2.1. Experimental

In this study, all slip casting experiments were carried out under 12 T rotating magnetic field using porous alumina bases and teflon lined glass molds. In order to evaluate the effect of glycerol (i.e. binder and dispersant) on dispersion of suspension is evaluated by comparing final texture degrees. Slip media with differing amount of glycerol were prepared. Mixtures of glycerol and water, containing 5, 10, 20 and 40 vol % glycerol on liquid basis, were used as suspension media where solid load was kept constant as 20 vol % ZnO. A commercial ZnO powder, used in this study, has ~300 nm mean particle size (JIS1, HakusuiTech co., Ltd., Osaka, Japan). 0.5 wt % poly(ammonium acrylate) (A6114, Toagosei CO., LTD.), based on solid load, was used as a dispersant. The samples were cold isostatically pressed after compaction at 392 MPa for 10 minutes. To evaluate the effectivness of the glycerol on the Lotgering factors calculated from XRD pattenrs and density values were compared. Observable shift in the XRD patterns are attributed to measurement artifacts while sattellite peaks are attributed to Cu $K_{\alpha 2}$ radiation. Effects of sintering temperature on

texture and density was investigated by sintering samples at 1100, 1200 and 1300°C. The effects were evaluated by comparing texture and microstructure development in different samples via calculating their Lotgering factors (see equation (4) page 50) and relative sintered densities, respectively. Lotgering factors were calculated from the XRD patterns of sintered specimens. Microstructures were characterized by scanning electron microscopy (SEM). Effects of template addition on texture and density were investigated by preparing slip compositions containing 2, 5, 10 vol % templates. In addition, combined effects of templates and glycerol were investigated by adding different amounts of templates into the composition, containing the determined optimum amount of glycerol. General notation for samples was, XcYrZg(12 or 0)T; X is the percentage amount of commercial powder, Y is the percentage amount of rod-like template powder. Z is the percentage amount of glycerol based on liquid content. 12 or 0 T is the strength of magnetic field used during the compaction.

2.2. Results and Discussion

2.2.1. Effect of glycerol addition on texture development

The addition of certain amount of glycerol into the suspension, results in an increase in the orientation behavior of the particles under magnetic field, which is accompanied by an increase in the relative intensity of (0002) peak, both in green (Figure 2.1) and sintered samples (Figure 2.2) (peak shifts in these patterns are attributed to measurement artifacts). Even the addition of 5 vol % of glycerol enhances initial orientation characteristics as shown in Figure 2.1. If the XRD patterns of sintered samples are compared to those of green compacts there seems to be a contradiction in results, since although having a worse initial orientation, f of sintered 100c40g12T is higher than 100c12T (See Figure 2.3) (i.e. texture fraction Lotgering factor, f). This is believed to be a result of disruption of surface orientation during the evacuation of excess liquid from top of mold especially for 100c40g12T sample since it took quite a long time for this sample to dry which in turn is attributed to the high amount of glycerol in the suspension composition.100c0T sample which is slip cast in the absence of a magnetic field showed almost no preferred orientation. Lotgering factor for the green compact is 0.014. Upon sintering of this random sample, no considerable changes in the peak

intensities relative to (0002) are observed. The f, of sintered 100c0T sample was calculated to be 0.008, indicating there is no preferred orientation in this sample.

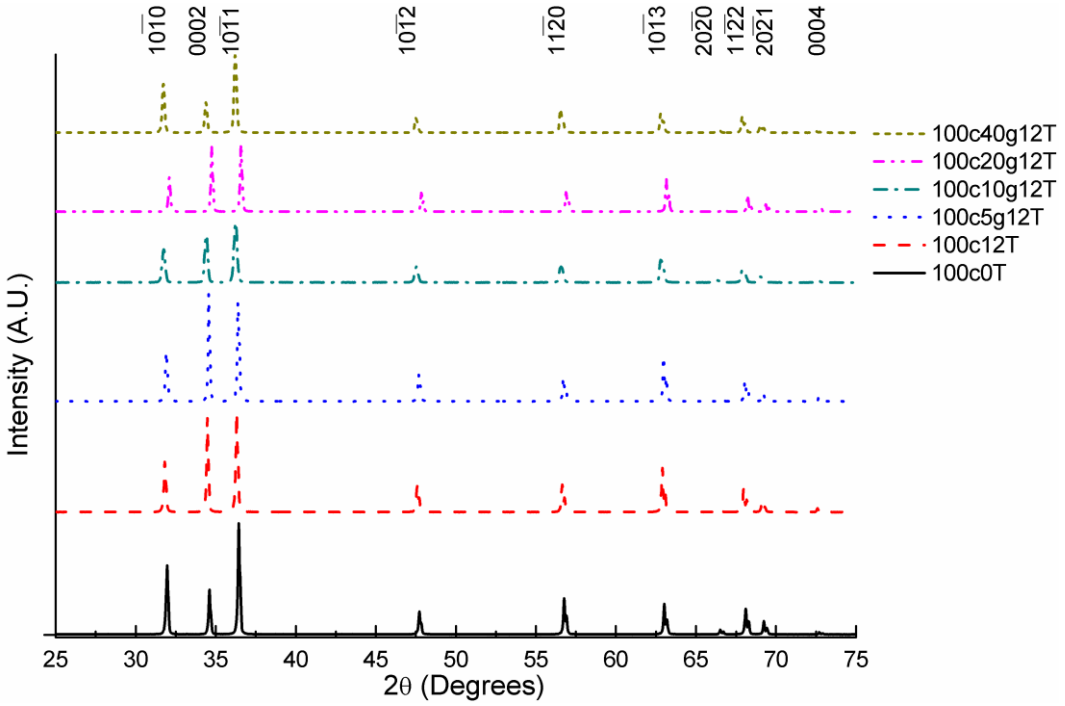

Figure 2.1 XRD patterns of samples 100c0T, 100c12T, 100c5g12T, 100c10g12T, 100c20g12T and 100c40g12T in the green state

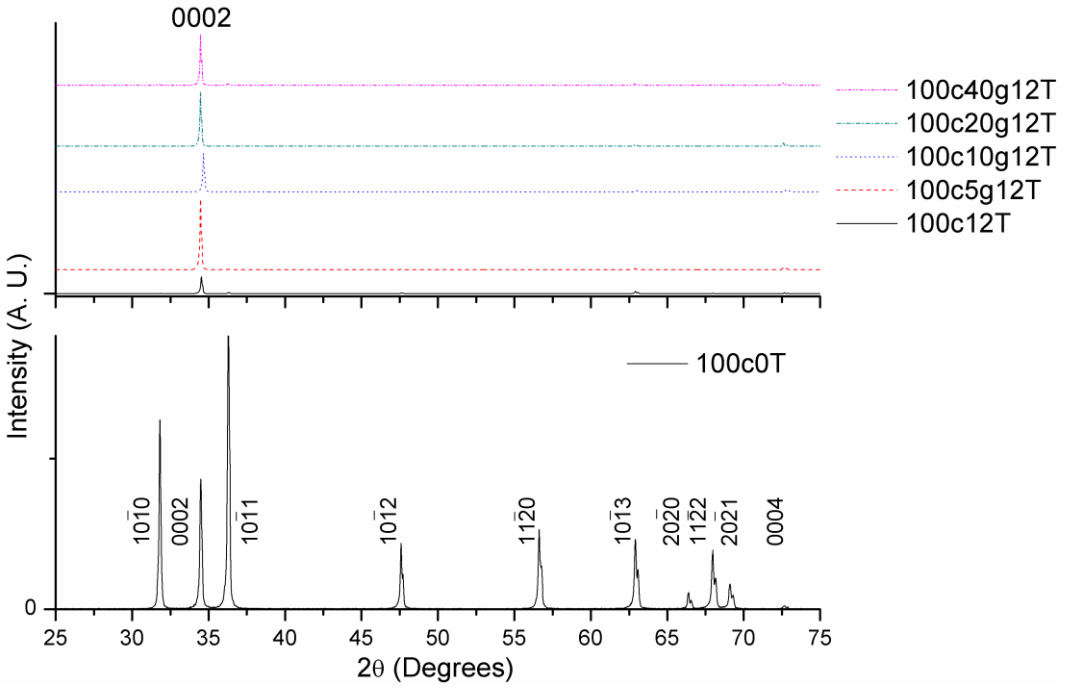

Figure 2.2 XRD patterns of samples 100c12T, 100c5g12T, 100c10g12T, 100c20g12T and 100c40g12T after sintering at 1200°C

The effect of glycerol addition on texture is most profound in sintered samples by a sharp increase in the (0002) peak intensity with incorporation of 5 vol % of glycerol into the ceramic suspension (Figure 2.2, 2.3). Further addition of glycerol caused relative intensity of (0002) peak to decrease slightly. Nevertheless, texture strength was higher in all samples prepared with glycerol when compared to sample prepared in the absence of glycerol. The sharp increase in the value of f by the glycerol addition (Figure 2.3) is attributed to the reported property of glycerol to enhance dispersion characteristics of polyelectrolyte dispersants as reported previously by other researchers [24], [25]. This interaction between dispersant and glycerol made orientation of ceramic particles under magnetic field easier. Thus, giving rise to good initial orientation and final texture in the sintered sample. Although glycerol molecules are considered to decrease particle-particle interaction by enhancing steric hindrance, in some cases the mechanism of glycerol interaction with dispersant is not very well understood. Contradictions of the effect of glycerol addition into ceramic slurries are discussed by Sofie and Dogan [24].

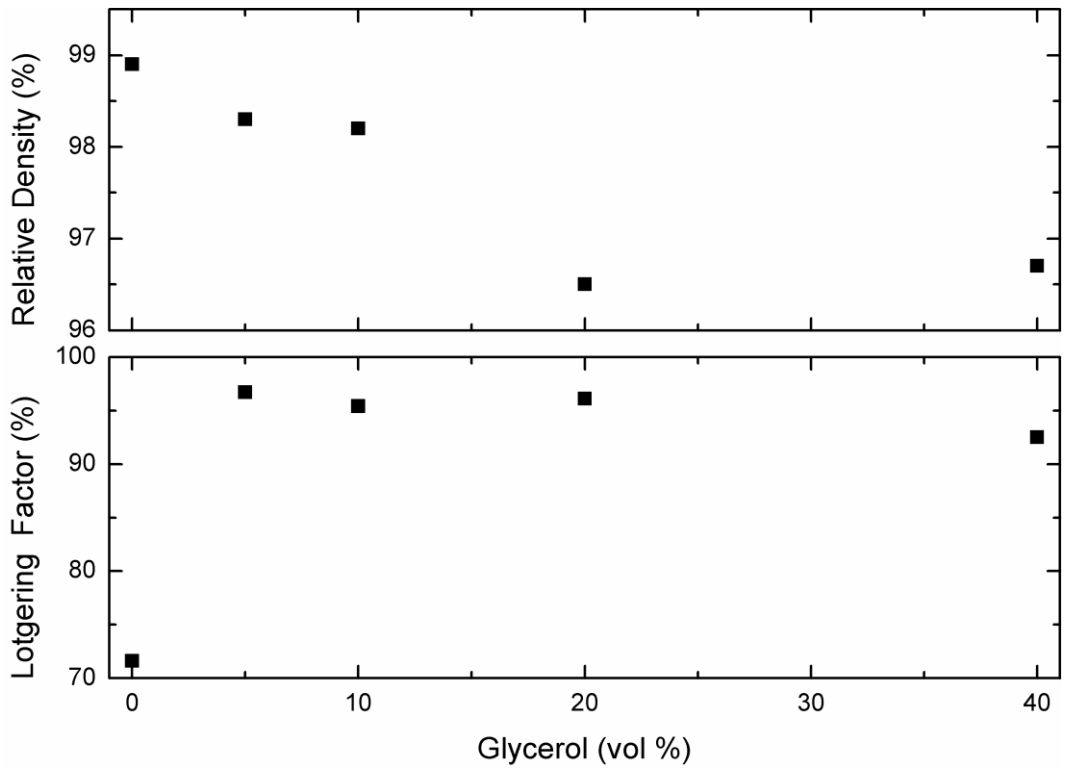

Figure 2.3 Lotgering Factors based on (0002) peak for 0.5 wt % dispersant containing samples after sintering at 1200°C. B = 12 T.

Further increase in glycerol content seems to have an adverse effect on orientation and slight decrease in (0002) relative peak intensities and consequently in the f values. These results suggest that as there is more and more glycerol among ceramic particles, they are forced to stay further apart from each other and that makes it difficult to obtain high density material after sintering. For example relative densities of sintered 100c12T, 100c5g12T, and 100c40g12T are ~99, ~98, and ~96.5 %, respectively. On the other hand, since there is a good initial orientation of particles in the green compact, due to good dispersion of slurry, even in samples whose sintered density is lower due to high glycerol concentration there are still a high degree of orientation. These results underline initial orientation of green compact and grain growth as key elements in texture development. However, the highest possible sintered density is desirable in order to eliminate pores from microstructure since they degrade the quality of texture and many other physical properties. Negative effect of glycerol on density can be explained on the basis of its positive effect on texture fraction. Glycerol increases the effectiveness of dispersant by enhanced steric hindrance [24]. Glycerol molecules basically interact with dispersant molecules by covering dispersant molecules, effectively increasing particle-particle distance and fill the space between particles, so there is more space between particles which should be closed during sintering. This inevitably reduces the sintered density. The figure 2.4 shows the effect of glycerol addition on microstructure and texture development. Microstuctures show significant increase in the number of anisometric grains as the glycerol is incorporated in to the suspension (Figure 2.4). This is in strong agreement with the increased Lotgering factor in the sintered samples. It should be underlined that these samples did not contain anisometric (rod-like) templates. Microstructures showed that initially isometric (equiaxed) particles in the green compact, aligned in the c-direction manufacturing process (as verified by XRD), were grown along radial direction during sintering process. This is the result of faster growth rate of prismatic planes than that of basal planes [13] and microstructures were anisometric similar to those obtained in other studies [13], [20]. When the initial alignment of the particles is relatively high, similar planes (prismatic-prismatic and basal-basal) confront each other during grain growth ultimately leading to a micro-

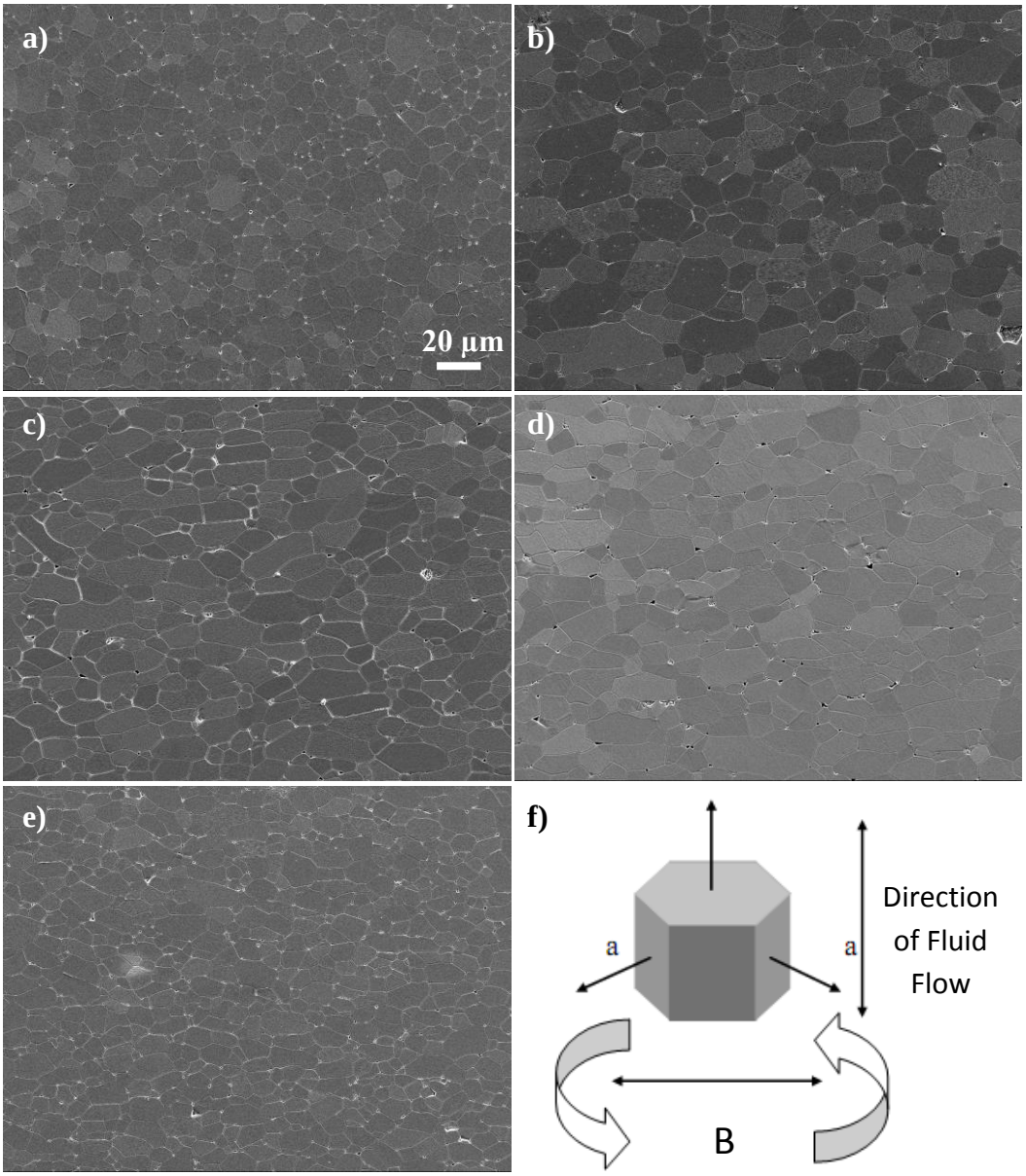

Figure 2.4 Micrographs, taken from ab-direction, of samples produced from slurries containing 0 (a), 5 (b), 10 (c), 20 (d) and 40 vol % (e) glycerol by volume and schematic describing the setup for aligning the crystallites in the slurry (f). Scale bar applies to all images

structure composed of anisometric grains and a high degree of crystalline orientation with coarser grain size. On the other hand, when the initial orientation is worse, as in the case of sample without glycerol (Figure 2.4, a), grain boundary movement seems to be hindered. This leads to a finer microstructure with less number of anisometric grains and lower degree of orientation (as shown above). When observed from c-axis direction in SEM (Figure 2.5) no anisometric grains were observed as expected. Furthermore, the pore characteristics were, different compared to radial-direction observations. Relatively larger pores were found on the grain boundaries suggesting there might be an anisometry in the pore morphology.

2.1.1. Effect of sintering conditions texture and microstructure development

There was an increase in the relative intensity of the (0002) peak in the XRD pattern for all samples after sintering (Figure 2.6). This can be explained by the growth of bigger particles in the expense of smaller ones. In case of slip casting under high magnetic fields, the attribute “bigger” means that particles which are large enough to be able to orient under applied field by overcoming the thermal motions in the suspension (Please see the first chapter for the conditions of magnetic alignment, for a more comprehensive discussion of equations governing diamagnetic alignment considering torque acting on particles and viscosity see the review of Kimura [18]). For a ‘big’ particle with larger volume, the reduction in magnetic energy would be greater meaning the driving force for alignment will be larger. Thus, in slurry composed of particles with many sizes only a certain percentage of particles can be aligned with the magnetic field for given ambient temperature and magnetic field strength. Since it is easier for ‘bigger’ particles to be oriented under magnetic field, basically they provide the initial preferred orientation in the green sample. Upon sintering, these pre-oriented particles grow by consuming smaller particles via Otswald ripening type process [23], ultimately causing a crystallographic texture in the final material. This process can be viewed as bigger isometric particles, in the powder with a size distribution, act as templates in the compact. The template particles do not necessarily need to be anisometric as in mechanical shaping methods such as tape casting or extrusion because the nature of slip casting under magnetic field lets

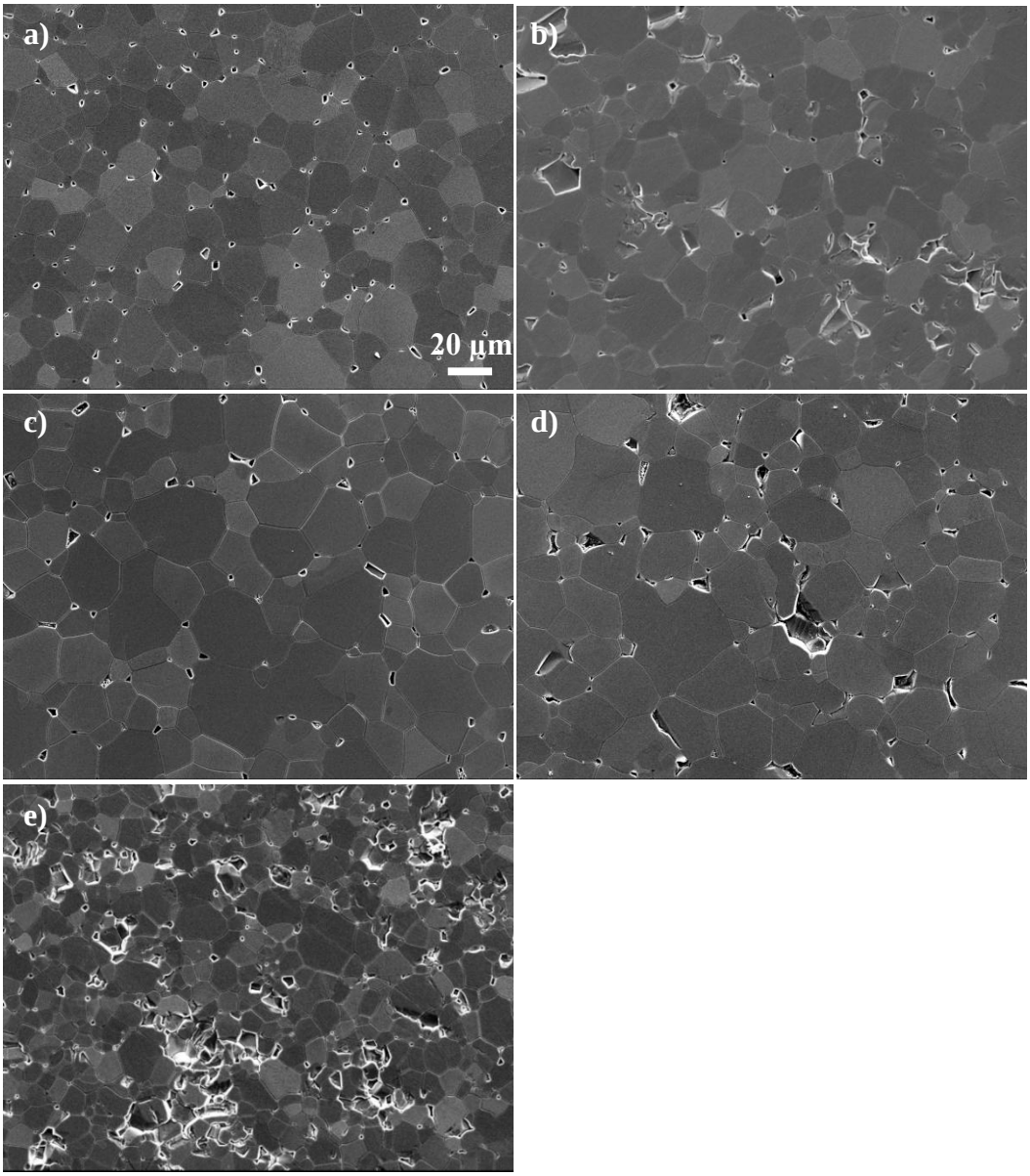

Figure 2.5 Micrographs, taken from c-direction of samples produced from slurries containing 0 (a), 5 (b), 10 (c), 20 (d), and 40 vol % (e) glycerol by volume. Scale bar applies to all images

orientation of particles regardless of their shape [2]. In this sense process of slip casting under strong magnetic fields can be visualized as some sort of to templated grain growth technique.

Micrographs of sample sintered at 1100°C shows a fine grained microstructure in comparison to samples sintered at higher temperatures (Figure 2.7 (a)). Also the microstructure was quite heterogeneous as there are some areas which seem to be composed of only smaller particles which are sintered together. As the sintering temperature increased the grains became coarser and more homogenous thanks to grain growth of bigger particles consuming smaller ones and increasing the homogeneity of the microstructure (Figure 2.7 (b) and (c)). Sintering at 1200°C favored both densification and grain growth leading to higher density whereas sintering at 1300°C seems to favor grain growth more than densification. Issues such as decomposition and subsequent evaporation of ZnO and de-sintering phenomena due to pore growth at higher temperatures, especially at 1300 - 1400°C, must be considered to play a role of slightly lower density for the sample sintered at 1300°C.

When 100c12T sample is sintered at different temperatures, Lotgering factor increased with increasing sintering temperature (Figure 2.9). Although Lotgering factor was almost the same for the samples sintered at 1200°C and 1300°C, the density of the latter was slightly lower.

Figure 2.8 shows the micrographs of samples, taken from c-axis direction. The microstructure consists of only isometric grains in this plane. The sample, which was sintered at 1100°C, shows quite fine microstructure in comparison to other samples sintered at higher temperatures. Figure 2.8 (a) shows a large grain size distribution. There are some sites which composed of only fine particles as it is discussed above. In samples sintered at higher temperatures no such heterogeneity is observed. 1200°C was the optimum sintering temperature as it resulted in the highest density and provided a good Lotgering factor at the same time. As a result 1200°C is adopted to be sintering temperature for further experiments.

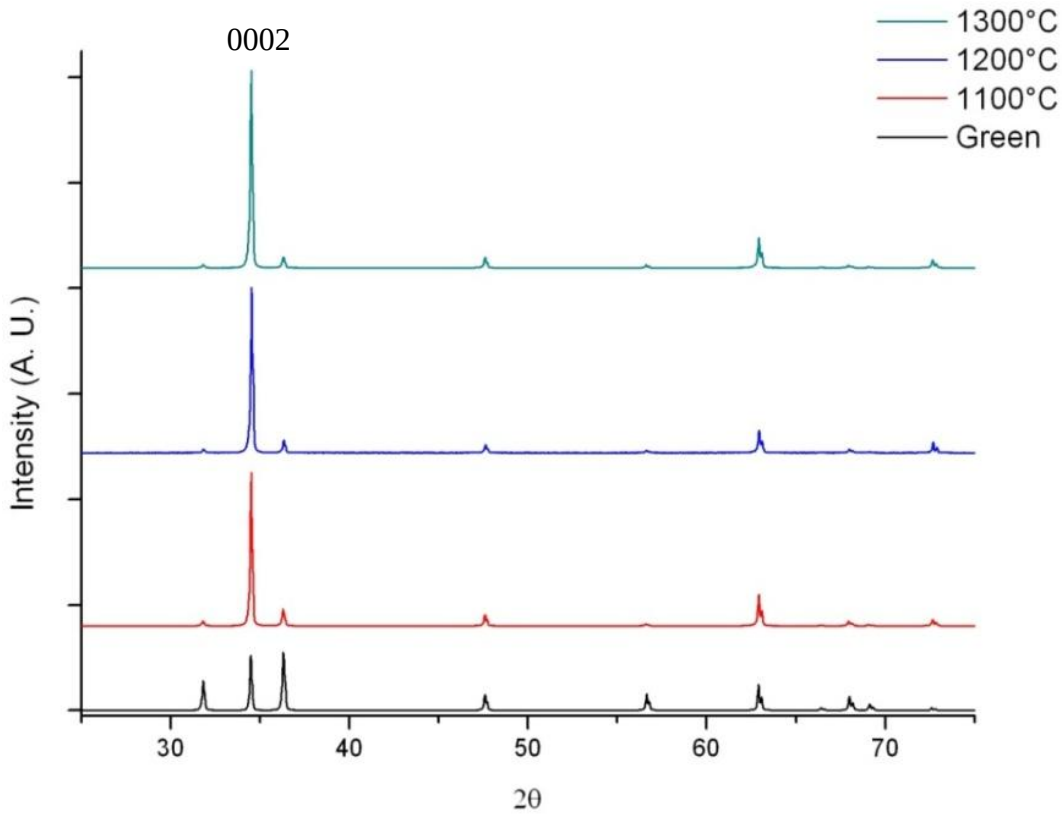

Figure 2.6 XRD patterns of 100c12T green and sintered samples

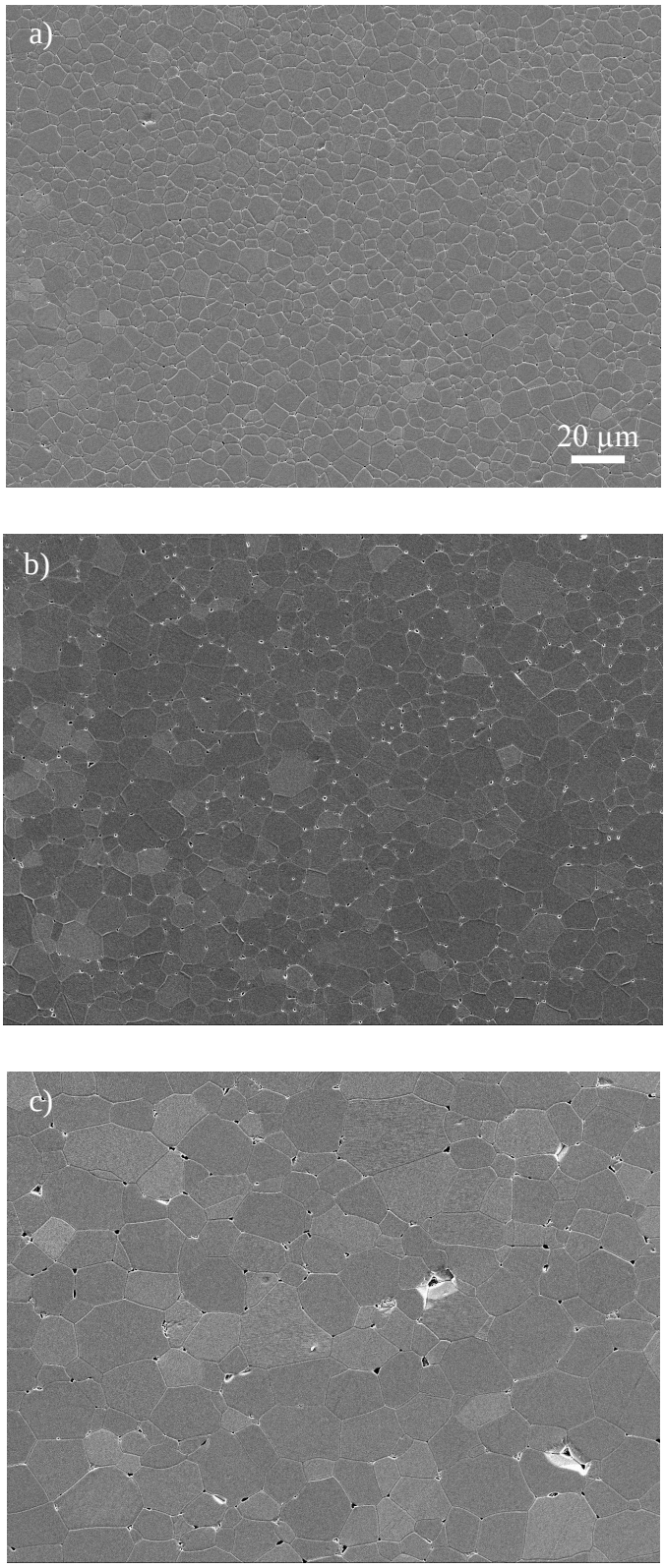

Figure 2.7 Micrographs of 100c12T samples from radial-direction which are sintered at 1100°C (a), 1200°C (b), and 1300°C (c). Scale bar applies to all images.

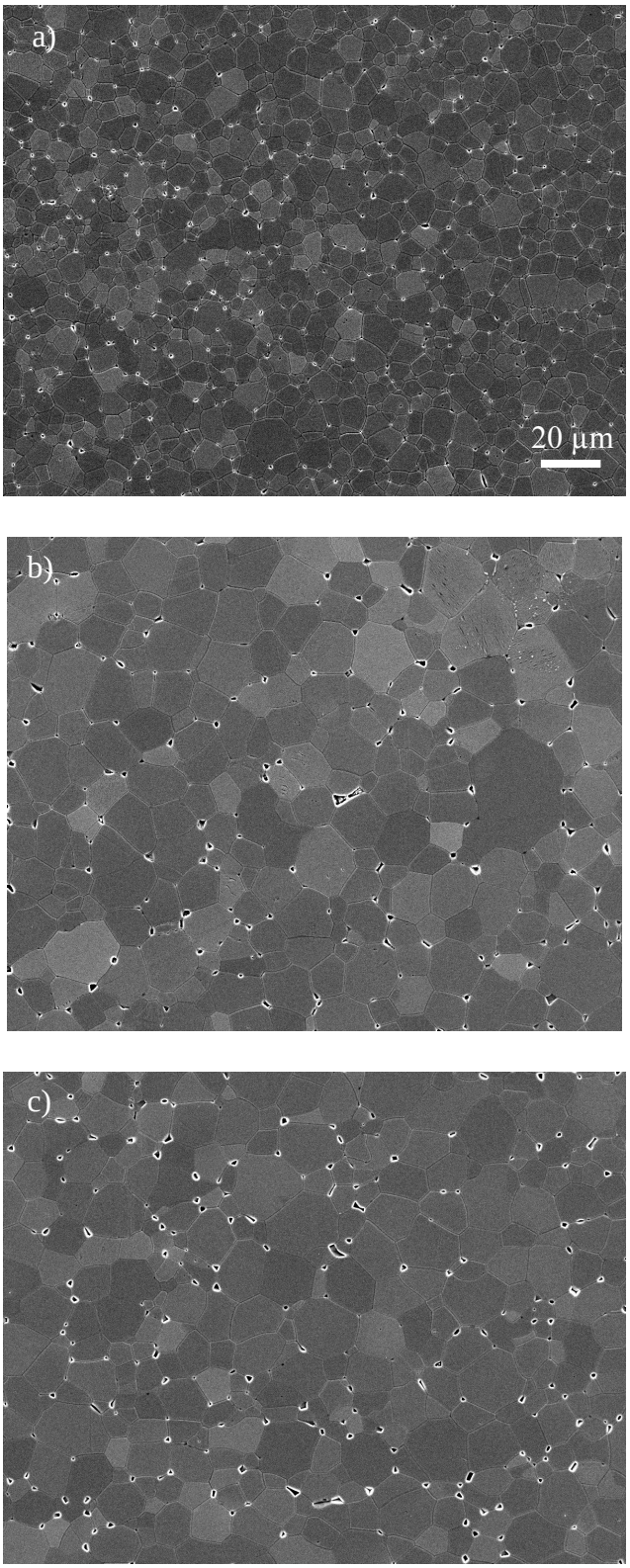

Figure 2.8 Micrographs of 100c12T samples from c-direction, which are sintered at 1100°C (a), 1200°C (b), and 1300°C. Scale bar applies to all images.

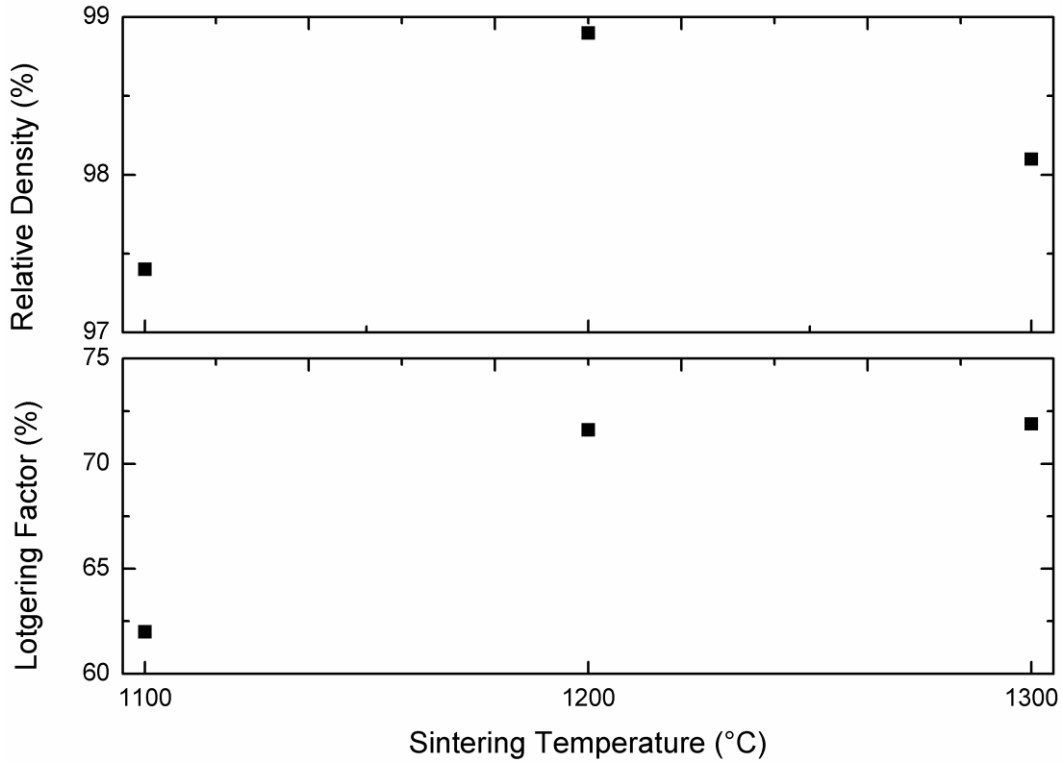

Figure 2.9 Effect of different sintering temperatures on Lotgering Factor for Sample 100c12T

Decrease in density of samples sintered in 1300°C (Figure 2.9) can be explained by heating rate. The heating rate employed in these experiments was 10°C/min after binder burn out step. So as the sample is heated to 1300°C with this rate, grain growth becomes dominant and full densification becomes difficult. This suggests that a higher degree of densification can be achieved by a slower heating rate. So, further experiments were carried out with 5°C/min heating rate and different holding durations. These experiments showed that with lower heating rate and longer heating durations sintered density can be improved (Figure 2.10). It is believed that with further optimization of sintering regime, near full theoretical density can be achieved. If previous studies of textured ZnO some of which employed higher sintering temperatures and/or longer sintering times [20], [26] are considered, it has been shown in this study, that the optimization of sintering program could lead sintering of ZnO ceramics up to very high densities at least 100°C lower and with relatively shorter holding times.

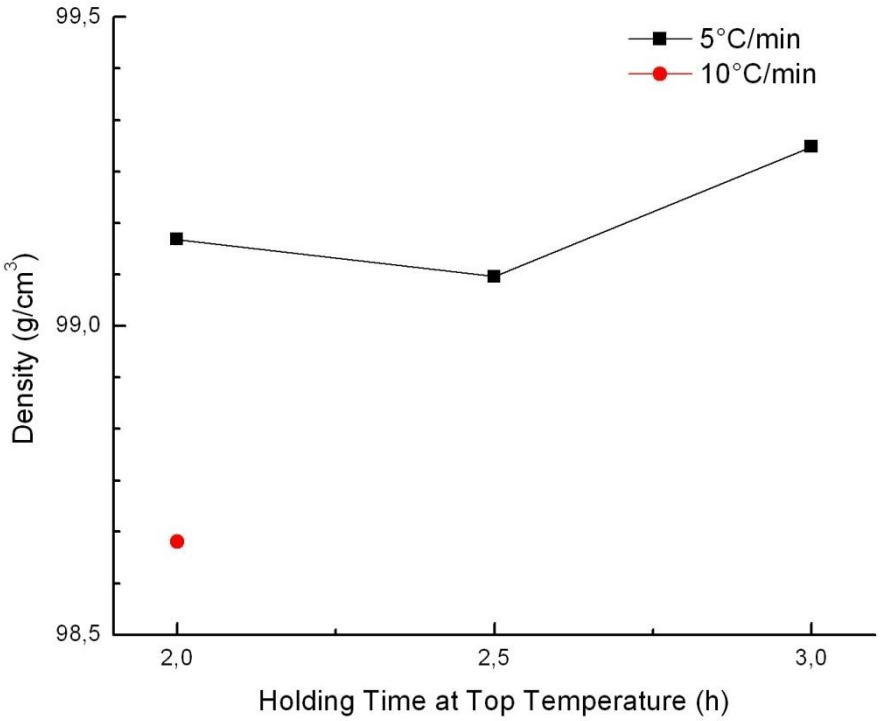

Figure 2.10 Effect of heating rate and sintering time on density of 100c5g12T sample

2.1.2. Effect of rod-like, template particles on microstructure and texture development

Addition of a small amount of rod-like template particles (2 – 5 vol %) in to the slurry in the absence of glycerol increased the relative intensity of the (0002) considerably (Figure 2.11), increasing the Lotgering factor, f, of sintered material by 20% to 25% at the same time. Being much bigger than isometric matrix particles, templates are much more easily oriented with magnetic field according to the Equation 1. Thus, the texture strength increase with initial increase in template content, when there is no glycerol in the system. Further increase in template concentration (10 vol %) decreased the orientation factor significantly (-30%), (See Figure 2.12). This decrease in texture strength can be attributed to either worsened dispersion characteristics of slurry by the addition of large amount of template or increased interaction among templates. In addition, the 10 vol % template particle decreased the sintered density which may also be a reason for reduced orientation (Figure 2.12). This decrease in sintered density for 5 and 10 vol % template systems is believed to be caused by constrained sintering induced by rod-like template particles. This hypothesis is investigated by thermo mechanical analysis experiments which will be discussed in the next chapter.

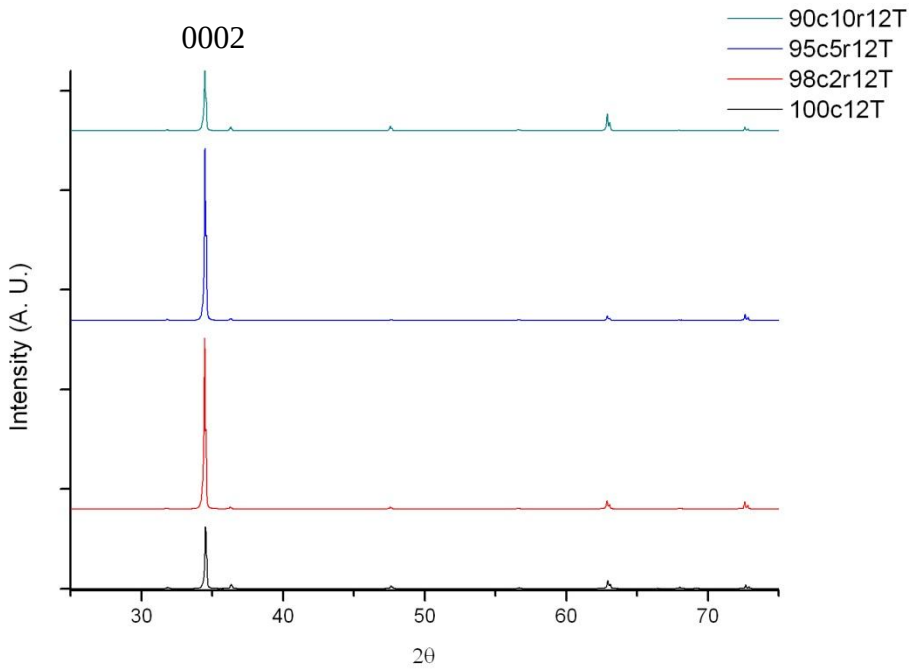

Figure 2.11 Patterns for samples 100c12T, 98c2r12T, 95c5r12T and 90c10r12T (all samples are sintered at 1200°C)

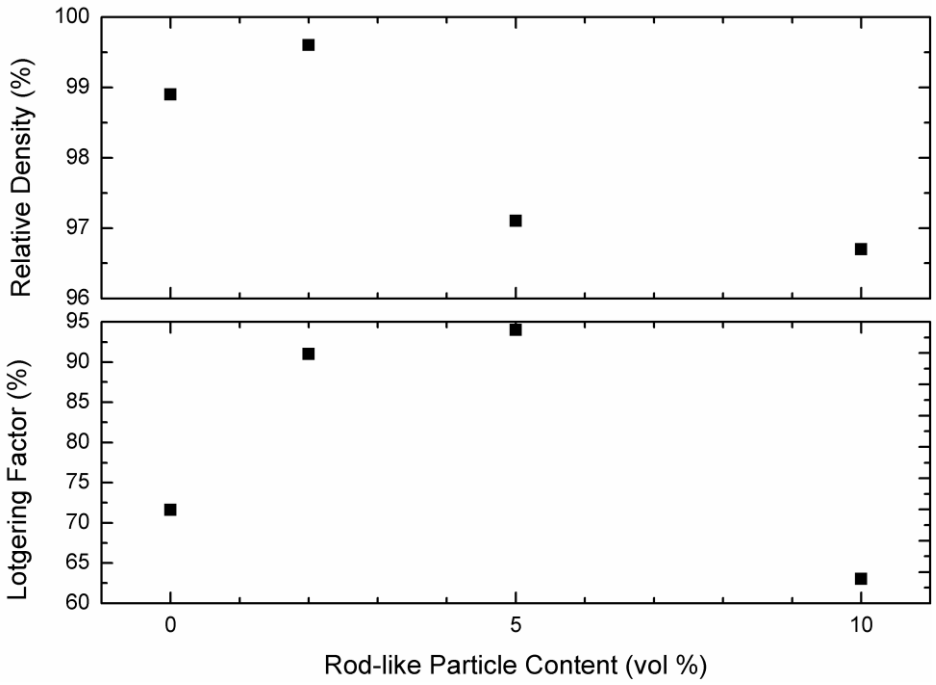

Figure 2.12 Effect of Rod-like template addition on degree of texture

Previously, it was reported that, in a slurry composed of only rod-like particles, it is very difficult to orient these particles as their long axis parallel to fluid flow (// to gravity for this system) direction due to pronounced effect of gravity on the particles [27]. However, in this study we were able to successfully incorporate rod-like particles into an isometric particle matrix to enhance the texture strength. This indicates that the anisometric template particles are tolerable to a certain extent under these conditions (the presence of matrix particles).

Incorporation of rod-like particles resulted in a coarsened microstructure (Figure 2.13). This observation is in agreement with the increased orientation factor by the addition of rod-like particles. However, as the content of rod-like particles reaches 10 vol % the microstructure becomes composed of very coarse grains and a high porosity and also anisometric grains disappear. This suggests that only a small percentage of rod-like particles can tolerate effect of gravity and enhance the orientation by templating the grain growth in the sintered sample. An increase in the sintered density is observed in the sample with 2 vol % rod-like particles. But as the template content increases, the sintered density decrease slightly. The reason for this may be the percolation of anisometric template particles which are far bigger than the matrix thus leading to voids in the microstructure which are difficult to eliminate by sintering. It is important to note that although enhanced crystallographic texture was determined by XRD, the microstructures suggest that all the template particles are dissolved into the matrix during sintering which results in loss of morphological texture.

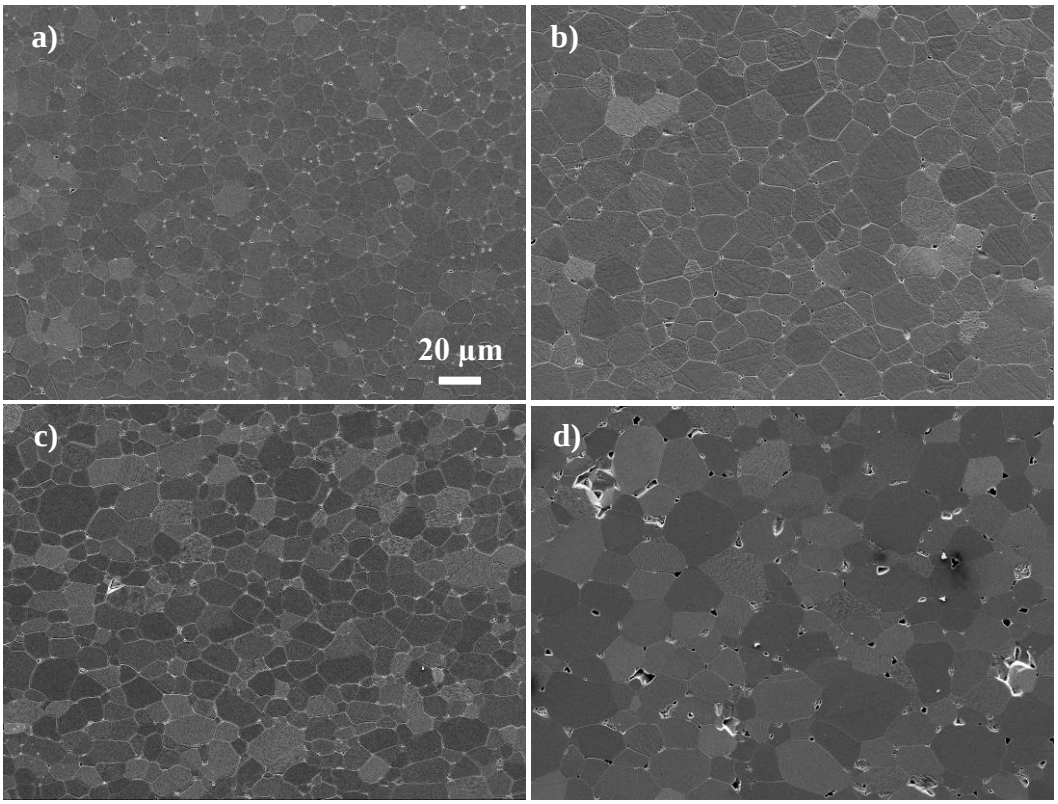

Figure 2.13 Micrographs of Samples taken from ab-direction of 100c12T (a), 98c2r12T (b), 95c5r12T (c), and 90c10r12T (d). Scale bar applies to all images.

2.1.3. Combined effect of template particles vs. glycerol on microstructure and texture development

Figure 2.14 shows the XRD patterns of samples after sintering. When template particles are incorporated to slurries prepared by 5 vol % glycerol, slight decrease in orientations of 2 and 5 vol % is observed while glycerol addition seems to enhance orientation behavior of 10 vol % template containing system. Generally addition of glycerol results in a slight decrease in sintered density for all samples (Figure 2.15). This can be explained by considering the above mentioned mechanism of glycerol to enhance stabilization once again. In this mechanism, glycerol molecules cover dispersant molecules and forces ceramic particles further apart by steric hindrance. So, as particle-particle distance increases it is more difficult to remove these pores during sintering. This situation results in a slight decrease in density of samples sintered under identical conditions.

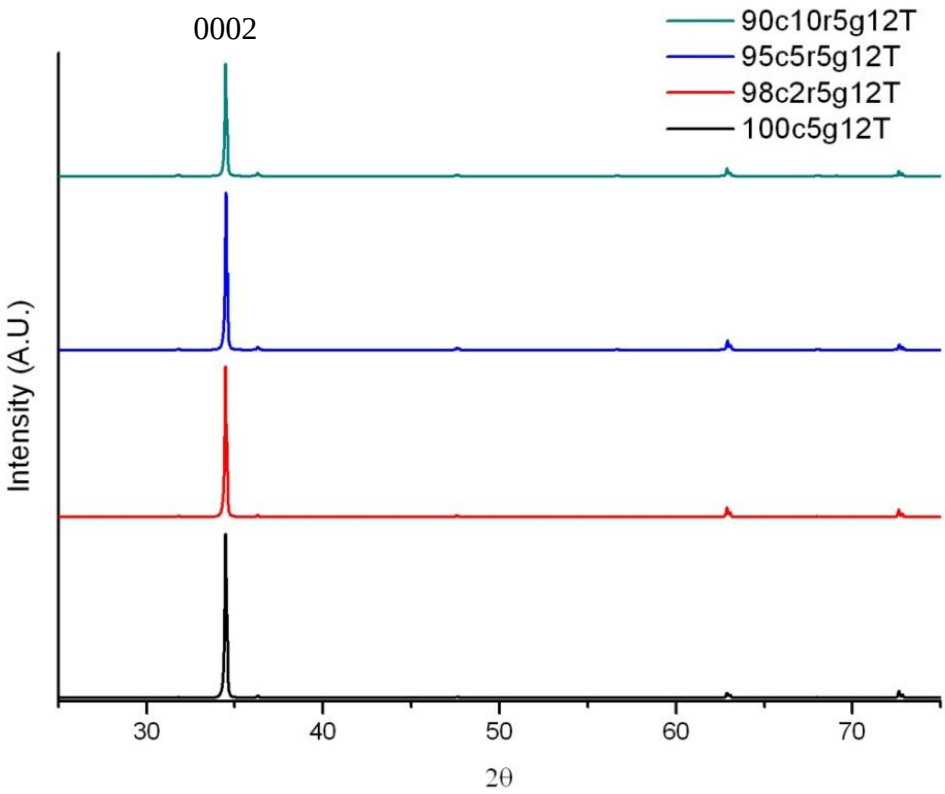

Figure 2.14 X-ray diffraction patterns of 0, 2, 5 and 10 vol % template containing samples prepared from glycerol incorporated slurry

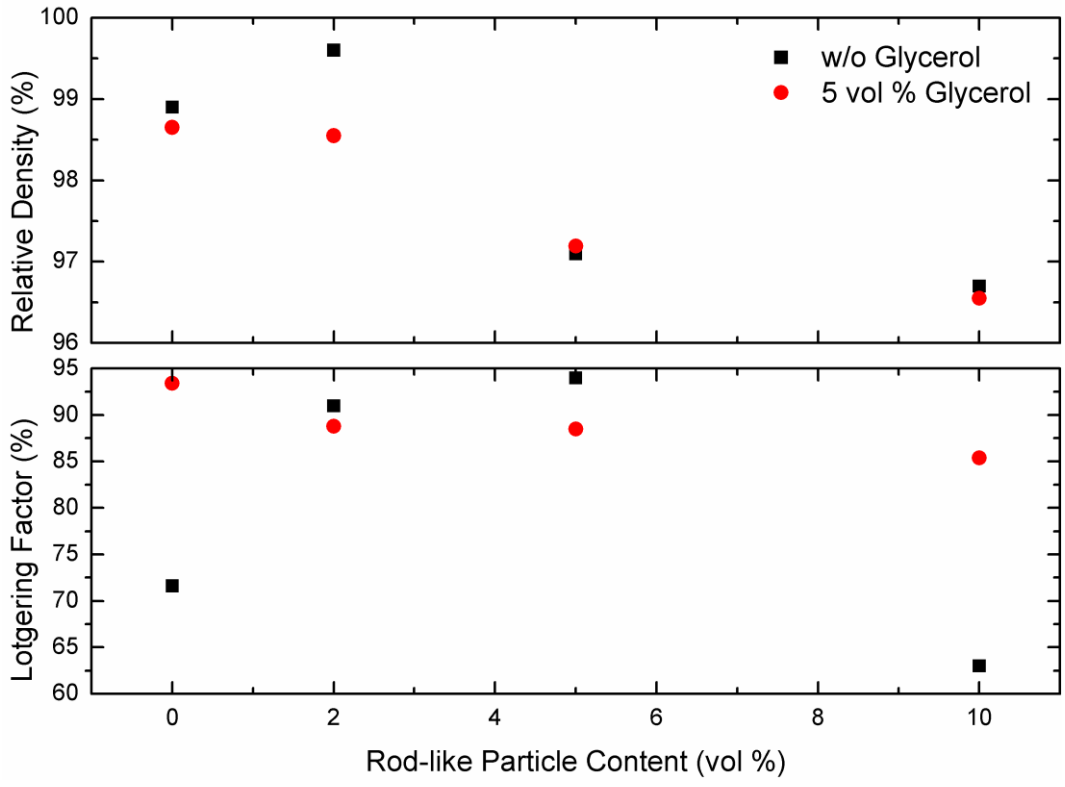

Figure 2.15 Comparison of template containing systems prepared with and without glycerol

2.2. Conclusions

It has been shown that the glycerol has a positive effect on the texture by improving the dispersion characteristics. On the other hand, glycerol adversely affects the densification when it is added >5 vol %. Therefore, further experiments were carried out with 5 vol % glycerol addition.

Optimum sintering temperature was found to be 1200°C giving high degree of texture and the highest density. Sintering at higher and lower temperatures resulted in lower densities. Addition of templates into the glycerol containing system decreases the texture due to slight misalignment behavior of the templates. An unexpected increase in the density was observed in the 2 vol % template system. This will be further in detail in the following chapter. Addition of the 5 vol % glycerol into the template system improves texture characteristic substantially while not affecting the density significantly. The parameters which were optimized in this part were utilized in the further sections of the thesis.

3. ANISOTROPIC SINTERING BEHAVIOR IN TEXTURED ZnO; EFFECTS OF MAGNETIC FIELD AND TEMPLATES ON SINTERING BEHAVIOR, TEXTURE AND MICROSTRUCTURE DEVELOPMENT

Despite the promises of texture engineering, there are some serious problems in the way of wide implementation of this interesting materials processing technology to the industry. Except from the problems associated with templates in TGG-type processes, scaling up of processes or high costs, there are sintering problems such as loss of dimensional control and residual stresses caused by anisotropic sintering shrinkage of textured ceramics. Anisotropic sintering shrinkage in several systems has been investigated but still there is more to understand about this phenomenon. Several causes of anisotropic sintering shrinkage which are reported to date are; i) green compacts which are completely composed of oriented anisometric particles [28], ii) non-densifying oriented large anisometric inclusions in randomly oriented matrixes [29], [30], iii) anisotropic surface or grain boundary energy in largely oriented green compacts [31], [32], and iv) anisotropic pore morphology and contact anisotropy [33], [34]. It should be noted that these sources are, sometimes, interrelated and in certain cases they might co-exist and in some other cases not. For example in an OCAP process anisotropic surface energy and contact anisotropy would be equally important whereas if spherical particles are slip cast under magnetic field anisotropic surface energy would dominate over other causes, if packing is assumed to be homogeneous and isotropic (i.e. no anisotropic pore morphology).

By combining different texture inducing methods such as TGG and magnetic alignment one can overcome some of the difficulties associated with individual production methods. For example by hybridization of TGG and magnetic field alignment techniques, it might be possible to decrease the required template amount and/or eliminate the necessity of introducing a liquid phase in most TGG family methods to achieve good texture properties. By eliminating the liquid phase one can achieve single phase textured materials. By combining magnetic field method with TGG one can hope to achieve good alignment of grains by a reduction in the required strength of magnetic field since templates are big particles and bigger particles are able to align at much lower magnetic field strengths [17]. Some recent studies with magnetic field can also be considered in

the context of hybrid processing. In these works anisometric, large inclusions are utilized in order to take advantage of their different properties [35], [36] than matrix material. In conventional TGG process, matrix particles around templates are usually randomly oriented whereas the matrix particles would be oriented in the same manner as the templates when such hybrid process is carried out. Accordingly, the idea of process hybridization may become important to overcome some of the difficulties related with individual processes and remove the obstacles before the texture engineering technology.

Therefore, research objective of this study was to investigate the effect of hybridization of TGG and magnetic alignment processes on processing characteristics such as sintering and microstructure development and subsequently on texture via a model material system. Zinc oxide (ZnO, $P6_3mc$, a=b = ~0.3249 nm, c = ~0.5206 nm), an important multifunctional oxide, with highly anisotropic properties, due to its hexagonal wurtzite structure, was chosen as a model material system in this study. A wide band gap (~3.3 e.V. at room temperature) [37] compound semiconductor, ZnO demonstrates properties such as piezoelectricity, luminescence [37], [38], and thermoelectricity [20]. Although available as single crystals [39-41], polycrystalline ZnO is also quite important for practical applications; therefore, textured ZnO ceramics may find interesting applications.

3.1 Experimental Procedure

Since high quality rod-like particles are not commercially available, rod-like ZnO template particles were synthesized, prior to further experiments, via hydrothermal method as previously described by Lu and Yeh [42]. Initially, 0.5 M clear zinc solution was prepared by dissolving zinc nitrate hexahydrate (Merck GmbH, Darmstadt, Germany) in distilled water. Zinc hydroxide was precipitated by mixing the zinc solution with 0.1 M aqueous ammonia (NH_4OH) solution. After precipitation, precipitate was washed rigorously with distilled water. That was then fed into a hydrothermal reactor. Hydrothermal reaction was carried out in a polytetrafluoroethylene lined stainless steel autoclave at 100°C for three hours under autogenous pressure. During hydrothermal synthesis the reactor was mixed at a stirring rate of 50 rpm. Then the synthesized powder was washed with distilled water by centrifugation. Finally, the powder was dried by freeze drying.

ZnO samples which contain template particles from 0 to 10 vol %, were prepared by slip casting with and without 12 T rotating magnetic field. Schematic of the experimental setup and model structure are shown in Figure 3.1 a). Suspensions with 20 vol % solids loading were prepared by ZnO powder (JIS1, HakusuiTech co., Ltd., Osaka, Japan), with 5 vol % (based on liquid volume) glycerol containing aqueous suspension medium. The commercial ZnO powder was composed of particles with a wide variety of morphologies, generally with small aspect ratio (Figure 3.2). 0.5 wt % poly(ammonium acrylate) (A6114, Toagosei CO., LTD.), based on solid load, was used as a dispersant. Suspensions were homogenized by ultrasonication for 10 minutes. In the text, 100c0T represents the sample which was cast without magnetic field and contains no templates while 100c12T refers to sample which was slip cast under 12 T rotating magnetic field and had no templates. 98c2r12T, 95c5r12T and 90c10r12T samples contain 2, 5 and 10 vol % (based on solid content) templates, respectively. These samples were slip cast under 12 T rotating magnetic field. After compaction under magnetic field, all samples were cold isostatically pressed at 392 MPa for 10 minutes.

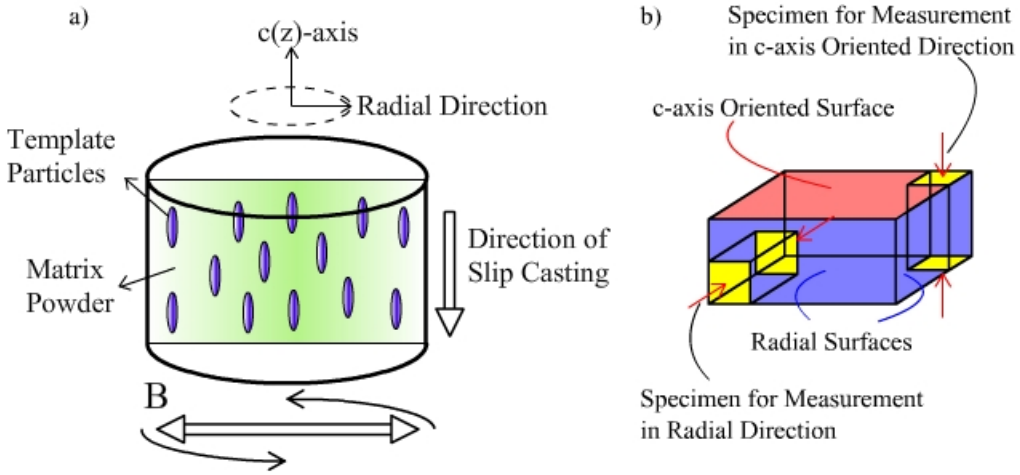

Figure 3.1 Experimental setup and cross-section view of the aimed model a), and schematic drawing showing the specimen preparation b).

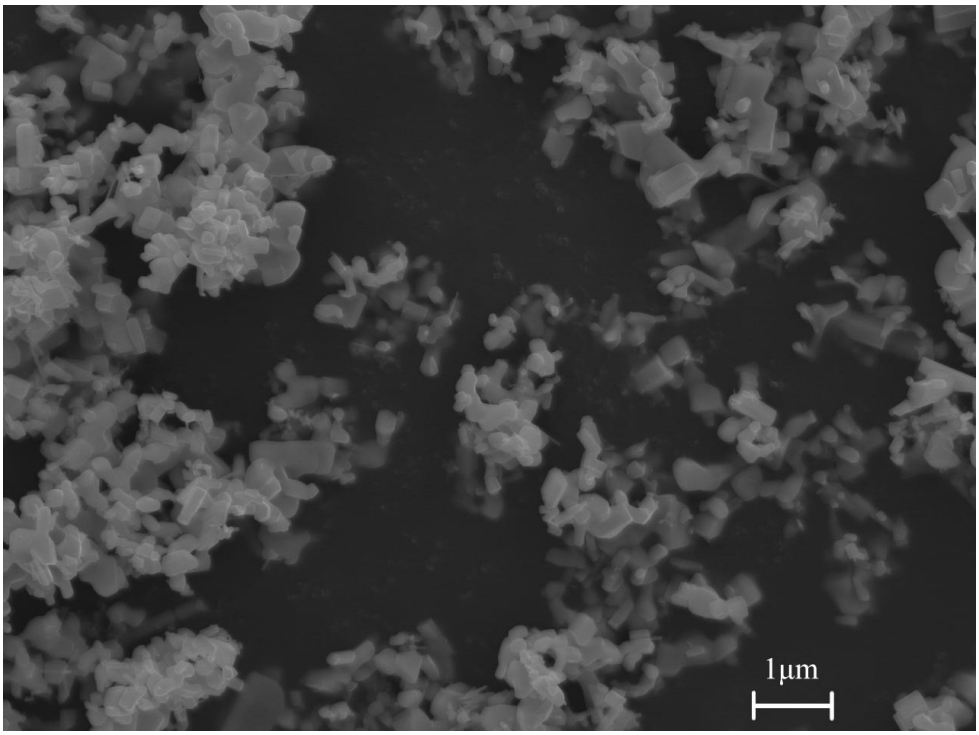

Figure 3.2 SEM micrograph of as received commercial ZnO powder

Green densities of samples were calculated from shrinkage values by assuming that the shrinkage in transverse direction is symmetric. To study the sintering behavior of green samples, specimens were cut as rectangular prisms in which longer axis is normal to either the basal or prismatic plane oriented faces for thermomechanical analysis (TMA). For randomly oriented sample (100c0T) TMA specimens were cut in a way that the measurement direction was parallel to the sample z and radial directions. For all textured samples, strongly oriented crystallographic c-axis, [0001], was parallel to sample z-axis and weakly $(10\bar{1}0)$ oriented directions were parallel to sample radial (See Figure 3.1 b)). In TMA, organic components of slip compositions were burnt out at 400°C for 2 hours. Then, specimens were heated at 5°C/min to 1200°C for sintering at this temperature for 2 hours. Sintered densities of the specimens were measured by Archimedes' method. Top surfaces of c-axis oriented samples, which were sintered at TMA, were polished down to 0.02 μm for electron backscatter diffraction (EBSD) study. (0001) Pole figures obtained from the EBSD data were averaged over entire azimuthal angle range and thus the pole figure profiles were obtained. Then, these orientation distribution profiles were fit to March-Dollase equation [11], [43];

$$P(r,\omega) = (r^2 Cos^2(\omega) + r^{-1} Sin^2(\omega))^{(-3/2)} \quad (3)$$

In the equation (3), r parameter can take a value between 0 and 1 and it defines the quality of the texture, i.e. the width of the orientation distribution function. Accordingly smaller r means finer quality. ω is the angle between sample normal and the normal of the basal plane of ZnO crystal (c-axis).

3.2 Results

Figure 3.3 shows hydrothermally synthesized ZnO particles which were used as templates in this study. The templates have the average dimensions of 7 μm in length and 1.5 μm width. When x-ray diffraction pattern of rod-like particles was compared with the XRD pattern of the commercial powder, preferred orientation in $(10\bar{1}0)$ plane was observed (Figure 3.4) (Although there are minority impurities such as Si and Fe in the templates due to x-ray fluorescence analysis (not shown) the 0.42 degrees of shift in peak positions, in template particles, is attributed to the analysis conditions since same shift is observed in all peaks).

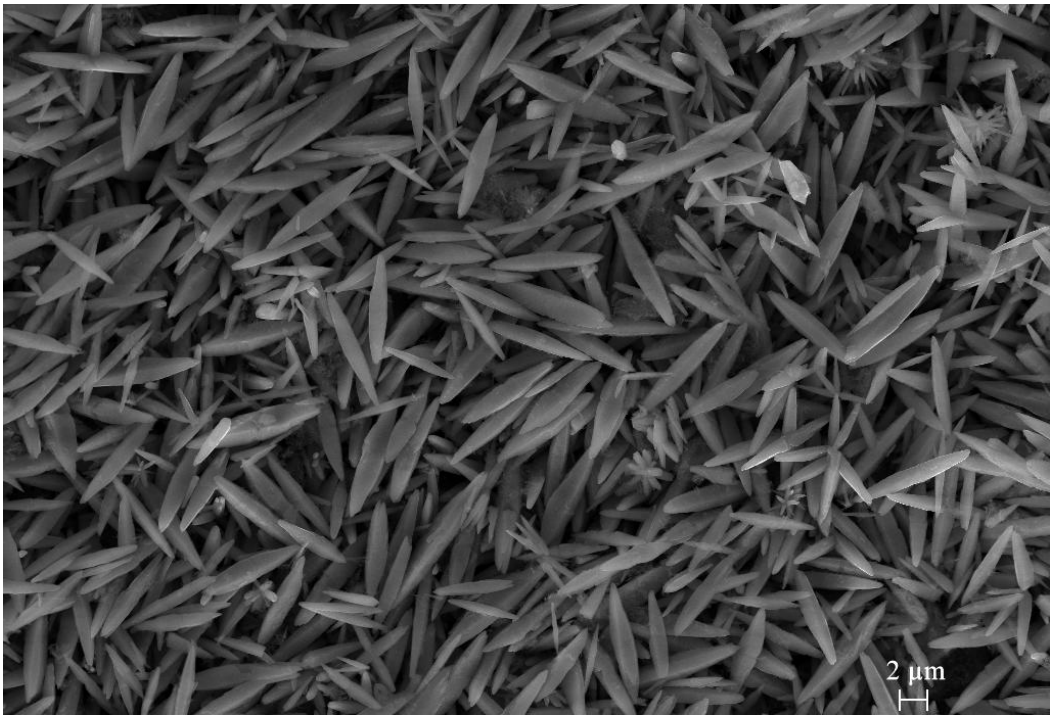

Figure 3.3 Scanning electron micrograph of rod-like ZnO template particles.

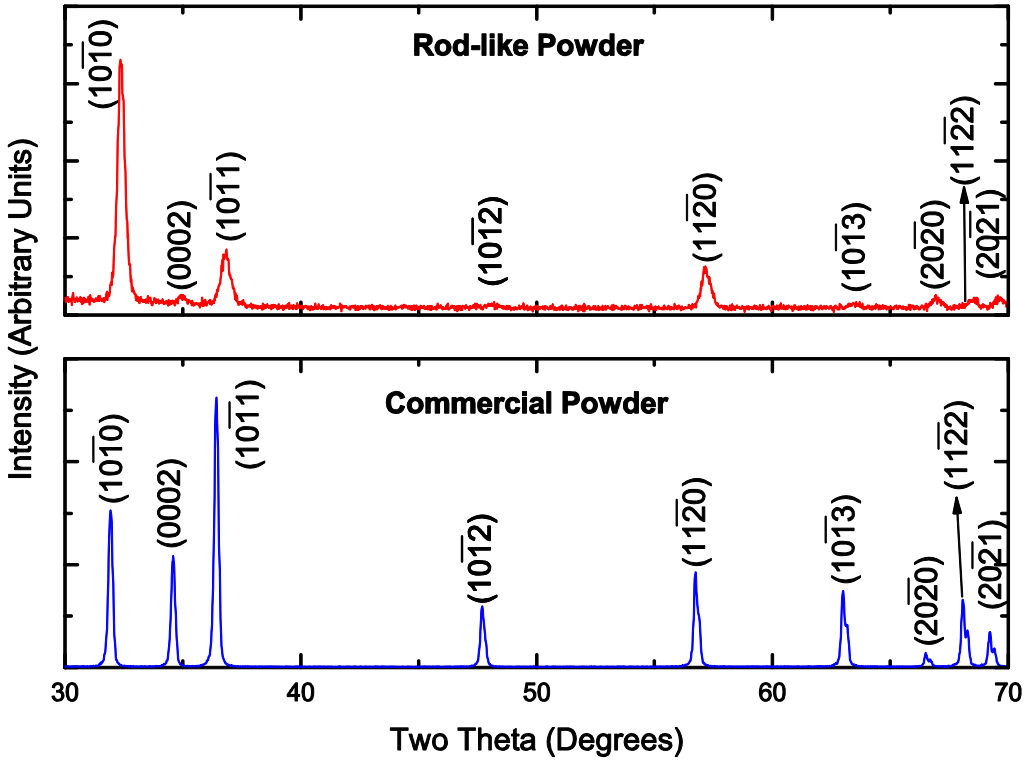

Figure 3.4 X-ray diffraction patterns of rod-like ZnO powder and commercial ZnO powder.

This preferred orientation is caused by the shear due to smearing, during the preparation of the XRD sample. The same preferred orientation can be observed in elongated morphology of the templates (Figure 3.3). This result confirms that, long axes of templates are parallel to crystal c-axis direction, whereas, short axes were grown along prismatic plane normals. As stated above anisotropic diamagnetic susceptibility of ZnO forces c-axis to align perpendicular to the applied rotating magnetic field which means that rods must align their long axes perpendicular to the rotating magnetic field. Accordingly, Figure 3.5 shows clearly, that the model shown in Figure 3.1 is almost completely achieved after slip casting under rotating magnetic field. Several template particles can be seen to be aligned perpendicular to the magnetic field direction as well as a few slightly misaligned templates. Figure 3.6 shows sintering characteristics of the systems that were studied in this work. 100c0T sample which was slip cast in the absence of magnetic field and template particles exhibits anisotropic shrinkage and shrinks about 14 % in z direction and a little less in radial direction (~13 %, See Figure 3.6 (a) and Figure 3.6 (f)). In addition, it should be noted that shrinkage in z direction starts later, at around 815°C, than shrinkage in radial direction which starts at 735°C (Figure 3.7).

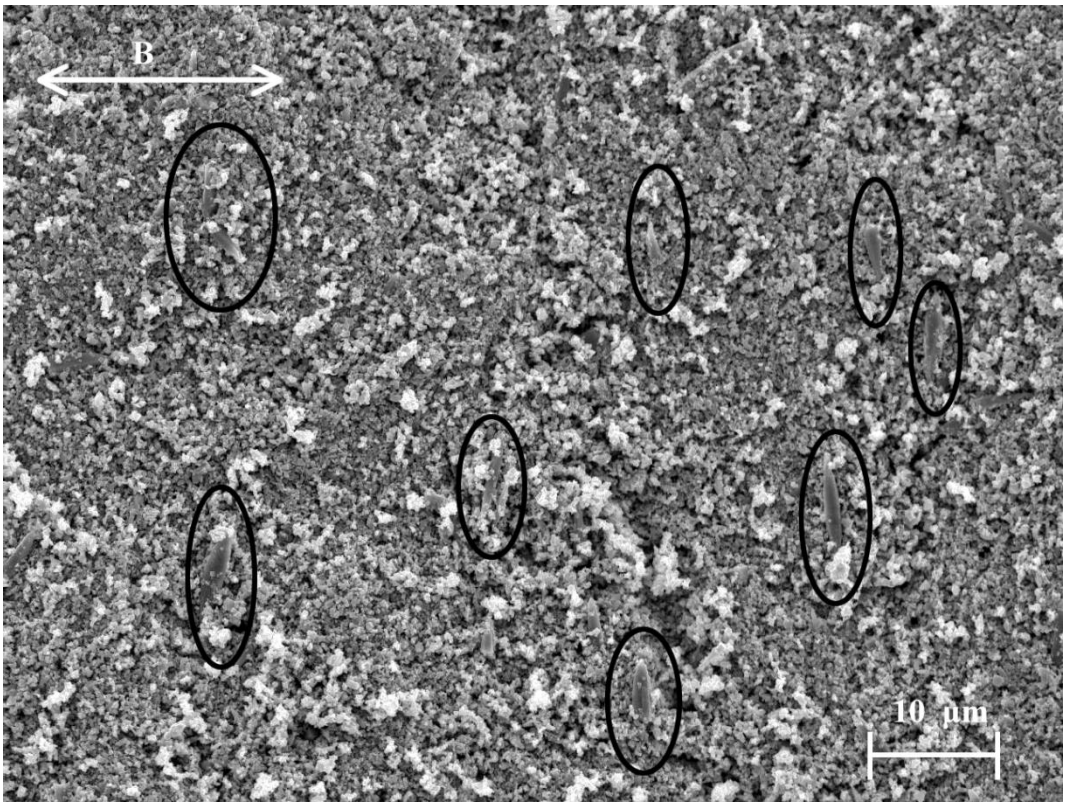

Figure 3.5 SEM image of green 95c5r12T taken from radial direction. Black markers show template particles which are oriented perpendicular to applied magnetic field B

Sample 100c12T exhibits less shrinkage in both the c-axis oriented direction (11.4 %) and radial direction (11.7 %), (Figure 3.6 (b) and (f)), with respect to random sample. Shrinkage in c-axis oriented direction begins at around 850°C while it occurs at around 740°C in radial direction (See Figure 3.7). Since the sintering curve in c(z) direction did not reached a plateau during the test (Figure 3.6 (b)) of this highly c-axis oriented specimen, it can be concluded that the shrinkage was not complete at the end of sintering dwell time. Interestingly, the sample with 2 vol % template addition (98c2r12T) demonstrates almost isotropic sintering shrinkage which are ~12.9 % and ~12.8 % for radial and c-axis oriented directions respectively (Figure 3.6 (c) and (f)). Shrinkage in 95c5r12T sample is, again, anisotropic and shrinkage in c-axis oriented direction starts first, at 757°C in contrast to radial direction which started at around 840°C (Figure 3.6 (d) and (f)). The effect of anisotropic shrinkage is most pronounced in the sample 90c10r12T sample (Figure 3.6 (e) and (f)), which has the total shrinkage values of 11.8 % and 8.8 % in radial and c-axis oriented directions, respectively. Figure 3.6 (f) shows

total sintering shrinkage of the samples at the 450th minute of the TMA analysis as a function of template content, magnetic field and direction. It is seen from this graph that although the random sample exhibits anisotropic sintering shrinkage, it shows the maximum total shrinkage among all samples. Final shrinkage values of samples for both directions of the 100c12T and 98c2r12T sample seem to be almost isotropic, although in the 100c12T sample sintering onset temperatures are different for two directions. However, as the template content increases, the shrinkage starts to become more and more anisotropic, which gives clues for constraining of matrix particles by the templates. Green densities of the samples increases slightly, as templates are incorporated into the system as can be seen from Figure 3.8. This can be attributed to high density of templates in comparison to matrix compact.

Figure 3.10 shows the backscattered electron diffraction orientation maps of samples which show individual orientations of each grain. The 100c0T sample shows almost randomly oriented microstructure after sintering (Figure 3.10 (a)) as expected, since there was no magnetic field applied during forming of the compact. On the other hand, the 100c12T sample exhibits high texture (Figure 3.10 (b)). Samples containing 2, 5 and 10 vol % templates demonstrate maximum multiples of a random distribution (MRD) values of 11.3, 9.1 and 11.7, respectively, which are far less than that of the 100c12T sample (i.e. 18.45) (Figure 3.10 (c), (d) and (e)). The higher maximum MRD value means there are more grains which are oriented along c-axis direction if we assume the information collection area on the sample is roughly the same. Figure 3.11 shows distribution of MRD values of (0001) pole figure profiles and March-Dollase fits for all samples. For a random sample, which is 100c0T in this case, the MRD value fluctuate about 1 for all degrees which means that there is almost same amount of matter oriented at each angle and its vicinity. The addition of templates results in shallower orientation distribution (Figure 3.11). Figure 3.10 (f) shows a typical microstructure belonging to 98c2r12T specimen which is taken from radial direction.

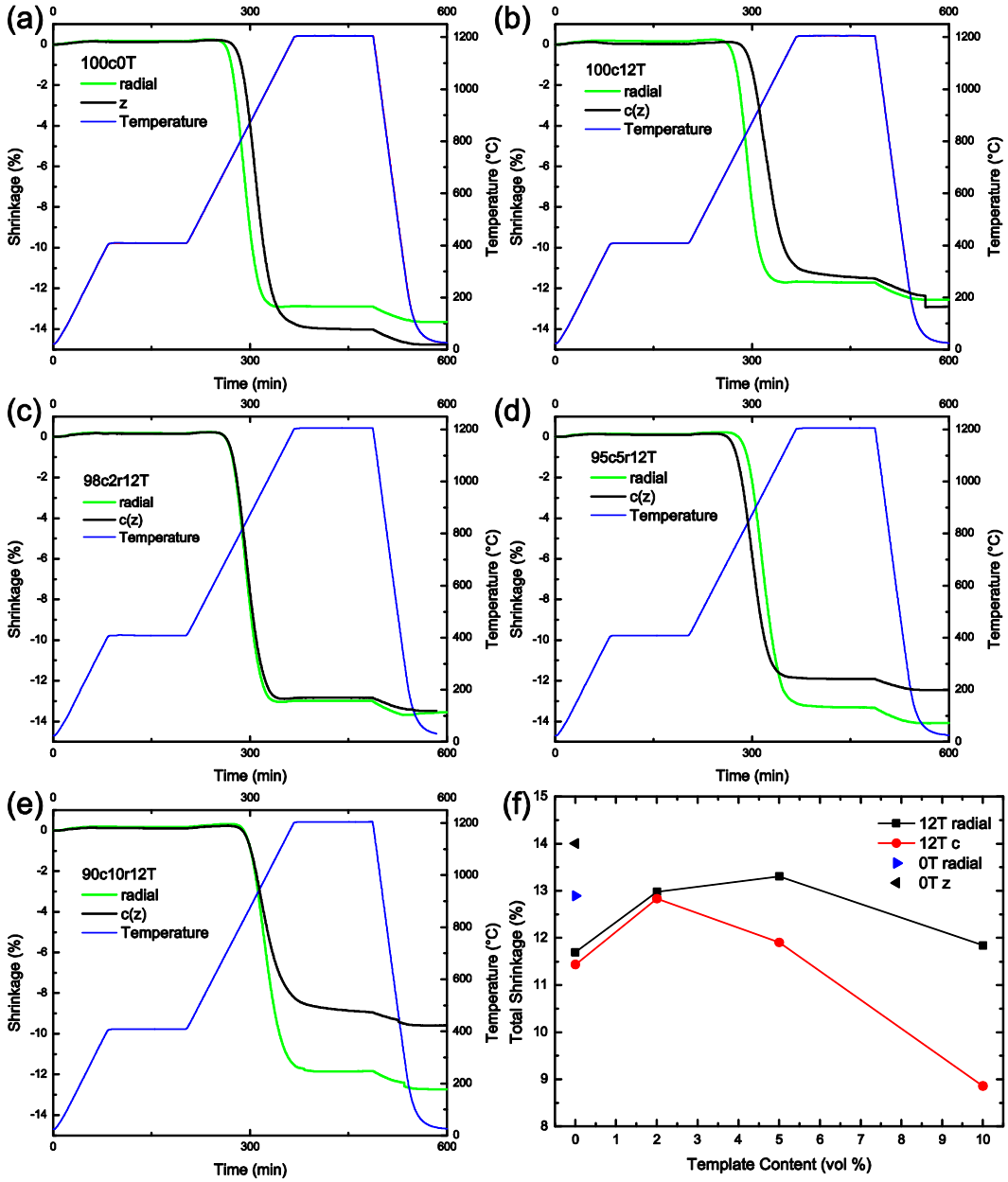

Figure 3.6 TMA shrinkage curves of (a) 100c0T, (b) 100c12T, (c) 98c2r12T, (d) 95c5r12T, (e) 90c10r12T samples, (f) change of total shrinkage values as template contents and magnetic field condition varies

3.3 Discussion

Even though it was manufactured in the absence of a magnetic field, and no preferred orientation can be observed from top surface (Figure 3.10 (a) and Figure 3.11), 100c0T sample, shows small amount of anisotropy in the final shrinkage and large difference in onset temperature values for radial and (z) directions of the sample (Figure 3.6 (a)). This sintering anisotropy may arise from two general sources; i) process related and ii) materials related causes. The former causes can be non-uniform distribution of polymeric additives and non-uniform packing and/or slight orientation due to processing conditions, whereas the latter causes include anisotropic particle morphology and surface energy anisotropy which is also related with curvature. Non-uniform distribution of glycerol is rather unlikely since glycerol has high solubility in water whereas amount of dispersant was negligible. Non-uniform orientation may arise from the effect of suction force on anisometric particles during the slip casting procedure. Although not directly observed in this case, anisometric particles are known to align in the presence of suction force as explained previously by Tanaka [44] and Chen *et al.* [45]. The effect of suction on anisometrically shaped particles is demonstrated in Figure 3.12 (a). However it should be noted that the orientation mentioned is rather small and further decreases as distance from mould surface increases, which is probably the reason that the EBSD analysis shows completely random distribution when it is carried out on the top surface. Even such heterogeneity at the vicinity of the bottom surface can cause some small anisotropy in the sintering shrinkage as shown in figure 3.6 a). The reason for this sample to exhibit the biggest shrinkage might be attributed to relatively low initial packing density (Figure 3.8) due to overall random distribution of particles in spite of the possible, small particle alignment at the bottom part. Generally random distribution is also confirmed with the almost identical shrinkage rate along radial and (z) directions (Figure 3.7). In highly textured 100c12T sample the predominant mechanism resulting in anisotropic shrinkage was the anisotropic surface energy due to strong fiber texture. Implications of this strong fiber texture on sample is as follows; in c-axis oriented direction which is parallel with sample z-axis, basal planes confront each other in the green compact resulting in a low lattice mismatch (i.e. low energy grain boundaries) whereas in radial direction different crystal planes come across

each other since rotations of crystals about c-axis are random, as shown in Figure 3.12 (b). Therefore, the grain boundary energy is higher in radial direction in comparison to that in c-axis oriented direction as a result of higher lattice mismatch. According to Zavaliangos *et al.* [31] this creates an anisotropy in grain boundary diffusivity rate which in turn results in sintering anisotropy. Furthermore, Shui *et al.* concluded that the anisotropic mass transfer rate causes sintering anisotropy in highly textured materials [32].

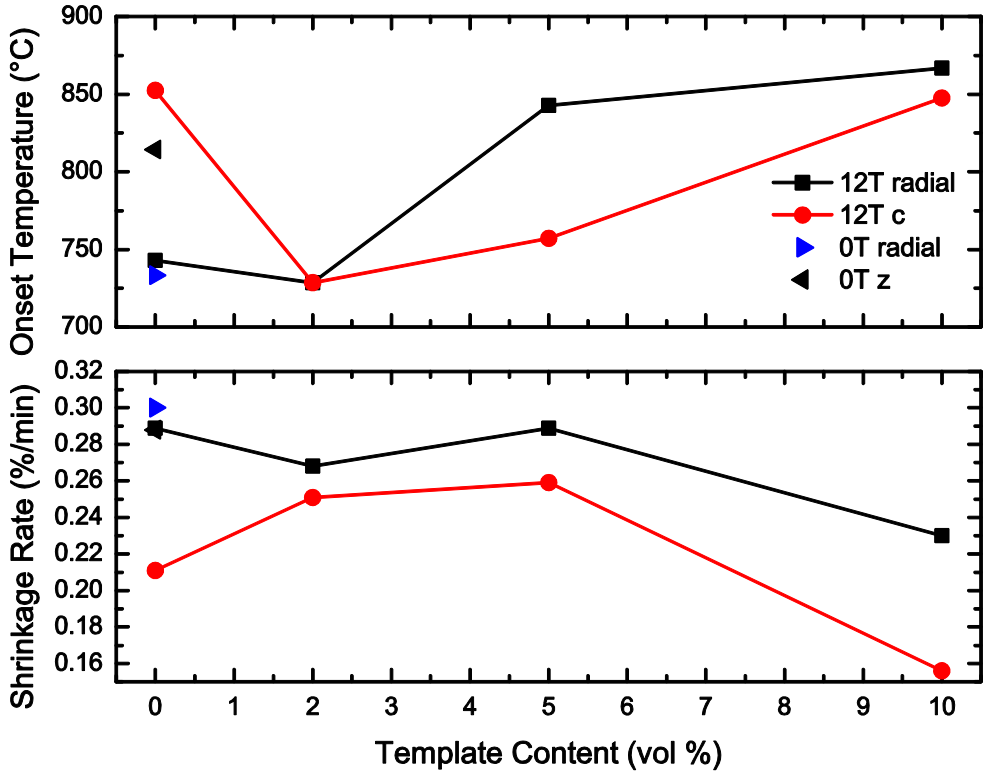

Figure 3.7 Graphics showing the dependence of onset temperatures of sintering and shrinkage rates on direction, on template content and magnetic field conditions

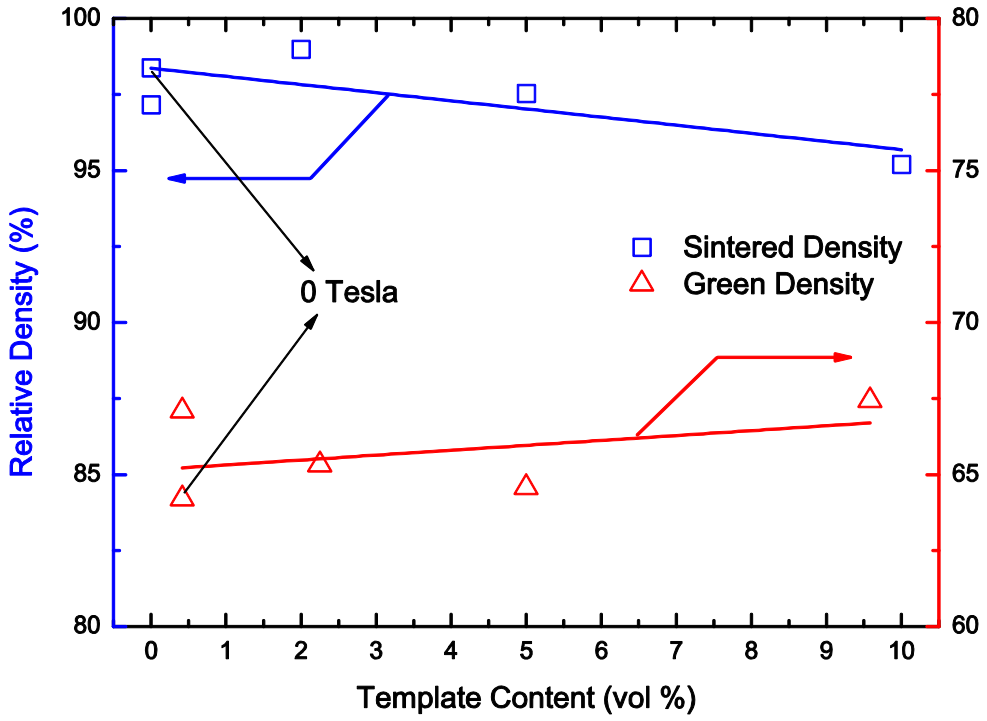

Figure 3.8 Relative green and sintered densities of samples, as a function of template content and magnetic field condition

Consequently, the sintering rates are different in the c-axis and radial directions. Anisotropic surface energy distribution also manifests itself in the difference in onset temperatures; sintering in radial direction starts at almost 110°C lower temperature than that in c-axis direction. Shrinkage rates also show the same trend; slower in shrinkage rate c-direction (0.21 %/min) is observed whereas in radial direction shrinkage rate is 0.29 %/min (Figure 3.7). This result is in very good agreement with above mentioned literature.

Sintering curves of the 98c2r12T sample from both directions are almost the same as well as their sintering rates and onset temperatures as shown in Figure 3.7. In addition, sintered density of this sample was the highest. This is an interesting result since templates, generally, retard sintering, slow it down and worsen the densification as it is widely documented in the literature which concludes that; rigid, non-densifying templates cause constrained sintering. In addition, when introduced into system in large amounts they tend to form a rigid skeleton via percolation thus reducing sintering ability [29]. However, Bocaccini and Olevsky proposed, for a hypothetical case, densifying inclusions can enhance densification as they would contribute to overall energy of the system [30], if the

particles have a surface energy that exceeds that of the matrix powder. Therefore, rigidity of the templates were investigated at sintering temperatures (Please, note that, here rigidity refers to the stability of the templates at high temperatures, i.e. ability to retain their shape during sintering. It does not refer to any particular mechanical property). When the templates were annealed at 1100°C for 2 hours it was observed that particles could not retain their initial anisometric shape and tend to reduce their surface energy by losing their well faceted morphology (Figure 3.13), suggesting that their initial shape is not thermally stable at the sintering temperature used in this study which was 1200°C. This result shows that in this case template particles can sinter with the surrounding matrix powders and can enhance densification. To clarify the reason why these templates act in such a fashion, crystalline structure was investigated in detail with Rietveld refinement method (Figure 3.9). The peak positions and broadening are good indicators of the crystalline structure but when the patterns are quantized then they give the most valuable informations. One of the best methods to quantize the crystal properties via x-ray diffraction is the Rietveld refinement method [46]. The xrd pattern of commercial powder (Figure 3.9, a)) has very narrow peak width and is considerably randomly oriented. The narrow peak width is a result of defect free crystallites in the powder [47]. Lack of preferred orientation in the pattern is due to the low aspect ratio of the crystallites in the powder. On the other hand, when the XRD pattern of the as synthesized template powder (Figure 3.9, b)) is inspected closely, considerable peak broadening is observed compared to the peaks in the xrd pattern of the commercial powder. This peak broadening can be attributed to the microstrain in the crystallites. This microstrain, in turn arises from the defects of the crystalline structure [47]. Each defect in a crystal causes local distortions in the lattice. These local distortions cause a strain which affects the crystal properties. These deviations from ideal crystal geometry can be observed by means of Rietveld refinement of x-ray diffraction patterns [48]. The maximum values for microstrain in commercial and as synthesized template powder are -1.3×10^{-10} and 0.002, respectively. The microstrain value of the templates is several orders of magnitude higher than that of commercial powder. The relationship between the defect formation and microstrain can further be concluded if the intrinsic defect formation probabilities are checked. Intrinsic

defect formation probability of commercial powder is $5.9x10^{-9}$ while it is 0.0043 for templates. Also, twin fault probability value of $5.9x10^{-9}$ for commercial powder increases to 0.0052 for templates. Rietveld refinement studies of the templates after annealing showed that the microstrain value drops to half (0.001) and intrinsic defect formation probability drops more than 3.5 times to 0.0014. Twin fault formation probability of annealed template powder is 0.002, more than 2.5 times lower than that of as synthesized template powder. All these results show two things; i) templates are defect-full instead crystallites, and ii) the microstrain decreases as defect numbers decreases upon annealing. So if we imagine the template particle in a matrix of commercial powder we can consider following scenario; initially the template has higher energy than its surrounding due to microstrain it possesses. When sintering proceeds, the templates start to evolve their shape in order to reduce shape, by this evolution the template loses its faceted geometry. With its new geometry the template surface has a smaller radius of curvature which lets it to sinter to the surrounding particles. This scenario is as close as possible to that is proposed by Boccaccini and Olevsky [30].

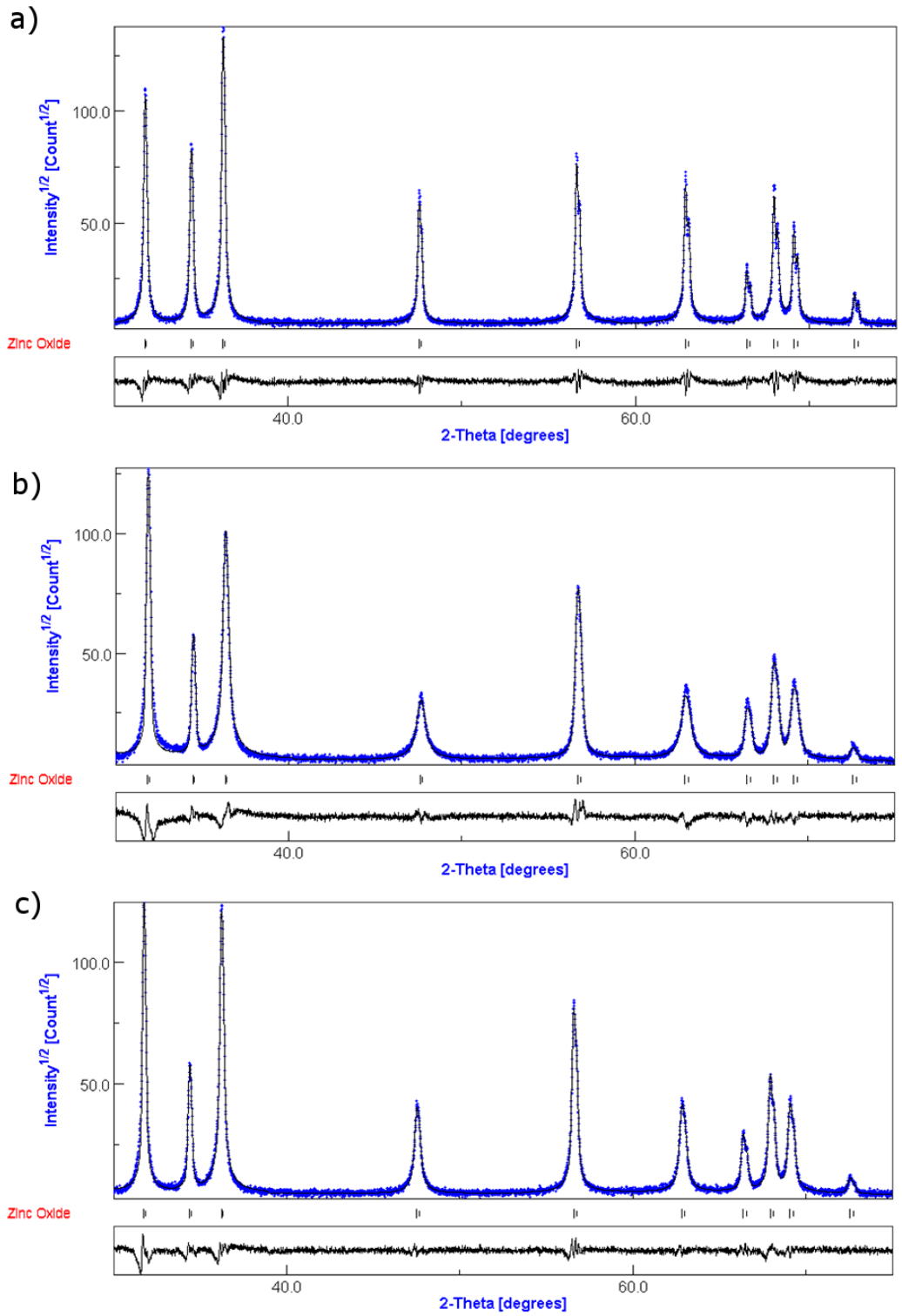

Figure 3.9 Rietveld refinement results of the a) commercial ZnO powder, b) as synthesized ZnO template powder, and c) template powder annealed at 1100°C for 2 hours. (Blue) Scatter dots represent experimental XRD data. Solid (black) line is the whole pattern fit result after Rietveld refinement. Vertical lines are the expected peak positions of ZnO. Bottom of each image is the residual plot (difference between the experimental values and fit).

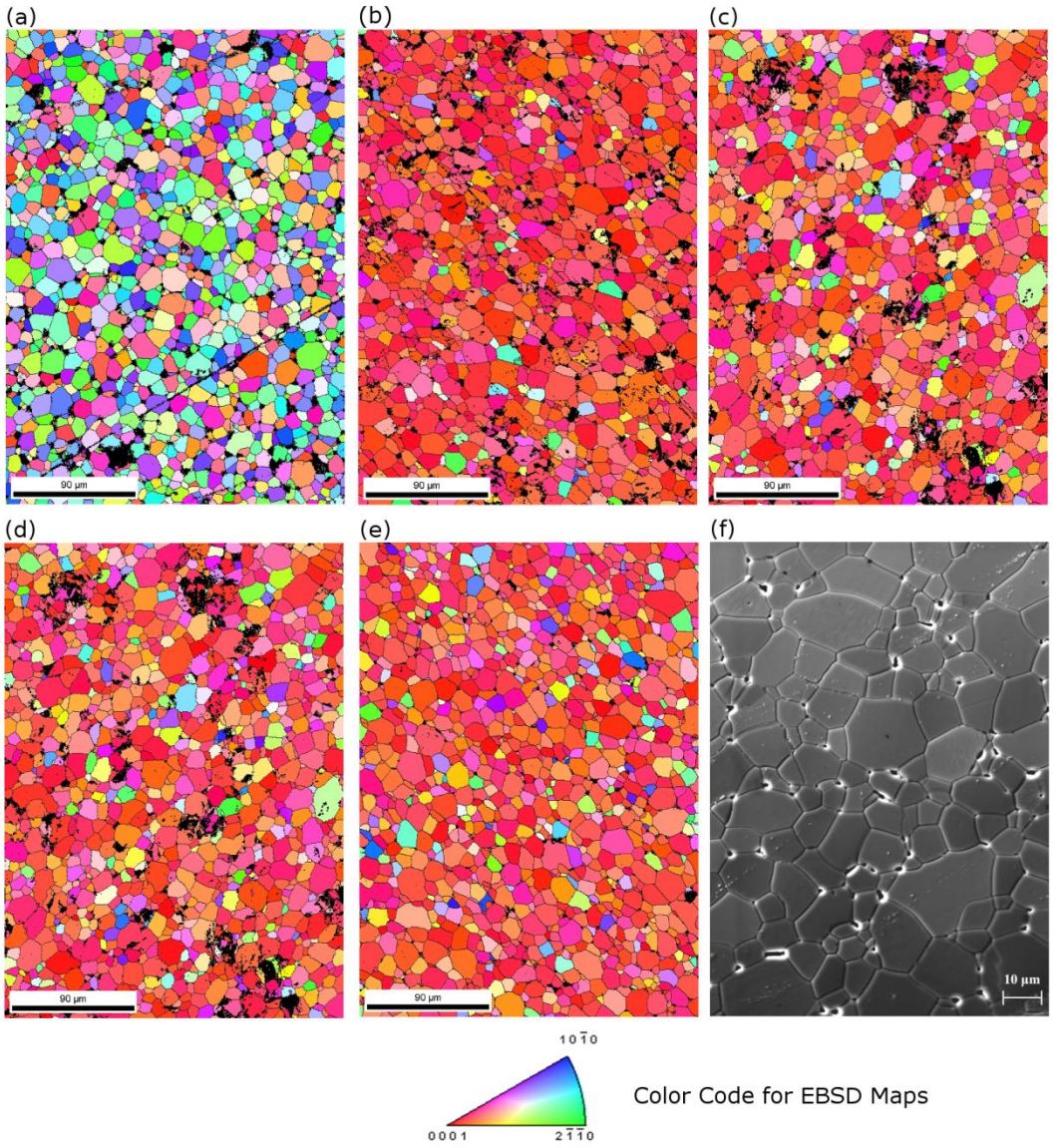

Figure 3.10 EBSD maps of TMA specimens from c-axis oriented faces; a) 100c0T, b) 100c12T, c) 98c2r12T, d) 95c5r12T, e) 90c10r12T, and f) a typical microstructure belonging to 98c2r12T from radial direction

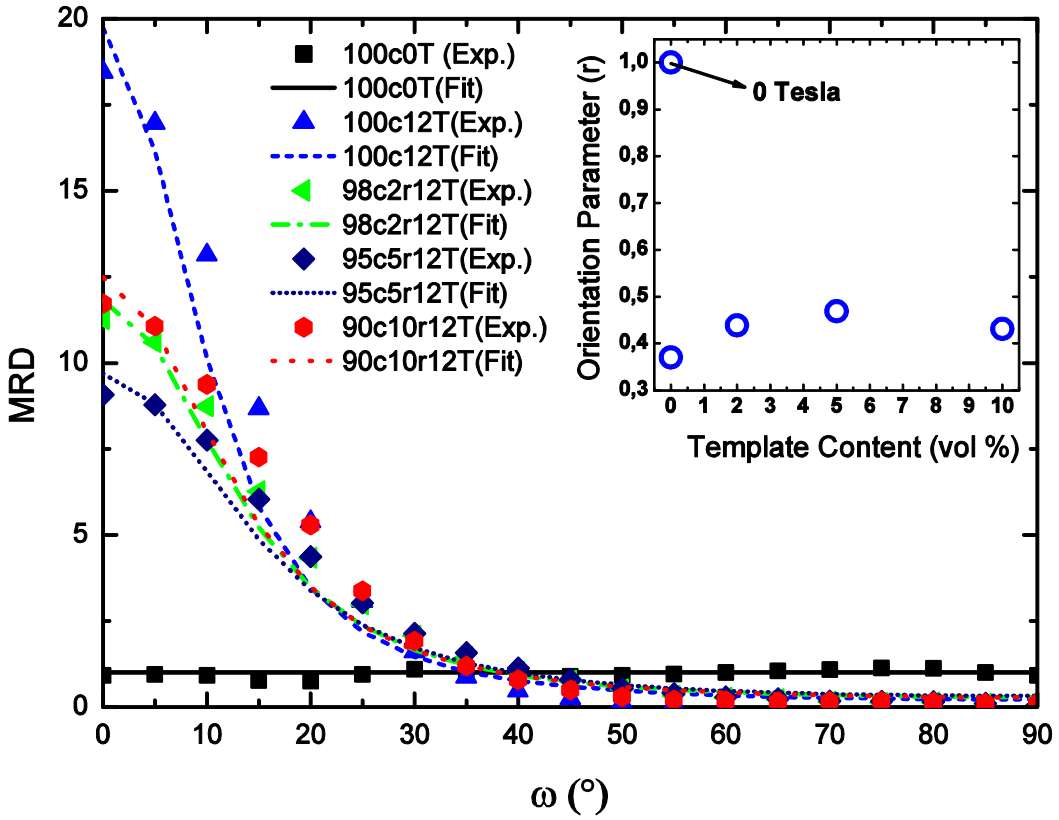

Figure 3.11 (0001) EBSD pole figure profiles of sintered samples. March fits to the MRD data is shown as curves. Inset shows dependence of orientation parameter, r, on template content and magnetic field.

Moreover, the decrease in the final texture (Figure 3.11 (inset)) can be attributed to the suction force on templates during slip casting. This suction force tends to align templates perpendicular to the gravity opposing the rotating magnetic field which tries to align templates parallel to the direction of gravitational pull. In addition, the negative effect of gravity on alignment of rod-like or whisker shaped particles is reported previously [23]. Apparently in the case of the system reported here (template + matrix) gravitational force was not enough to disturb the alignment of templates significantly as described in ref. [22]. On the other hand, from SEM image of raw 95c5r12T (Figure 3.5), which is typical of all systems, it can be seen that, occasionally, there are templates which are slightly misaligned. Therefore, when compared to 100c12T sample, 98c2r12T shows slightly lower texture quality (Figure 3.11 (inset)). Here it should be noted that the strong alignment of matrix particles might have an important role in the reduction of the anisotropic sintering shrinkage. To test this some further study was carried

out which will be discussed later in this text. This high degree of matrix particles alignment along with the templates can not be achieved in any other process than magnetic alignment. Matrix particles' alignment combined with densifying behavior of the templates with volumes less than a critical value resulted in a material with less anisotropic shrinkage, less constrained sintering and enhanced densification, which is comparable to the random sample.

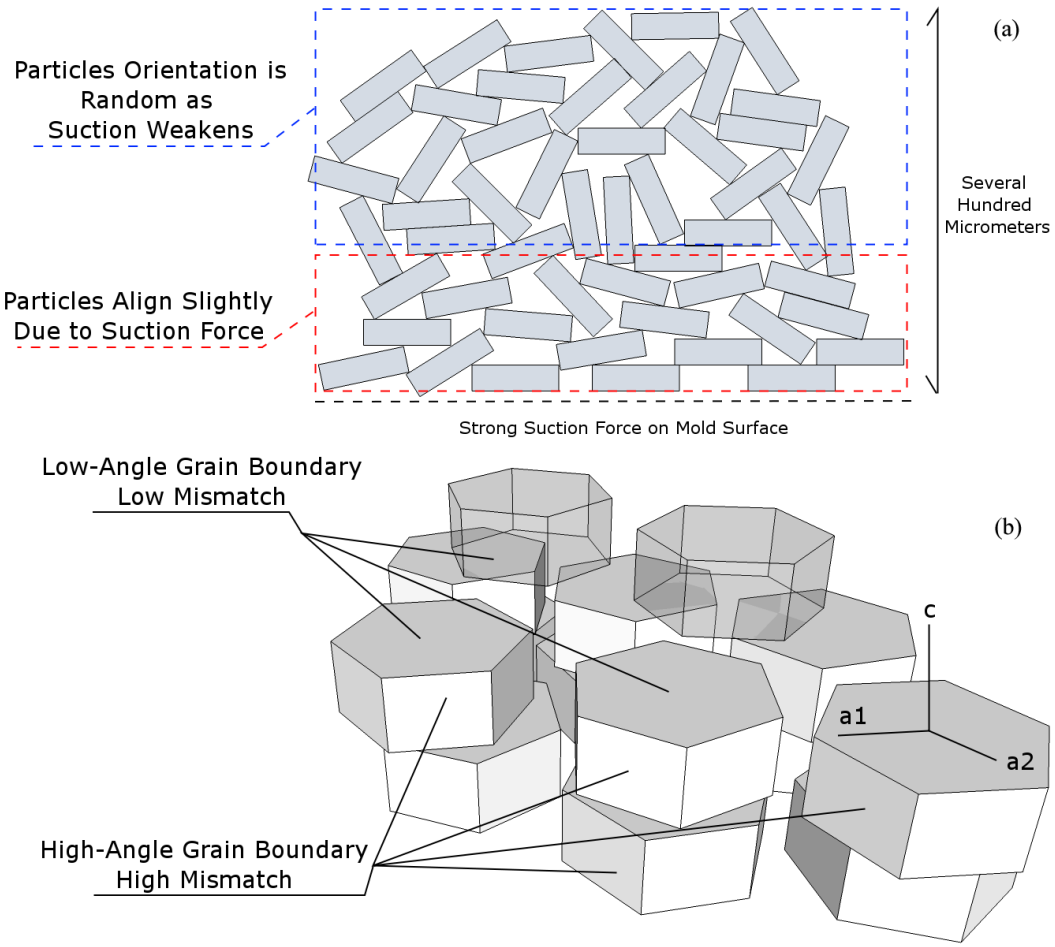

Figure 3.12 Schematic drawings of (a) influence of fluid suction on anisometric particles in the bottom of a slip casting slurry without applied magnetic field and (b) high and low-angle grain boundaries in a fiber textured material

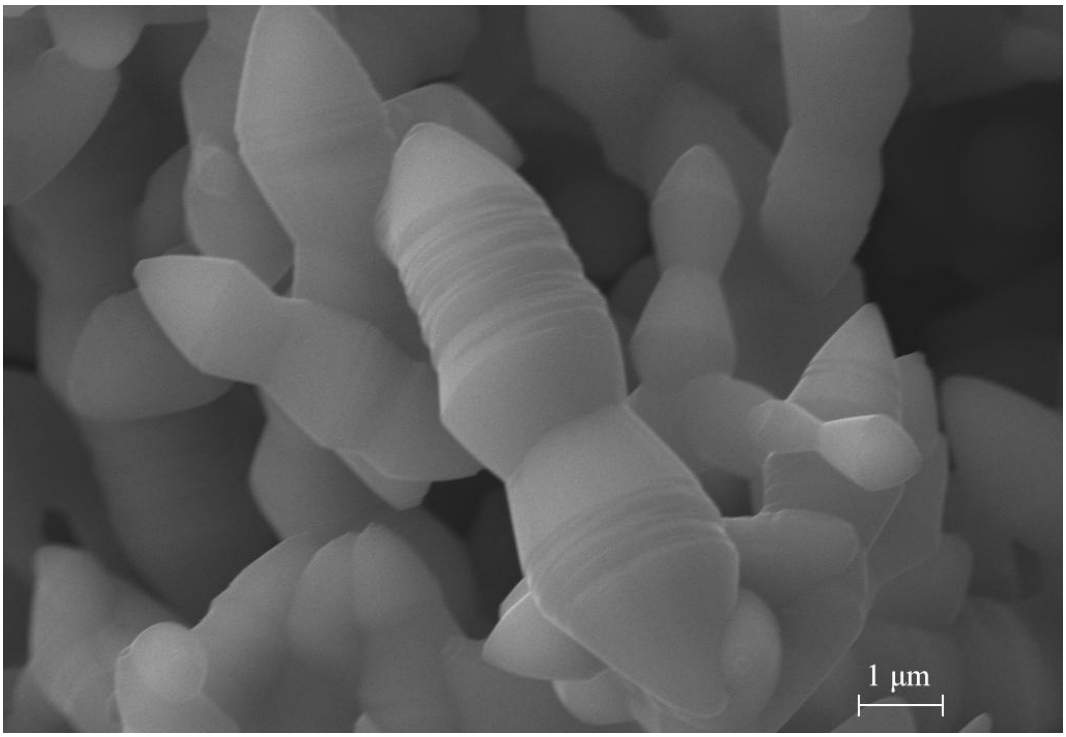

Figure 3.13 Rod-like ZnO templates after being annealed at 1100°C for 2 hours.

As the template content was increased from 2 to 5 vol %, anisotropy in the sintering reappears and relative sintered relative density decreases. This result suggests that there may be a critical amount of densifying inclusions (templates in this case) which may enhance the densification behavior as suggested by Boccacini and Olevsky [30]. Although shrinkage rates increase slightly, the increase of template content from 2 to 5 vol % also increases the onset temperatures (Figure 3.7) which may be due to increase in template content. In a previous study it was shown that [12], when the critical amount of templates is exceeded, individual template particles can come into close proximity and they begin to interact. This may result in more misoriented template particles. Similarly, as volume of templates increases from 2 to 5 vol %, effect of interaction may become more significant. This will result in the decrease in distance between two templates, which is combined with the increase in number of misoriented templates can lead to the reduction of density as in the case for 95c5r12T. The decrease in texture quality (i.e., increase in r value), can also be attributed to increase in number of misaligned templates since number of template particles increases.

As the template content is increased even further, to 10 vol %, anisotropic shrinkage becomes more dominant. For the 90c10r12T sample, difference in total shrinkage is the largest (Figure 3.6 (f)) and, onset temperatures for sintering are very high (as high as 865°C and 848°C for the radial and c-axis oriented specimens respectively) and shrinkage rates in both directions are 0.23 %/min and 0.16 %/min for the radial and c-axis oriented directions, respectively, which are the lowest values among all samples (Figure 3.7). These results indicate that constraining effect of template particles starts to dominate when their amount in the system exceeds the critical value. This sintering characteristic results in a reduced relative sintered density (Figure 3.8). Besides the constraining effect of misalignment of templates, the addition of such an amount of template into the suspension is not easy. This in turn affects rheological characteristics of the suspension and may cause non-uniform packing. While the bottom part of the 90c10r12T sample exhibits very low density top part of the sample was much denser (not shown). Reduced density in the bottom part might be a result of the sedimentation of templates as the dispersion of templates into the matrix becomes more and more difficult with the increase of template concentration. Due to sedimentation, the amount of template particles might become very high in the bottom part and these lead to a reduced density as observed in 90c10r12T. Sedimentation of templates also explains the higher orientation quality for this specimen. Since the template amount decreases in the top part, decrease in the r value with respect to the 95c5r12T (Figure 3.11 (inset)) can be attributed to reduction of template amount in the top part due to sedimentation and performing the EBSD analysis on the top surface of the sample.

Although not very dominant a morphological texture was also present in the samples when viewed in SEM from radial direction. This morphological texture can be quantified by measuring the grain sizes along c-axis direction and radial direction (Lince software, TU Darmstadt, Germany).

Figure 3.14 shows that the largest difference in grain sizes along radial and c-axis oriented directions is present in the 100c12T sample, which is highly textured. Grain sizes of specimens tend to decrease as template content increases in the system. The random sample, 100c0T, has an almost isometric grain shape according to the

Figure 3.14.

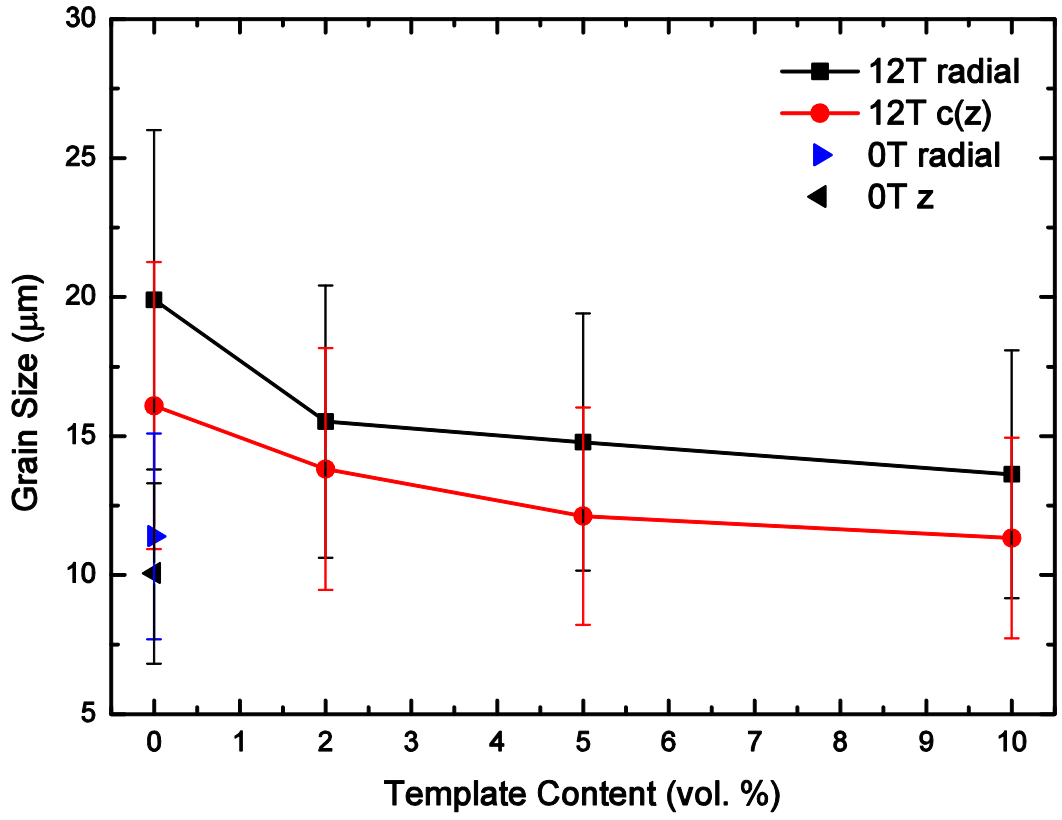

Figure 3.14 Change of grain size as template content and magnetic field condition during processing changes

To test the effect of matrix orientation on texture development, 0 and 2 [% template systems were tape cast. When densified, the shrinkage and orientation characteristics were investigated. The 2 vol % system showed less densification and slightly more anisotropic shrinkage (Figure 3.15). The 2 vol % template containing, tape cast system shrank less in the casting direction which contradicts orientation dependence typically seen for the slip casting under magnetic field technique. This is attributed to worse orientation (or random characteristic) that is achieved by matrix in the tape cast system. Even though templates were very well aligned in the green compact, neither sample were able to show good orientation (texture) after sintering which is probably a consequence of negligible matrix alignment in the green compacts. Lotgering factors [49] of two systems were similar and a very small degree of texture is present (See Figure 3.16). These

results show that the matrix alignment is crucial to obtain texture development in undoped ZnO system via TGG-type processes.

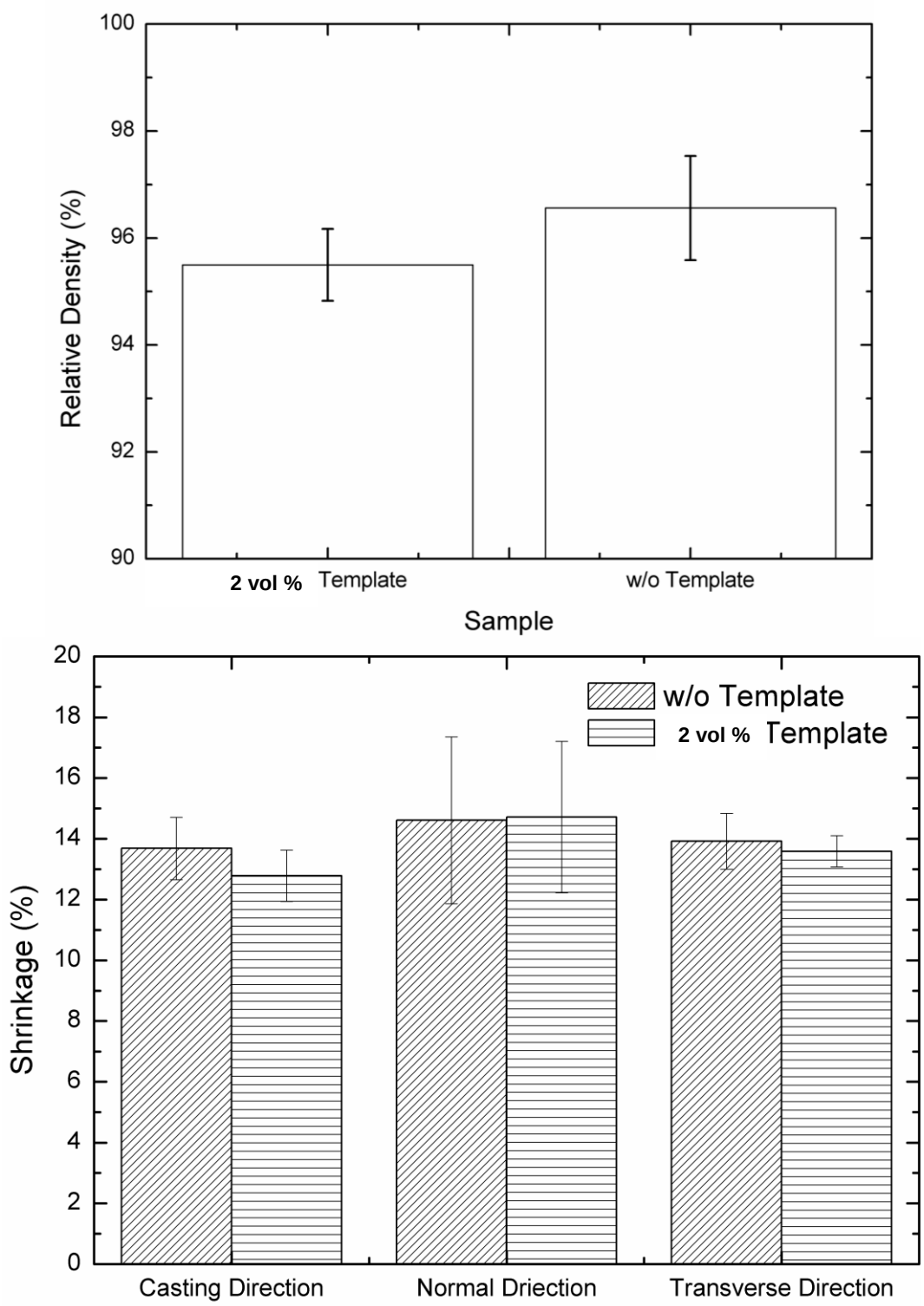

Figure 3.15 Relative sintered density (top) and sintering shrinkage data (bottom) comparing tape cast 2 vol % template system with the system which contains no templates.

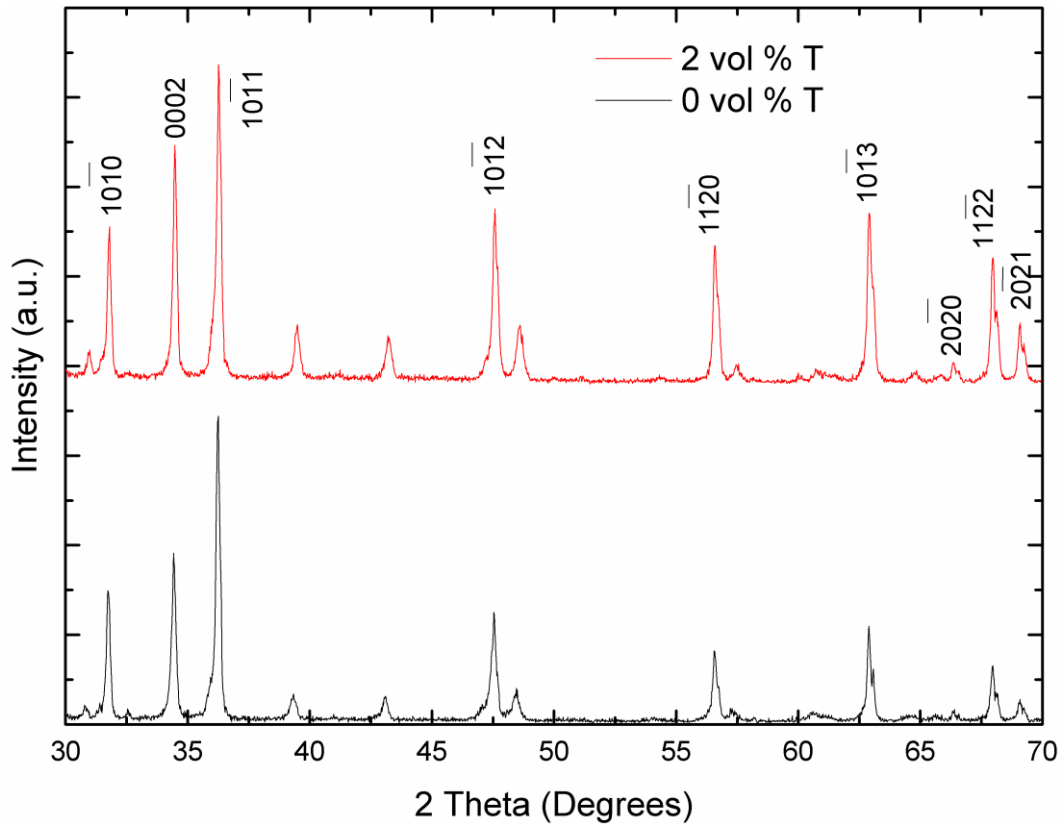

Figure 3.16 XRD patterns of the tape cast 0 and 2 vol % template containing systems after sintering. Non-named peaks belong to apparatus used for measurement.

In the light of above discussion, it can be concluded that the sintering can be enhanced by introducing small amount (below some critical value) of densifying template particles into the textured matrix system. By combining the results of this work with previous literature one can derive a hypothetical map for describing densification behavior in a system which is sintered without addition of theliquid phase. Oriented matrix and the low amount of oriented templates and densifying template behavior are desired parameters for a good densification (Figure 3.17). In Figure 3.17, there is a critical volume ratio of densifying and/or unstable template particles (i.e. V_c) over which, densification is inhibited whereas below this critical value densifying templates cause an enhancement of densification behavior by regulating the matrix powder. This volume ratio was found to be 2 vol % in this work. The densifying behavior of the inclusions is also

critical, since in a recent study by Zhu *et al.* [36], it has been shown that as low as 5 wt % rigid β-Si_3N_4 caused an anisotropic shrinkage of almost 3 times difference between the directions parallel and perpendicular to the whisker alignment direction. As discussed above, for a good densification and less anisotropic shrinkage, matrix orientation should be as high as the template orientation. The template content must be below the critical value and finally templates should be thermally unstable. Here, it is assumed that the template particles have the same orientation characteristics as matrix powder and there is no liquid phase since situation can be quite different if the matrix powder is randomly oriented and/or there exists a liquid grain boundary phase. There is a certain possibility that there might be a critical value for rigid template volume under which constrained sintering would be negligible, but such critical volume should be very small if any.

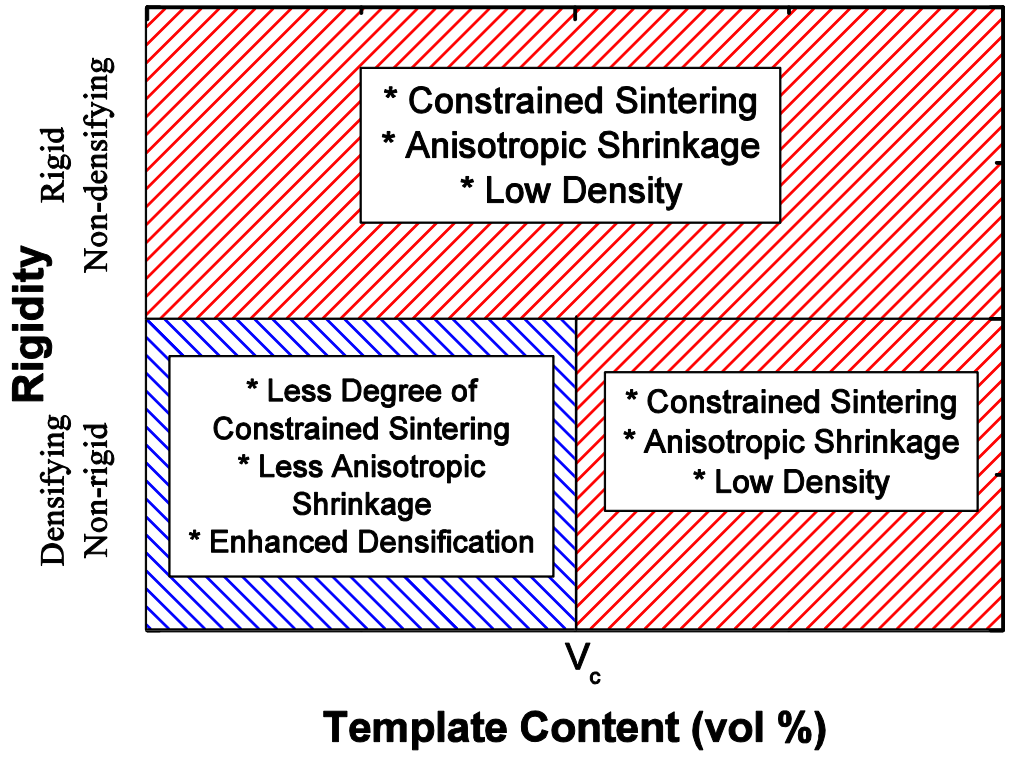

Figure 3.17 Control of constrained sintering, anisotropic shrinkage and density by template content and template rigidity.

One interesting outcome of the hybridization of TGG with magnetic alignment method is the fact that template particles in this process could have been merely equiaxed particles of larger size than matrix powder since

morphological anisotropy is not necessary as in conventional TGG process. This has obvious advantages such as the elimination of dependency on the anisometric templates. As a consequence of using bigger particles it might be possible to decrease the strength of magnetic field required, since aligning micron sized particles is much easier. This will have positive effects on the initial cost of magnetic alignment instrument. Yet another possibility is the engineering the process, by carefully selecting the template size distribution instead of using templates with narrow size distribution to reduce the effects of anisotropic shrinkage by regulating the particle size distribution for better initial packing which should result in enhanced sintering. However, these effects related to template size should be further investigated.

3.4 Conclusions

Hybridization of the TGG and magnetic alignment processes was successfully realized on model ZnO system. It has been shown that by introducing aligned non-rigid, densifying, template particles into a textured matrix of smaller size below a critical amount, densification behavior can be controlled. By doing so, effects of anisotropic shrinkage can be reduced if not eliminated completely. This kind of hybrid processing can be used to overcome the problems associated with the texture engineering by reducing costs and/or refining the raw material needs. Further studies are needed to clarify the effects of coarse densifying inclusions on sintering characteristics and mechanisms at work during their sintering and interaction with finer matrix particles.

4. TEXTURE – PROPERTY RELATIONS IN ZnO

ZnO is one of the most interesting materials, due to its multi-functionality. It exhibits several interesting properties and finds many applications from varistors [13] to sensors [50-52] and from transparent conducting oxide coatings [53] to surface acoustic wave devices [54-56]. In addition, ZnO, which has hexagonal wurtzite structure, exhibits highly anisotropic properties. Many studies have been carried out to enhance the properties of this material via production of oriented microstructures [26], [57-59]. Formation of microstructural texture or orientation can be regarded as the non-random distribution of angular positions of crystallites with respect to each other. The fact that the characterization studies which have been performed on the materials with textured microstructures started just about with the first x-ray diffraction studies shows the importance of the field (papers on preferred orientation can be dated back to 1920's and possibly before).

This special interest is especially due to potential of the crystallographic texture to transfer the crystallographic anisotropy (dependence of properties on crystallographic directions) to macro dimensions. Anisotropy in the properties arises as a result of the crystal structure. Some crystal structures such as cubic crystals are more symmetric, whereas triclinic crystal system has the lowest symmetry among all crystal systems. There are 32 point groups and 230 space groups, a single crystal can belong to. For example, ZnO has 6mm point group and $P6_3mc$ space group symmetry (Wurtzite type crystal structure). This point group is in fact the reason for which the ZnO has anisotropic properties. The symmetry elements of a single crystal should be present in the symmetry elements of its properties as stated by von Neumann's Principle. The Neumann's principle was extended to the polycrystalline materials (and anything in general) by Curie's Principles;

- Symmetry elements of the effects must be present in the causes;
- Effects can be more symmetrical than the causes themselves;

So it is possible to utilize a process with certain symmetry elements to create a polycrystalline material with at least same symmetry. For example, a material which is slip cast under magnetic field should have (at least) the symmetry of the magnetic field. Suspension being slip cast adopts the symmetry

of the applied field and final compact has the symmetry imposed by the magnetic field which in turn manifests itself as texture in the material. From Curie's principles it can be expected that this texture has the symmetry elements of the magnetic field utilized during the slip casting process. If the same principles are applied to the properties of the textured material, then one expects to find same symmetry elements of the process and texture in the properties too. Therefore, it is possible to control the properties by controlling the texture of the material. This symmetry can be controlled by designing the texture of the material via processing conditions (as discussed previously in chapters 1 and 2). For example, by utilizing a magnetic field, a texture can be imposed on a material. By changing the application type of magnetic field (static or rotating) it is possible to obtain different textures with different anisotropy degrees. As expected, texture results in symmetry in the material. Furthermore, due to principles of Curie and Neumann, this texture must manifest itself in the symmetry of the properties. Symmetries that can be attained by the polycrystalline materials are called Curie Groups (they are also named Continuous Groups or Limiting Groups). In Figure 4.1, geometric representations of the seven Curie Groups can be seen. Please see reference [60] for a discussion on the Curie symmetry groups and the materials that possess such symmetries.

If it is possible to control the symmetry of a material through control of texture, then properties can be tailored accordingly. The control of properties without touching to the chemical composition is very desirable. By use of magnetic field alignment it is possible to produce single phase textured materials. In order to exploit the texturing for tailoring the properties it is necessary to develop a fundamental understanding how properties are related to texture characteristics. Therefore, the purpose of this study was to investigate the property texture relationship in polycrystalline ZnO. Up to date, the research on the textured ZnO is generally focused on the thin films and on specific properties with a limited view. On the other hand, in this study relationship between hardness, thermal conductivity and electrical conductivity and texture were investigated. Also, the relationships are discussed in the light of the microstructural features. Previous studies also lack the comparison between the properties of highly, moderately textured and random samples.

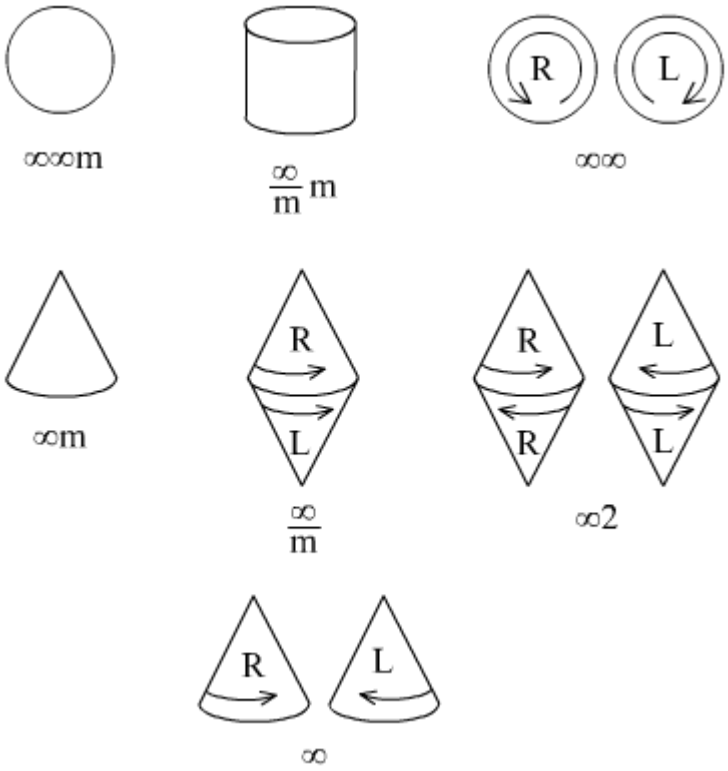

Figure 4.1 Seven Curie groups that can be found in polycrystalline materials.

4.1. Experimental Procedure

Pure ZnO compositions were slip cast with and without the application of a 12 T rotating or static magnetic field. Teflon lined glass moulds on porous alumina was used for slip casting purpose. After compaction the green part is removed carefully from the mould. The green compacts were then cold isostatically pressed at 392 MPa for 10 minutes. The samples were held at 400°C for 2 hours and than sintered at 1200°C for 4 hours. Heating rates were 5°C/min for all heating segments. Cooling rate was 10°C/min. Densities were determined by Archimedes method via boiling the samples in ultrapure water. Samples were first lapped to make sure their top and bottom surfaces are parallel to each other. The lapping was carried out by hand using a metallic ring and a cylinder to ensure even distribution of force. Grinding papers with successively finer mesh were used in lapping. For analyses, specimens were cut out of the 1, 2 and top surfaces of the sample A, B and C by a precision diamond wire saw cutter (Well Diamond Wire Saws, Switzerland). Sample and specimen designations are described in Figure 4.2. Specific procedures regarding specific test specimens are given below.

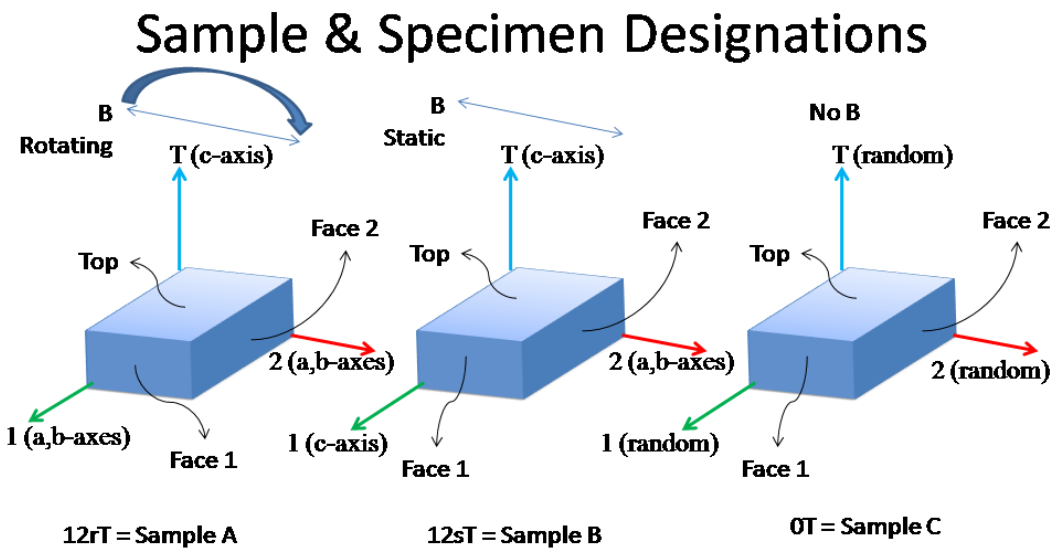

Surface	A – 12rT		B – 12sT		C – 0T
	Orientation	Strength	Orientation	Strength	Orientation
Top	c-axis	Very Strong	c-axis	Weak	Random
Face 1	a,b-axes	Strong	c-axis	Weak	Random
Face 2	a,b-axes	Strong	a,b-axes	Strong	Random

Figure 4.2 Sample and specimen designations as they are utilized throughout this chapter (top), as well as expected orientation and texture strengths of respective surfaces.

4.1.1. Microstructural and Texture Characterizations

Specimens were polished down to colloidal silica and chemically etched with a dilute nitric acid solution in deionized water until the grain boundaries become visible in the optical microscope. Microstructures of the samples were observed by an optical microscope with a digital camera installed, at 20x magnification. Image analyses were carried out on these microsctructures to obtain the grain size distributions as well as grain aspect ratio distributions. For image analyses the grain boundaries were traced by hand first. Then computer software was utilized for the rest of the analyses (FIJI, Image J bundle). Textures of the samples were evaluated by means of x-ray diffraction and electron backscatter diffraction (EBSD) on specimens without chemical etching. Lotgering factors were calculated from XRD patterns and pole figures were obtained via EBSD analyses. Lotgering factors were calculated using the formula below [49];

$$F = \frac{\sum(I_{(00l)}/I_{(hkl)}) - \sum(I_{0(00l)}/I_{0(hkl)})}{1 - \sum(I_{0(00l)}/I_{0(hkl)})} \quad (4)$$

4.1.2. Hardness

Three specimens with their wide surfaces normal to 1, 2 and T axes were cut out from the samples A, B and C. These specimens were mounted with a hot mounting press (Struers GmBH, Germany) at 180°C and 6 MPa for 10 min. Mounted specimens were then polished down to colloidal silica. Before hardness tests, the specimens were ultrasonicated and washed thoroughly with water in order to make sure no silica particles remain on the surface. Hardness tests were carried out by microhardness equipment at 0.5 N for 10 seconds. At least three measurements were carried out on each specimen and three specimens were tested for each surface of A, B and C. Results were averaged and standard deviations were calculated in order to obtain hardness values as a function of orientation and texture degree.

4.1.3. Electrical conductivity

At least three specimens as rectangular prisms were cut out with their long axis parallel to the 1, 2, and T directions of the samples A, B, and C. Surfaces normal to the measurement directions were lapped with a 1200 mesh silica paper. After lapping surfaces were cleaned by ultrasonication. Measurement surfaces were then coated with Au-Pd alloy via sputtering as a contact for measurement probes. After coating specimens were annealed at 200°C for 2 hours. Two terminal measurement method were utilized in determining the electrical conductivity. Voltage was sweeped from -2 V to 2 V while measuring the current. Three measurements were carried out on each specimen. These measurements were averaged and standard deviations were calculated.

4.1.4. Thermal Diffusivity

Specimens with face normals parallel to 1, 2, and T directions were cut and lapped and coated with carbon in advance of thermal diffusivity measurements. Thermal diffusivities of the specimens were measured by laser flash method. Cape – Lehmann model was applied for measurement of thermal diffusivity of the specimens. Measurements were carried out from room temperature to 1000°C under nitrogen atmosphere. Three measurements were taken at each temperature and the results were averaged.

4.2. Results and Discussion

4.2.1. Microstructure and texture

Relative sintered densities of the samples were higher than 97 % in all cases (Figure 4.3). Random samples showed the highest density as a principle. This is an expected result since texture results in an anisotropic surface (grain boundary) energy distribution in the green compact. As discussed in part 3, higher crystallographic mismatch in the grain boundaries results in better densification. Therefore, random sample (sample C) with the highest lattice mismatch in the grain boundaries, has the highest relative sintered density. Sample B which is slip cast in the presence of a static magnetic field is expected to have moderate texture and it has a wider density range than other two sample types. The second highest and lowest densities were obtained in sample type B. On the other hand sample A has a more narrow density range when compared to sample B. Since sample A is compacted with an applied rotating magnetic field it is expected to have a strong texture. From these results it can be deduced that with utilization of a rotating magnetic field the sample density can be better controlled. However with an increase in texture degree, a reduction in the density can be expected. This can be explained by the anisotropic sintering shrinkage behavior of the textured specimens as discussed in part three. This behavior results in a low density.

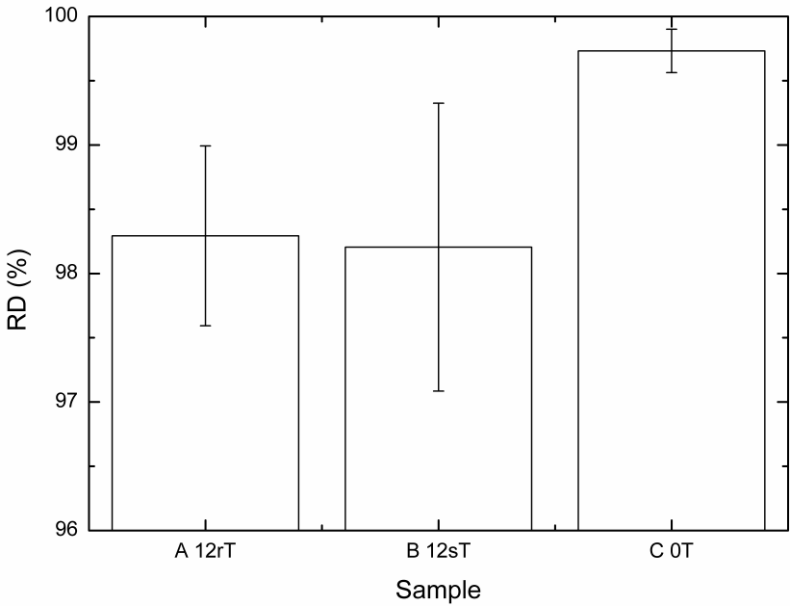

Figure 4.3 Relative densities of the samples used in measurement of the properties

Optical micrographs of the polished and chemically etched 1, 2 and T faces of sample A can be seen in Figure 4.4. Pores are located on the triple junctions and no intragranular pores were observed. There are some occasional pullouts due to the polishing. From the optical images it can be stated that there is no readily observable morphological texture. The grain shapes are almost isotropic and all three faces show similar grain structure characteristics. To investigate the grain microstructure in more detail image analysis was needed. Aspect ratio and grain size distributions were obtained from these analyses (Figure 4.5). Image analyses showed that the grain aspect ratio distributions were similar for 1, 2 and T faces of sample A. This is also in agreement with the lack of observable morphological texture. The aspect ratio distributions show that, large number of grains concentrate around an aspect ratio of 1.5, for all three specimens. It should be noted that the grains or particles with aspect ratios smaller than 1.5 are not considered to be anisometric [12]. Grain size distributions are again similar for three specimens of this sample. Grain size distributions peaked at around 15-20 μm. The lack of morphological texture can be attributed to the extended duration of sintering at 1200°C for 4 hours. When compared with the results from part 3, it can be concluded that the morphological texture worsens as the sintering duration extends (sintering duration was 2 hours in part 3). This is attributed to desintering behavior of the ZnO [61]. This situation was also observed in the specimens, which were sintered at 1300°C (second chapter, Figure 2.9). There was a decrease in density when samples were sintered at 1300°C. It seems that this also happens when the sintering duration increases at 1200°C. The general trend of decrease in density was observed when the sintering time is doubled (2 to 4 hours) (see Figure 2.9 and Figure 4.3). So it seems that a decrease in density is accompanied by a decrease in morphological texture in the specimens. This phenomenon is attributed by ref. [61] to pore growth in the final stage of sintering accompanied by reduction in the number of pores.

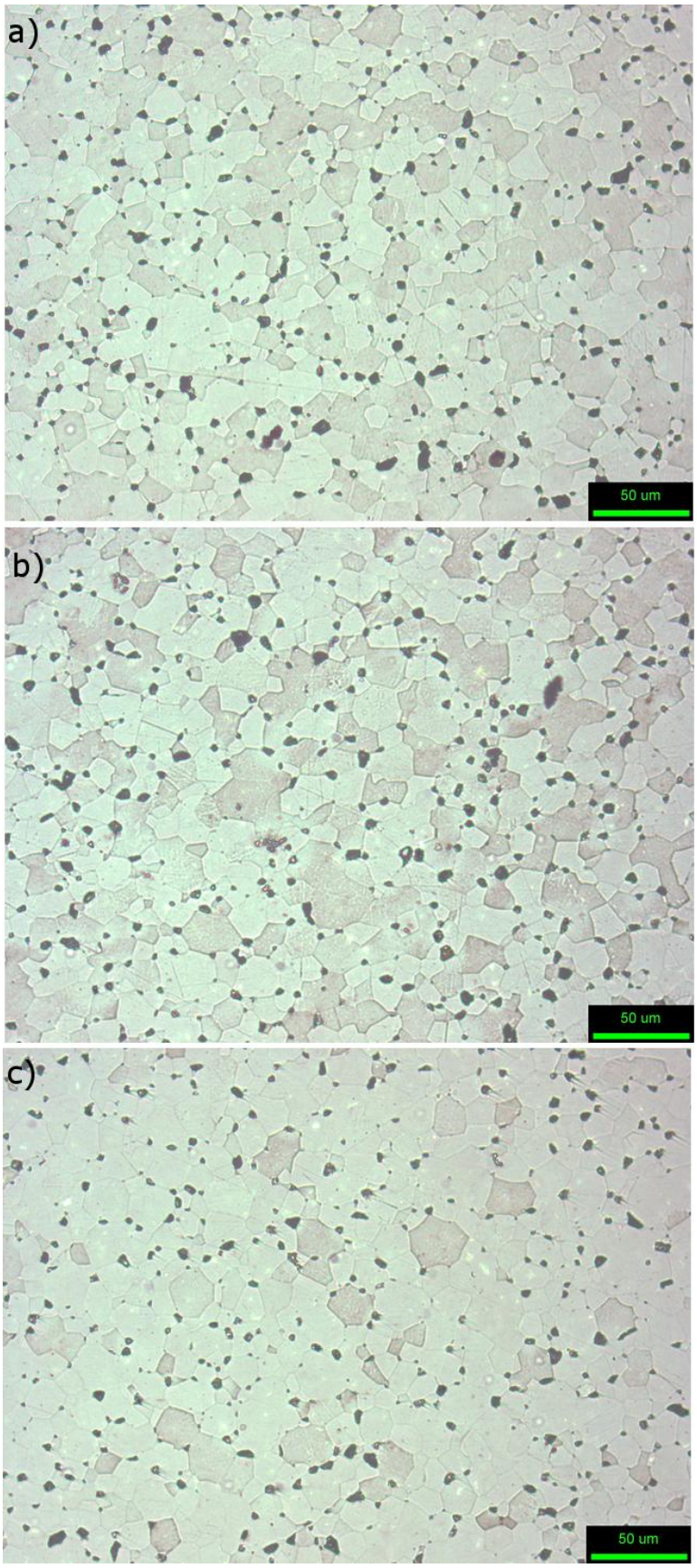

Figure 4.4 Optical micrographs of the a) 1, b) 2and c) T surfaces of the sample A.

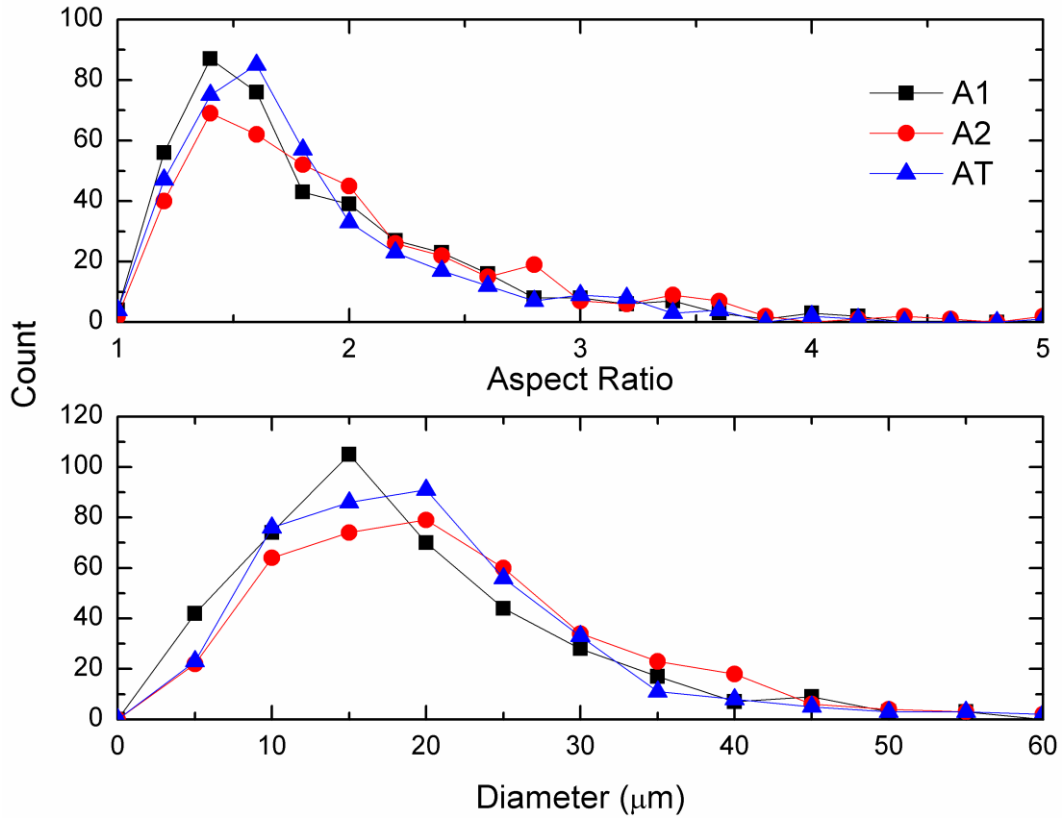

Figure 4.5 Top; grain aspect ration distribution, bottom; grain diameter distribution of the specimens A1, A2, and AT.

If we examine the x-ray diffraction patterns of the different surfaces of sample A we can see a strong preferred orientation in c-axis as seen in Figure 4.6. The XRD pattern of surface T shows a strong reflection at around 32 degrees which belong to (0002) reflection of ZnO. The axis T which is the normal of surface T is perpendicular to the direction of the rotating magnetic field (see Figure 4.2). When ZnO crystallites tried continuously to orient their c-axis perpendicular to the magnetic field also they align their c-axes parallel to the axis T of the sample A (see parts 1, 2 and 3). X-ray diffraction patterns taken from the radial surfaces, which are named 1 and 2, showed almost identical reflections. (0002) reflection is almost completely lost and the reflections coming from prismatic $(10\bar{1}0)$ and pyramidal $(10\bar{1}1)$ surfaces start to take over the preferred orientation. This is well expected since the rotating magnetic field locks the crystallites c-axis parallel to sample's T axis while rotation around these axes can not be controlled. Therefore this kind of texture is named fiber texture and has a cylindirical symmetry (Figure 4.1)

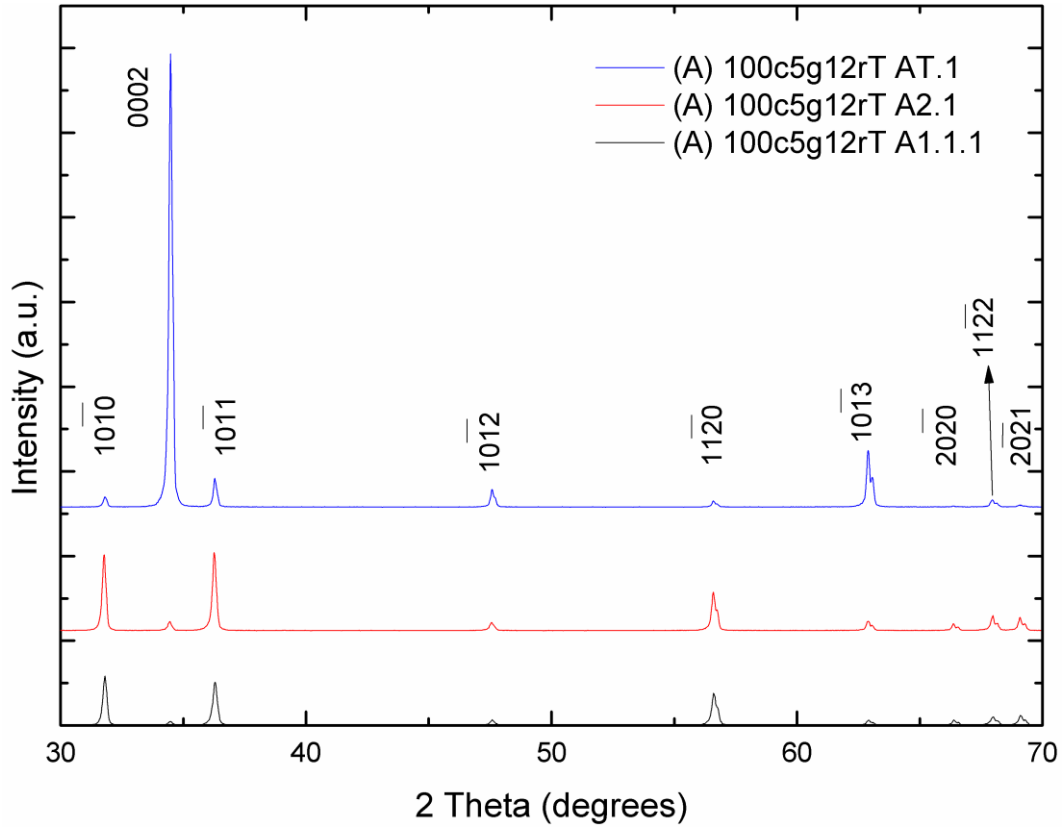

Figure 4.6 Representative XRD patterns of sample A from top surface and radial surfaces 1 and 2.

Although x-ray diffraction is a practical way of inspecting texture, it says nothing about the quality of the texture and the orientation distribution. Therefore, a more detailed analysis of the texture was needed. This need can be well met by means of electron backscatter diffraction method. In this method orientation characteristics of individual grains can be determined. And when this grain orientations are plotted in a pole figure it can be clearly seen that how well the orientations are distributed over the entire range. Figure 4.7 is a (0001) pole figure of specimen T of sample A. Here, the pole figure center corresponds to the (0001) plane (or [0001] direction). It can be sen that most of the orientations are centered on this center. A small deviation from the center is attributed to the misalignment of the EBSD detector. It should also be noted, a small deviation in the parallelism of the top and bottom surface of the specimen can be induced during the manual lapping process.

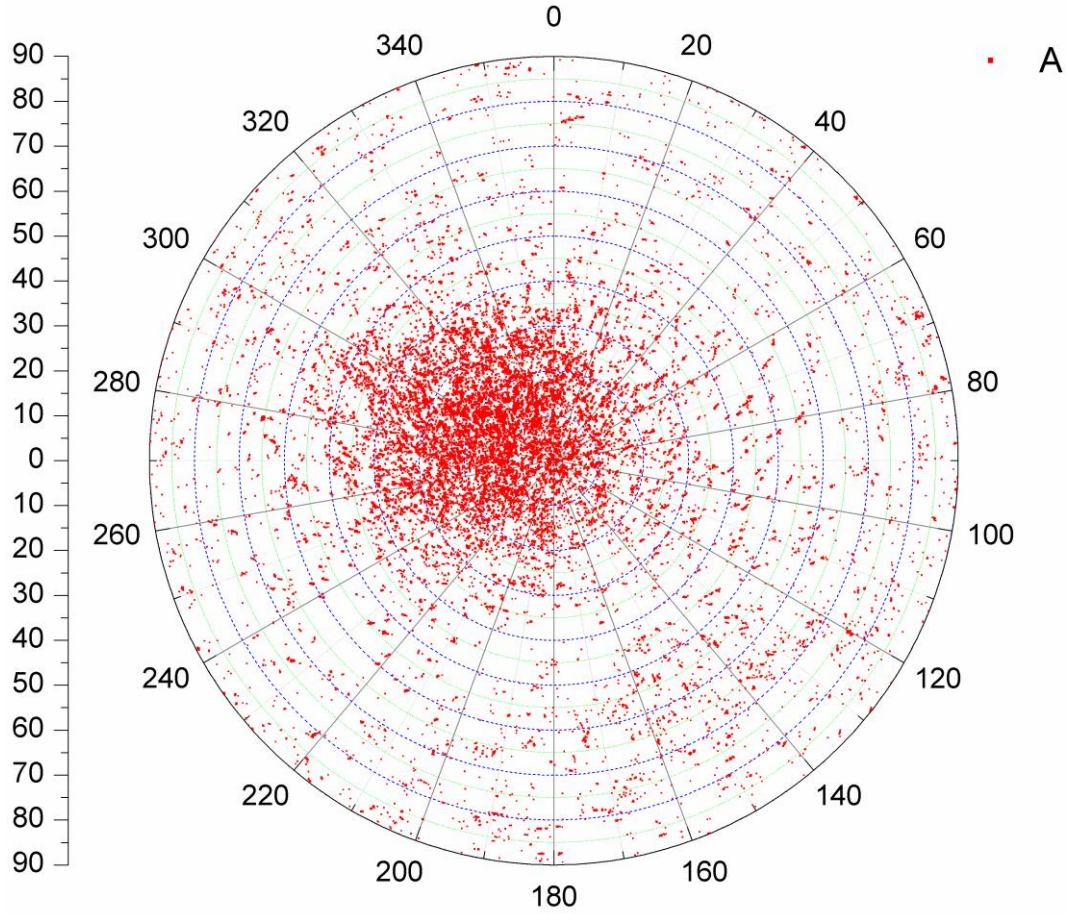

Figure 4.7 (0001) pole figure of sample A obtained via EBSD analysis from top surface.

The points which are located away from the center of the pole figure are the grains whose orientations deviate largely from the c-axis. It is useful to quantify the amount of this deviation from the ideal orientation, in order to form an opinion about the quality of the texture. For this purpose an orientation distribution function must be employed. In this study March-Dollase equation was utilized to evaluate the orientation quality of the texture [43] (See equation (3)). Figure 4.8 shows the (0001) pole figure reduced to a two dimensional plot. The pole profile is fit with equation (3) and orientation quality r was found to be 0.645. This value is almost two times worse than the sample which is sintered for two hours (See Part 3). So decrease in texture also represents itself in the decrease in texture quality. An explanation for the cause of reduction in texture degree after prolonged sintering duration can be the reduction in energy; as discussed previously surface energy distribution in a textured ceramic is anisotropic and this

resembles a non-equilibrium state for the material. When sufficient energy is given the system should try to reach a more stable state by decreasing this anisotropy via diffusion. These circumstantial evidences are not enough for proving the above mentioned hypothesis so more detailed studies will be needed, but the point is prolonged sintering times is not good for texture.

The texture characteristic in the sample A is a fiber texture with c-axis orientation axis being parallel to the sample T axis. This symmetry belongs to the cylindrical Curie group. Properties of this material is expected to have a similar values in the radial (along 1 - 2 axes) direction and different than the c-axis oriented direction (sample T axis). This will be discussed in detail in the next section.

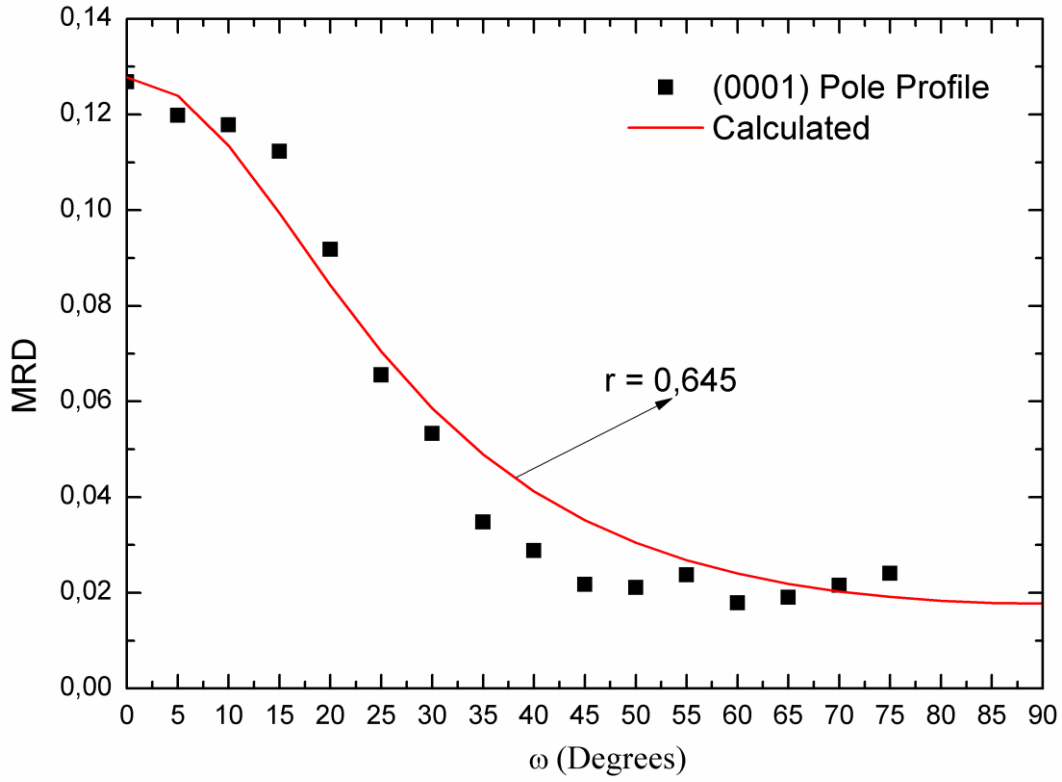

Figure 4.8 **(**0001) pole figure profile of specimen AT and corresponding March - Dollase fit

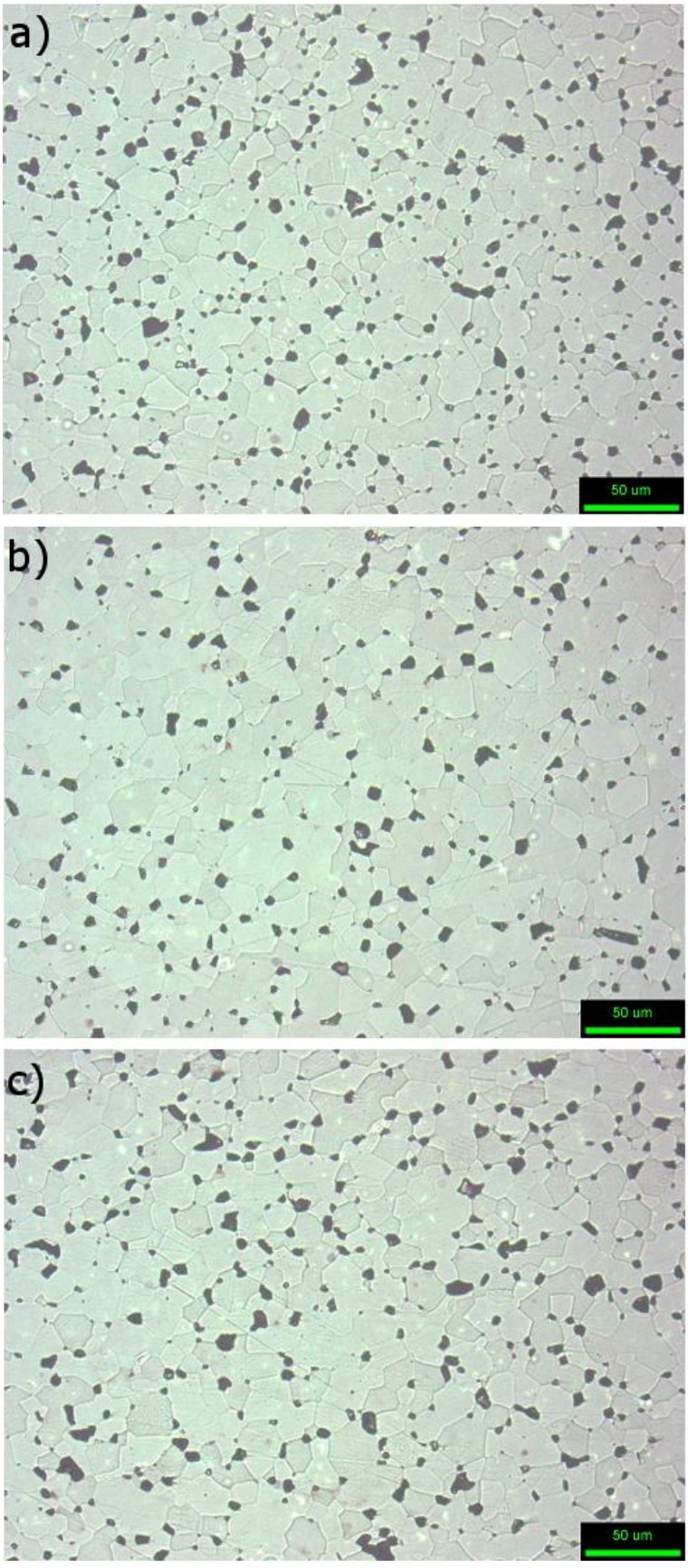

Figure 4.9 Optical micrographs of the a) 1, b) 2, and c) T surfaces of the sample B.

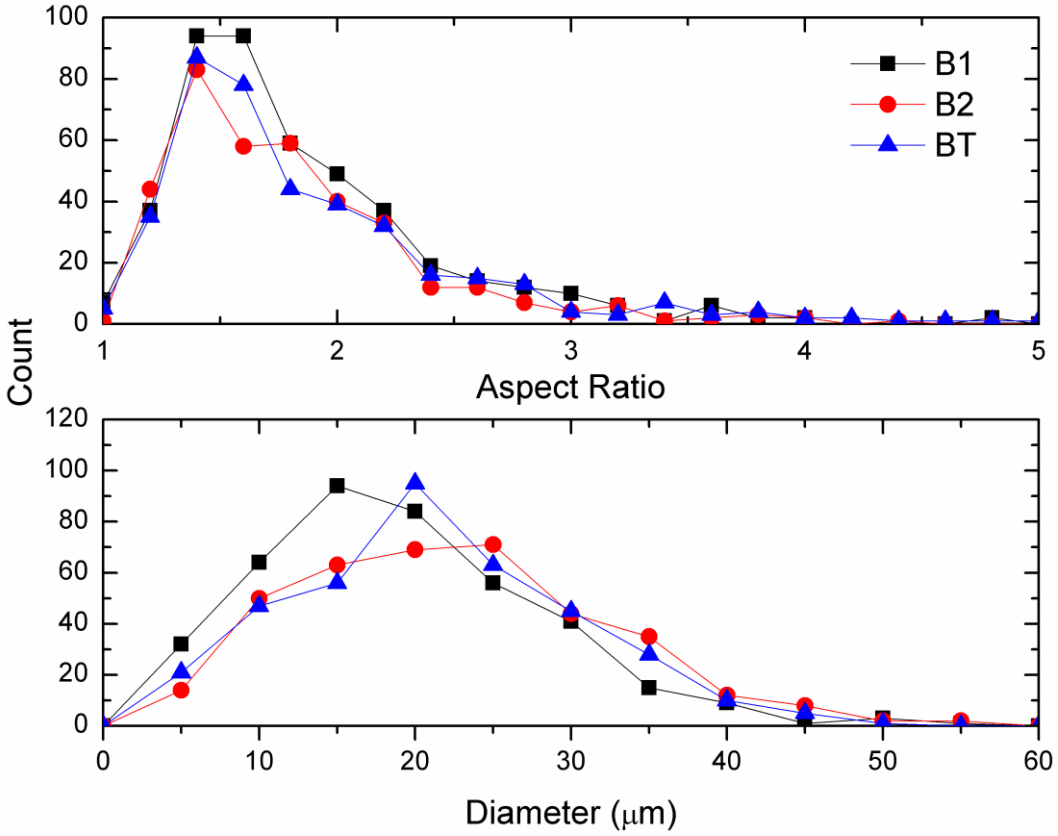

Figure 4.10 Top; distribution of grain aspect ratios, bottom; grain diameter distribution of specimens B1, B2, and BT.

Optical micrographs (Figure 4.9) and microstructural image analyses results (Figure 4.10) of the different surfaces of sample B, showed no evident morphological texture and again microstructures of the three faces were very similar. Only noted feature in the microstructure is the resemblance of the grain size distributions of the B1 and BT faces while the grain size distribution of B2 (which has different texture) has a broader characteristic. But this difference is very small to be called a sound morphological texture.

The microstructure is not very different from the microstructure of sample A in the sense that pores can be found again in the triple junctions. Again the pore structure of the faces with similar texture characteristics (1 and T) were similar while the face 2 has a slightly different pore structure (for example less number of pores). This is an example of the affection of microstructural features from the crystallographic texture.

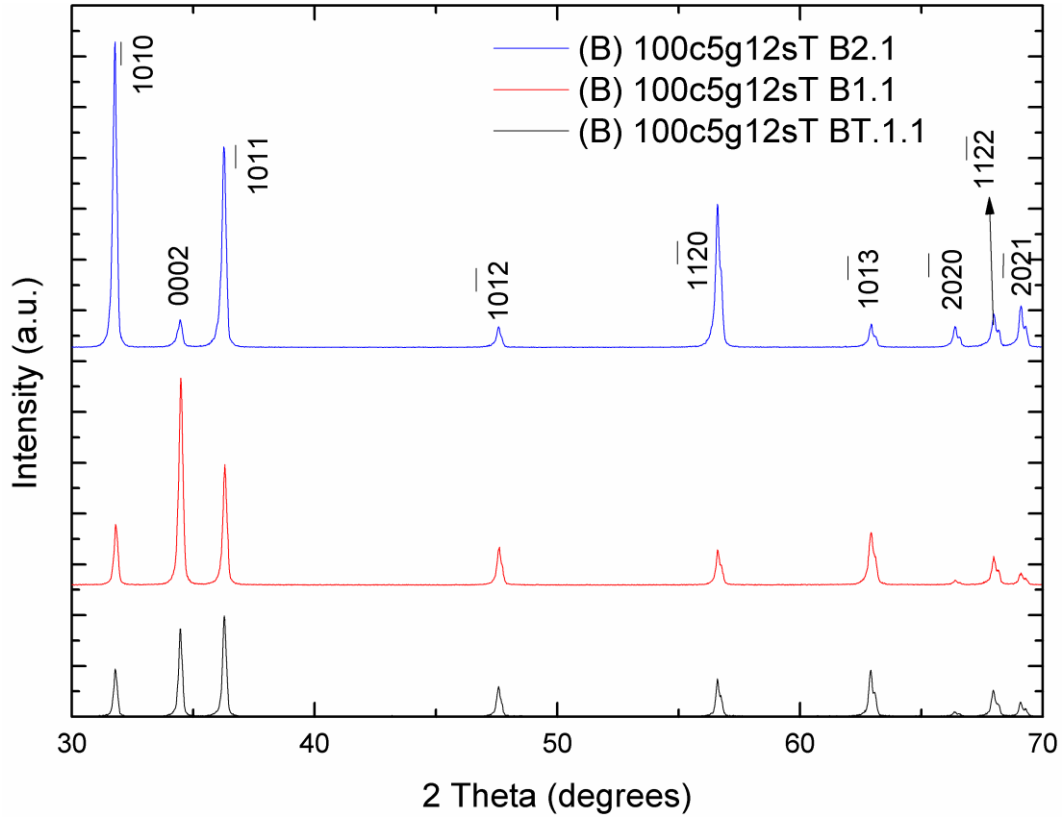

Figure 4.11 XRD patterns belonging to top and radial surfaces 1 and 2 of sample B.

When the XRD patterns of the B1, B2 and BT faces were compared (Figure 4.11), it is seen that the B2 surface which is orthogonal to the applied magnetic field shows reduced (002) reflection. Let us remember that the c-axis of ZnO crystals align perpendicular to the applied magnetic field. This means that they are locked, with their c-axis parallel to the plane which is orthogonal to the magnetic field. They are free to rotate within this plane. This configuration manifests itself as a increase in intensity of (002) peak relative to other reflections as it is the case for B1 and BT faces. The (002) peak intensity in the pattern of B1 is higher than the BT. The reason for that is the suction force acting on the anisometric particles and applying a torque on them during the compaction (See Part 3). During compaction of cast part, fluid flow forces anisometric particles (which are mostly rod-like) to align their c-axis perpendicular to gravitational pull. This disturbs c-axis texture in the BT face and forces particles to align more in the direction which is orthogonal to both the magnetic field and gravitational pull, B1. Therefore the (002) reflection intensity in this specimen is relatively higher when compared to that of the BT face.

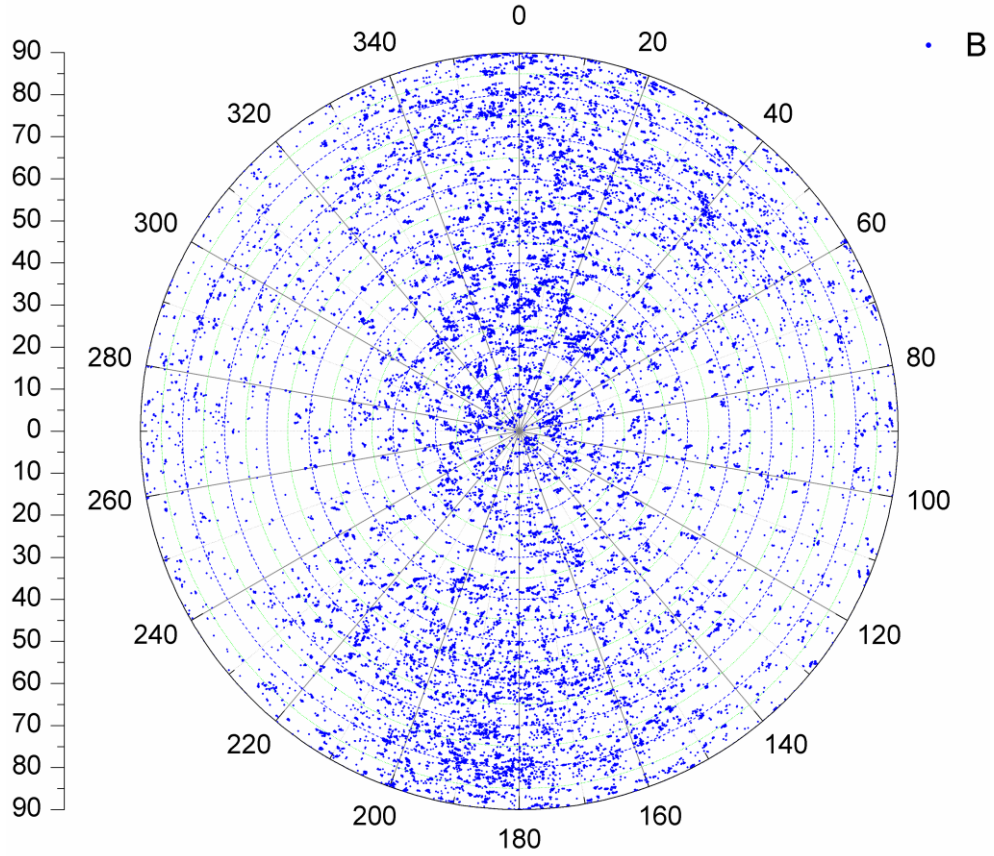

Figure 4.12 EBSD pole figure as taken from the top surface of sample B, centered on [0001] direction.

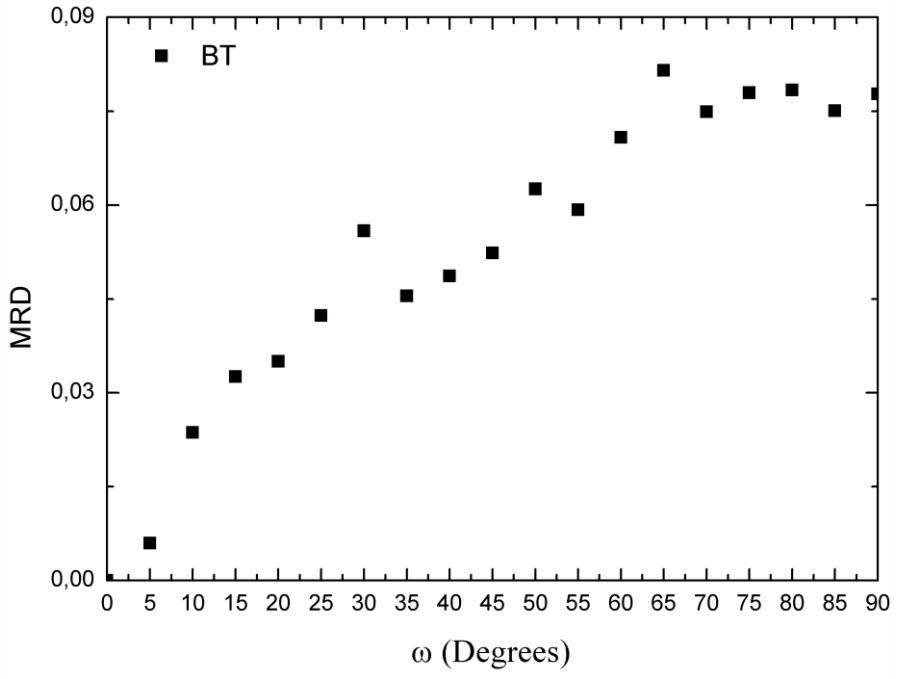

Figure 4.13 (0001) Pole profile of sample BT. MRD increases as the polar angle increases.

When the sample B is analyzed with electron backscatter diffraction from the top surface it was seen that the c-axes of the crystallites were distributed in the plane perpendicular to the applied magnetic field, as expected (Figure 4.12). The distribution is quite large and therefore the texture is weak when compared to that of the sample A which is slip cast in the presence of a rotating magnetic field. It is also seen from the pole figure that there is a collection of the orientation population in the higher polar angles of the pole figure (Figure 4.13), this again, supports that the rotation of anisometric particles in the plane perpendicular to magnetic field occurs and is the reason for better texture in the B1 direction. The kind of texture of this sample is not a fiber texture, therefore, it can not be defined by the March – Dollase equation.

From the above discussion it can be concluded that, the system again tries to adopt the symmetry of the process, but the forces due to gravity and fluid flow disrupts the alignment and causes the system to deviate slightly from ideal, expected symmetry.

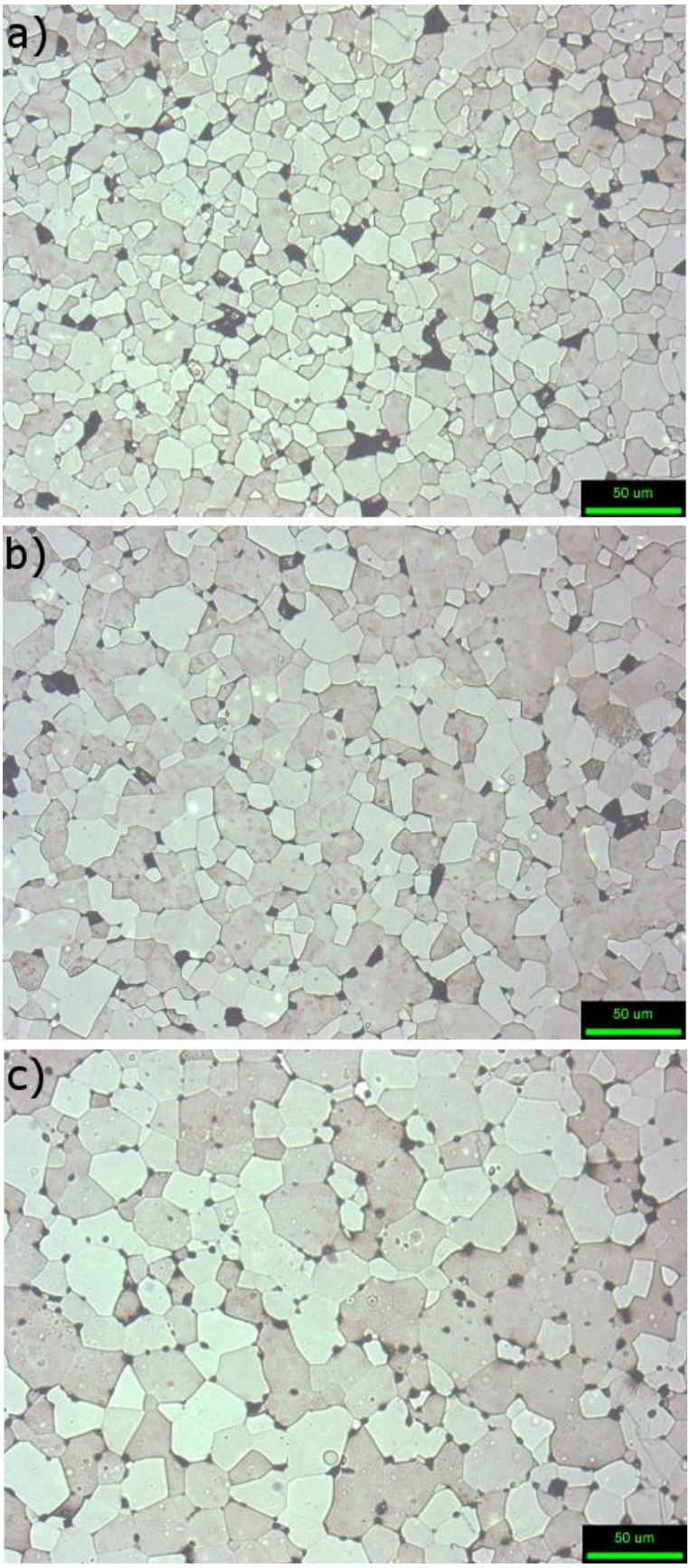

Figure 4.14 Optical micrographs of the a) 1, b) 2, and c) T surfaces of the sample C.

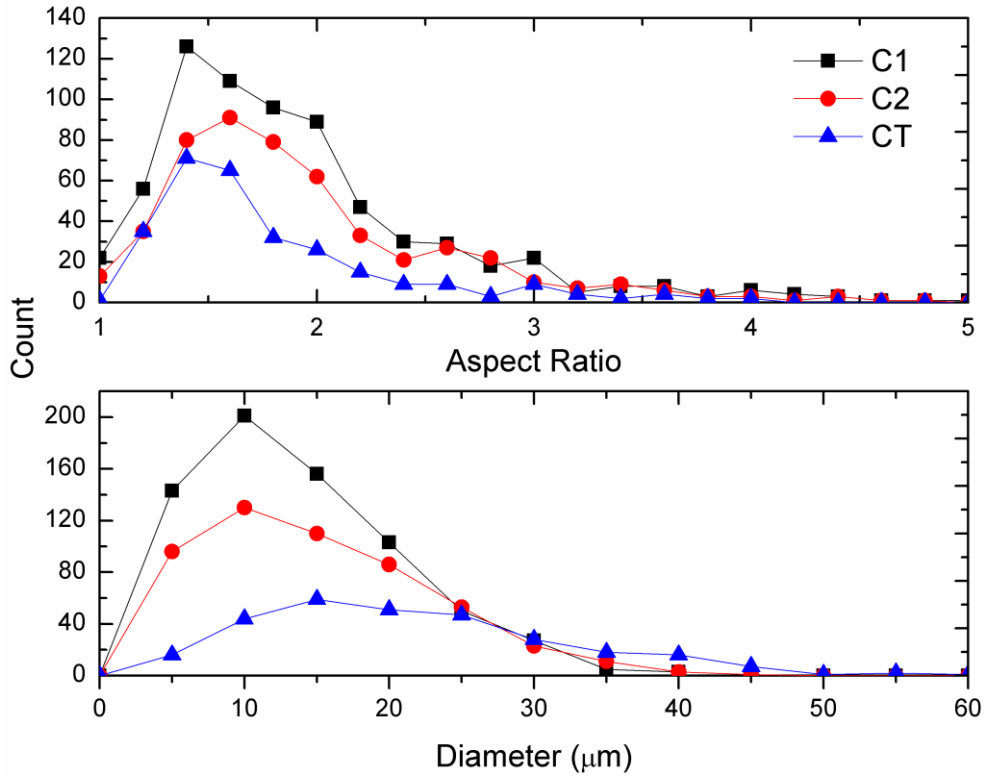

Figure 4.15 Top; distribution of the aspect ratio of grains, bottom; grain diameter distribution of sample C.

The microstructure of the sample C shows different properties when viewed from different directions (Figure 4.14). The grain morphology is not very different from other samples but the grain size distribution is slightly different especially in the CT face where the microstructure is composed of bigger sized grains (Figure 4.15). Moreover, the grain size distribution shifts to larger values for the CT face. In addition all of the faces show a general trend to have larger grain sizes when compared to the textured samples. This can be explained in the grounds of prolonged sintering duration. It seems that the random sample is more vulnerable to exaggerated grain growth than the textured specimen. This feature of random sample can be attributed to the larger grain boundary mismatches due to random distribution. These findings also suggest that the un-controlled compaction circumstance resulted in a non-controllable microstructure. Thus, the induction of texture in a material can be utilized also, for controlling the microstructural characteristics such as grain size and size distribution. The microstructure of the random sample is governed mainly by suction conventional process parameters.

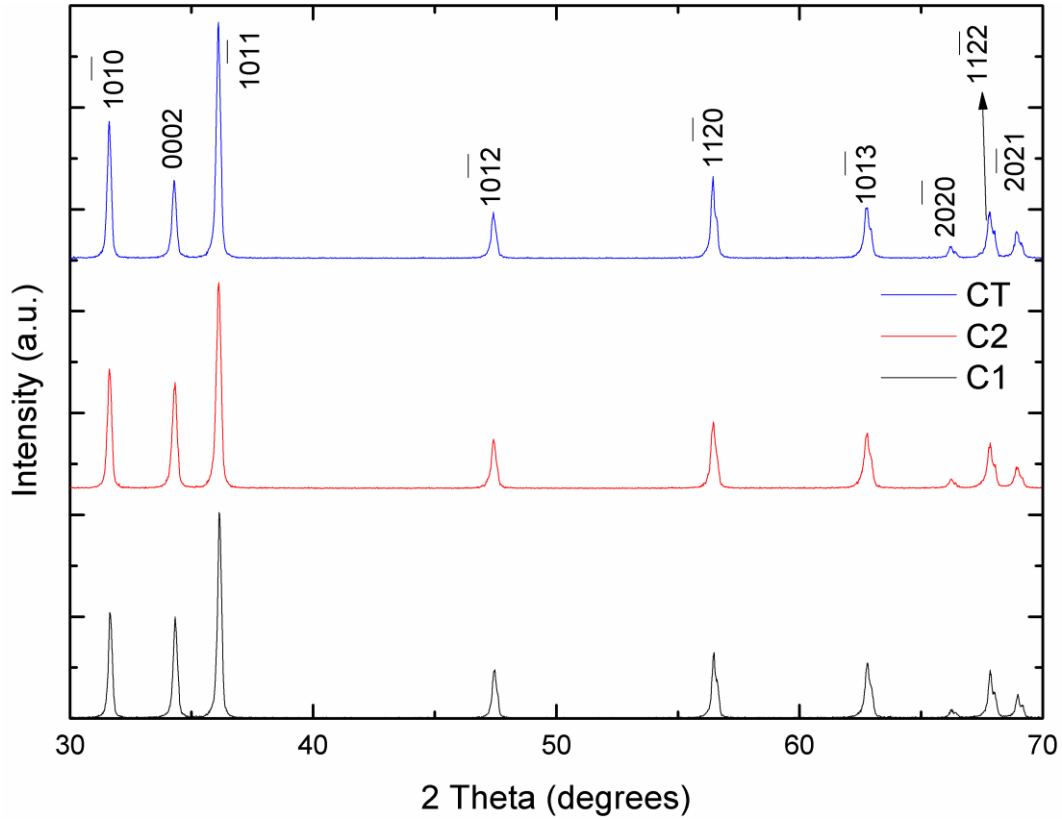

Figure 4.16 XRD patterns of top and radial surfaces 1 and 2 of sample C.

When XRD patterns of the faces of sample C is carefully observed it can be seen that the C1, and C2 surfaces have minute amount of preferred orientation. These faces' normals are perpendicular to gravity direction and therefore, it can be well expected, depending on the previous experience, that the c-axis of the rod-like particles align parallel to these face normals. Only the pattern of CT surface, which is the top surface resembles the XRD pattern of a completely random ZnO specimen. Thus we can conclude that the expectedly random sample C is not completely random. Since the orientation which is due to suction (fluid flow) or gravity (sedimentation) can not be controlled, the sample texture is out of controll when there is no external stimulus such as a mechanical gradient or magnetic field. This unctrolled orientation is exactly one of the main reasons for the different microstructures of differetn surfaces of sample C. On the other hand since this orientation is very weak in comparison to the sample A the overall high mismatch of the sample C resulted in a exagerated grain growth. To better elucide this texture characteristic we need to look into the EBSD pole figure of this sample in detail (Figure 4.17). The (0001) pole figure seems to be random but

when the orientation populations are averaged over the entire azimuthal range we see that there is a grouping of orientations in the higher polar angles. This can be better seen when the (0001) pole figure profile is plotted (Figure 4.17). In the pole profile there is an increase in MRD value in the higher polar angles. This is again an evidence that the particle orientation due to suction occurs.

Here a paranthesis should be open to discuss this results in the light of the studies described in chapter 3. When the pole profile of CT, is compared to that of the random sample (100c0T) in the chapter 3 of the thesis it can be seen that the results are contradicting. The orientation distribution of sample 100c0T flactuates around the value of 1 as the polar angle increases, which means it is mostly random whereas, sample CT's orientation distribution increases as polar angle increases. So, what is the reason for such contradicting results? The key point lies in the way specimens were prepared. Lets recall that the suction force was highest in the vicinity of mold colloid interface (Figure 3.12 a, [27], [44], [45]). In chapter 3, the EBSD data was collected on the top most surface of the sintered specimen. On the contrary, the specimen, CT, was taken out from the middle of the sintered specimen. If we take in to account that the total height of the samples were generally less than 1 cm. we have a proof that the orientation of the sample is not uniform throughout the whole sample. The prefferred orientation increases as the depth from the top surface increases. This evidence is also supports the hypothesized orientation of particles in the bottom part discussed in chapter three. In addition, the anisotropic sintering shrinkage in the sample 100c0T can now be associated with the non-uniform orientation distribution of due to suction force with more confidence.

As a summary, highly oriented material with a fiber texture, moderately textured and expectedly random materials were produced under rotating and static magnetic fields and without the application of a magnetic field, respectively. As a general trend texture materials have a lower sintered density in comparison to sample which is prepared without magnetic field. The sample without magnetic field has a small preferred orientation due to suction force. This suction force also plays role in the sample B. Also, effect of suction reflects in sample A as misoriented grains. The extended sintering duration resulted in excessive grain growth, expecially in the sample C.

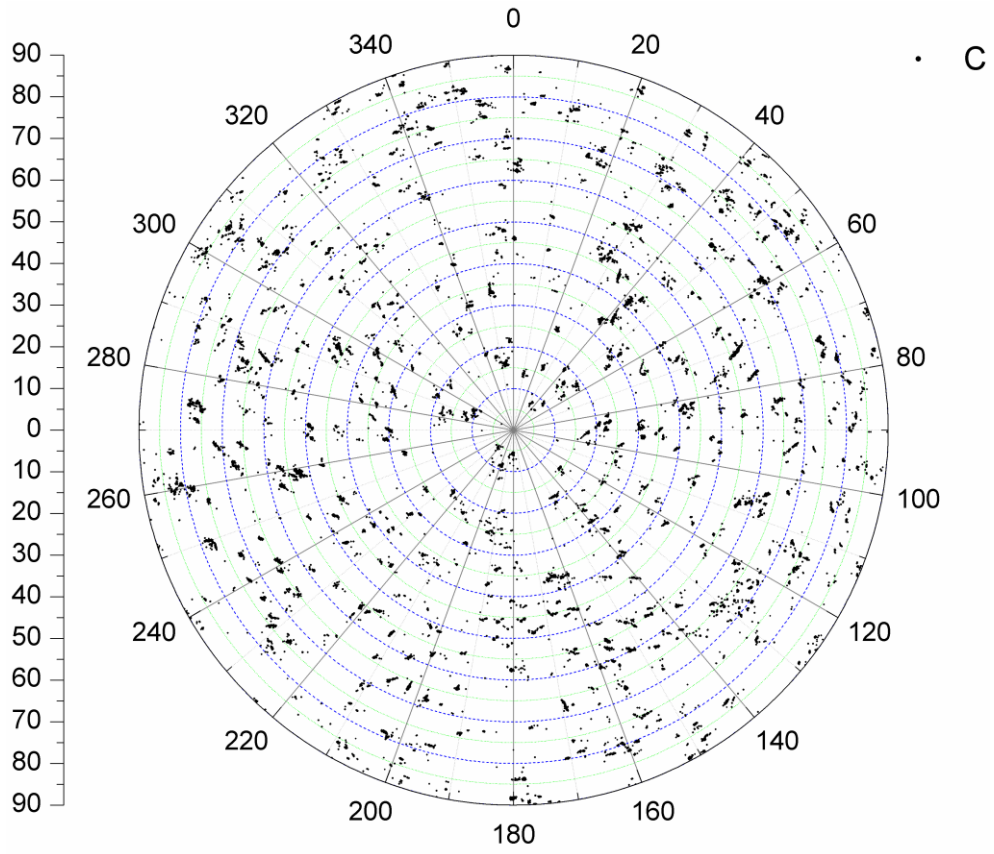

Figure 4.17 (0001) pole figure of C obtained from surface T via EBSD.

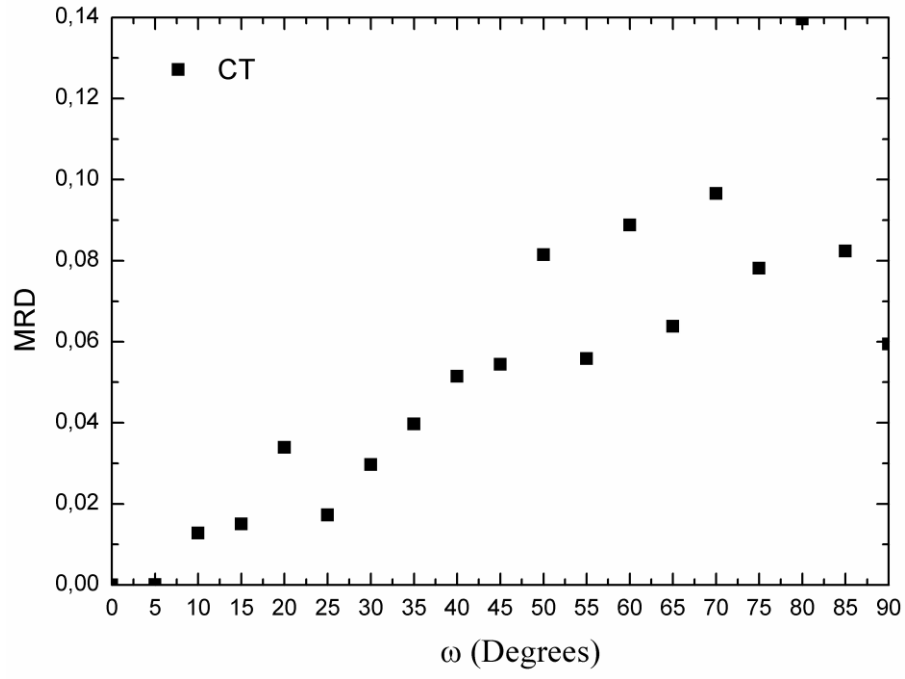

Figure 4.18 (0001) Pole profile of the sample CT. An increase in orientation in higher polar angles can be seen.

4.2.2. Hardnes

Demiantes *et al.* showed that the hardness' of the crystalline surfaces of ZnO single crystals are different from each other thus, anisotropic [62]. They also found out that the hardest surface of all is the (0001) plane at the studied temperature range. At room temperature the hardness of (0001) plane is around 4 GPa and the primary prismatic and pyramidal planes have the same value of 2 GPa (See [62] for a complete discussion).

Our findings showed that the hardest of all surfaces is the highly c-axis textured AT surface. This is in agreement with the literature saying that the hardest plane is the (0001) plane of ZnO but the Vickers hardness of the AT surface was around 200 kgf/mm^2 which translates roughly to1.96 GPa. This is almost half the value of the single crystal. What was expected is that the polycrystalline sample should have a higher hardness. The reason for not being so can be traced back into the microstructural features of the textured sample. Obviously microstructure plays a critical role in the hardness of the ceramic materials. In the case of sample discussed here two microstructural features that are different from the single crystals are; i) porosity, and ii) grains.

Hardness of ceramic materials increases as the sintering temperature increases [63]. This is due to the reduction of porosity at increased temperatures. Since the hardness is directly related with the bonding type and structure, and bond strength in particular, the porous materials are more vulnerable to the local plastic deformation. Therefore the porosity in the samples is one of the reasons for reduced hardness when compared to single crystals. The grain size also plays a role in the hardness. In the literature it is known that smaller grain sizes leads to increased hardness values. So when the temperature and/or sintering duration are over increased this cause extensive grain growth which reduces hardness [64].

A previous study found that the values of polycrystalline CsBr and CsI are slightly lower than that of the single crystals of the same materials [65]. No comment on the reasons was made in that work. The melt casting process used in that study might have caused exaggerated grain growth and also texture. No comments of these issues were made by the authors. These can be the reason for obtaining slightly lower hardness values for polycrystalline CsBr and CsI.

Another study on single crystal and polycrystalline of Nd.YAG material showed that the hardness of the latter is slightly higher [66]. In that work the polycrystalline Nd.YAG was prepared in the transparent form therefore. To be transparent polycrystalline ceramic materials need to have extremely low porosity and small grain size. The grain size of the polycrystalline Nd.YAG is in the order of 2 μm. This is much lower than the grain sizes of the samples reported here (See Figure 4.5, Figure 4.10, Figure 4.15). In addition to small grain size, lower porosity of the polycrystalline Nd.YAG let that material to have a higher hardness value than its single crystalline counterpart (See [66] for a more complete discussion).

Figure 4.19 shows the hardness values of the different surfaces of the textured samples are different. The radial surfaces of sample A (A1, A2), have very similar hardness values which are lower than that of AT. Since A1 and A2 has similar orientation characteristics this is in accordance with the expectations. Also, it is worth noting that the symmetry of the hardness of sample A, is cylindrical, same as the texture symmetry.

The B1 and BT surfaces have intermediate hardness values. Let us remember that the orientation characteristics have to be reflected by the properties somehow. Therefore, the B1 surface is little harder than BT, since it has a higher preferred orientation in c-axis. The B2 surface's hardness is similar to those of the A1 and A2. This is a highly expected result since the all of these surfaces (A1, A2 and B2) have same preferred orientation. The c-axis orientation in these surfaces is forbidden by the magnetic field. Those oriented such, are rotated into this forbidden direction by the effect of suction force.

Sample C's surfaces have average hardness values between those of the highly c-axis textured AT surface and A1, A2 and B2 surfaces. The reason is the mostly randomly distributed grain orientations. There are two features about the hardness values of the sample C; i) the standard deviations of the hardness' of the surfaces are generally larger than those of the textured sample surfaces, and ii) the values of the average hardness' of C1, C2 and CT were slightly different. These two features are results of the lack of control of particle orientations during compaction. The only force during compaction of sample C was suction force

which randomly acts on each particle. So there is no predictable outcome for the hardness for the sample C which is produced without magnetic field.

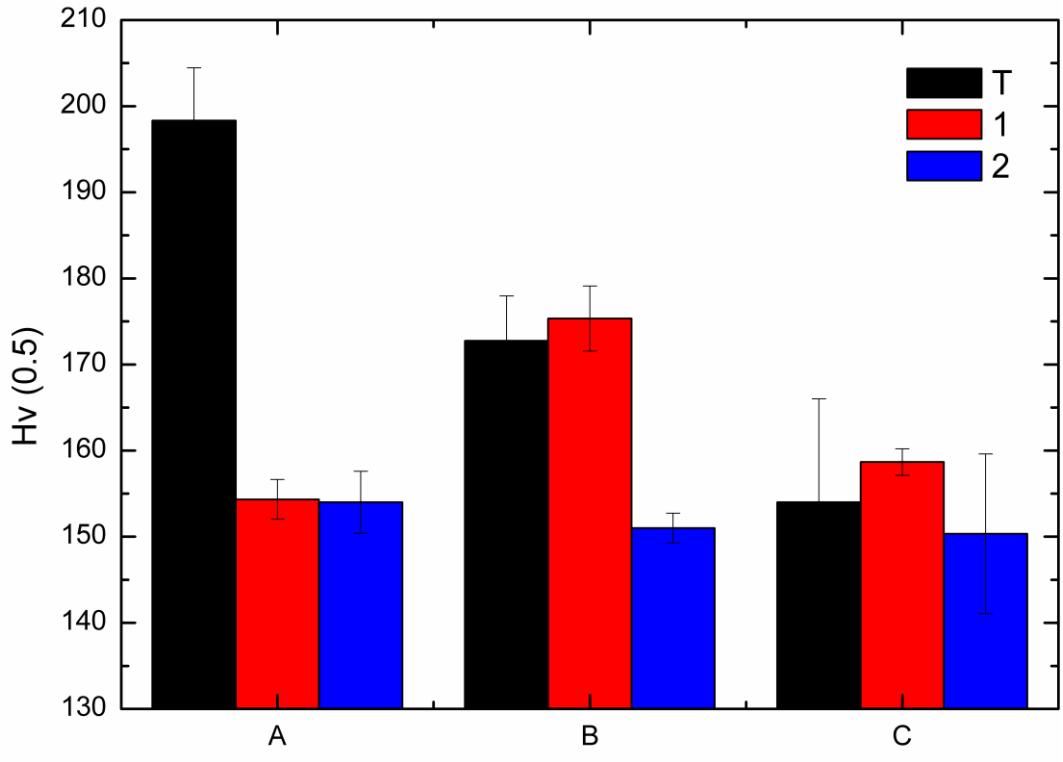

Figure 4.19 Hardness values of obtained by Vickers indentation tests on top, 1 and 2 surfaces of the samples A, B and C.

Now we know that texture causes anisotropy in the hardness, but how the hardness changes as texture degree changes? To find out, the texture degrees of the samples were described by the Lotgering Factor (f_{00l}) [49]. When the hardness value of each samples' surface with highest f_{00l} value is plotted against the Lotgering factor, we see that the hardness varies linearly with texture and increases when Lotgering factor increases (Figure 4.20). C1 has the Lotgering factor of almost zero. B1 has a Lotgering factor of around 27 % and lies on a strait line which extends to AT which has a f_{00l} equals ~75 %. The hardness' of the C1 B1 and AT surfaces are 160, 175 and 200 kgf/mm^2, respectively. It was already discussed that the hardness depends strongly on the microstructure, and there is a three fold effect of texture on microstructure; first is the reduction of grain size which tends to increase hardness, second increase of porosity which reduces hardness, and finally, third the increase of c-axis oriented grains as a direct effect; since the c-plane has the highest hardness this effect should increase the hardness.

As these effects compete, the average hardness of polycrystalline ZnO seems to increase linearly with increasing Lotgering factor.

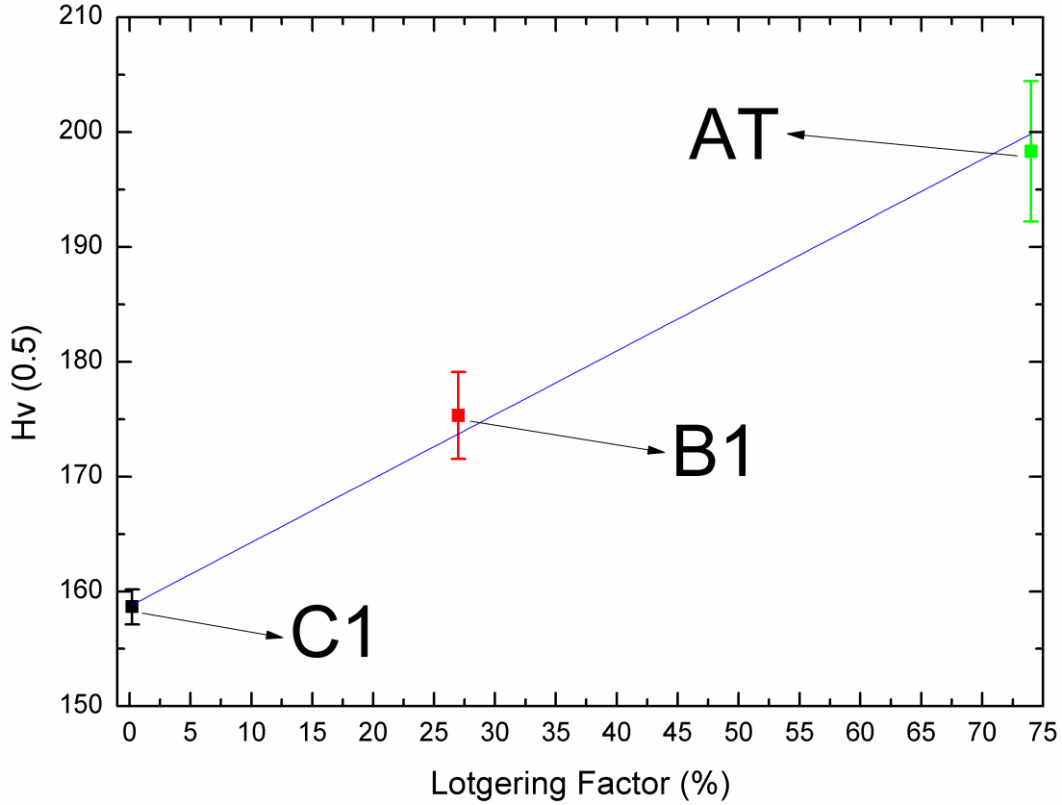

Figure 4.20 Change of Vickers hardness with Lotgering Factor. Hardness depends almost linearly only on c-axis texture.

4.2.3. Electrical Conductivity

Zinc Oxide (ZnO) is a highly popular, wide band gap (3.3 eV) semiconductor with a large exciton binding energy (60 eV) [38], [67]. It is widely used in several electronic applications such as thin film piezoelectric devices, voltage surge protectors, light emission, chemical sensing, and energy generation. Most of these applications exploit ZnO in thin film form. Since thin films have a tendency to have strong textures it is very important to know how the texture affects the properties. In addition to thin films, how the texture affects the elelctrical properties of bulk ZnO is of quite interest for certain applications such as varistors and thermoelectric. Although, from a scientific point of view, it is interesting to know, what is the relation between electrical conductivity and texture characteristic in ZnO, this has also practical impacts on the applications

discussed above. Therefore, the aim of this work was to study, in detail, how anisotropy in electrical conductivity forms as texture is induced in the system and also to what extend the texture affects the electrical conductivity.

Previously electrical properties of doped and un-doped textured bulk ZnO were investigated [26], [57]. In those works general approach to investigate the effect of texture on electrical conductivity was to prepare a highly textured specimen and a random control specimen then, compare the electrical properties of random specimen with the textured specimen. That kind of approach overlooks the effect of texture on the properties of individual samples and tends to fall short in demonstrating the anisotropy in the textured samples. Moreover, what is not present in those studies on textured ZnO, is the samples with intermediate texture degrees. In this study, on the other hand, we tried to elucidate how the texture characteristic and microstructure affects the electrical conductivity of individual samples in different directions, therefore we were able to map the anisotropy to a certain extend. In addition, the sample which was prepared with a static magnetic field has intermediate texture which is utilized to observe the effect of texture degree on the electrical conductivity.

Figure 4.21 shows the change of current density of sample A in directions parallel to 1, 2, and T axes, with varying electric field strength. It can be seen that annealed Au-Pd contacts showed Ohmic behavior and the dependence is fairly linear. The AT curve has a slightly steeper slope than other directions which means that electrical conductivity in the T direction (which is highly c-axis oriented) is higher than those in the radial directions. The dependence of current density in 1 and 2 directions is almost same. The only noticeable difference between the curves 1 and 2 is the slightly narrower standard deviation of the curve 2. Here we see a behavior that resembles the dependence of hardness in direction for sample A. The symmetry of the property is again belongs to the cylindrical Curie group and is same with the symmetry of its texture and thus the applied magnetic field. What we see is a perfect accommodation of Neumann's and Curie's principles by the textured, bulk ZnO.

The reason why the AT direction has the highest conductivity is not fully understood but it is most likely due to the lower mismatch in the grain boundaries in this direction. Lower grain boundary mismatch might have caused less

scattering during electronic transport. It has to be noted that, this is almost pure speculation. The investigation of this issue is beyond the scope of this thesis, but it is interesting and worth studying in a future work.

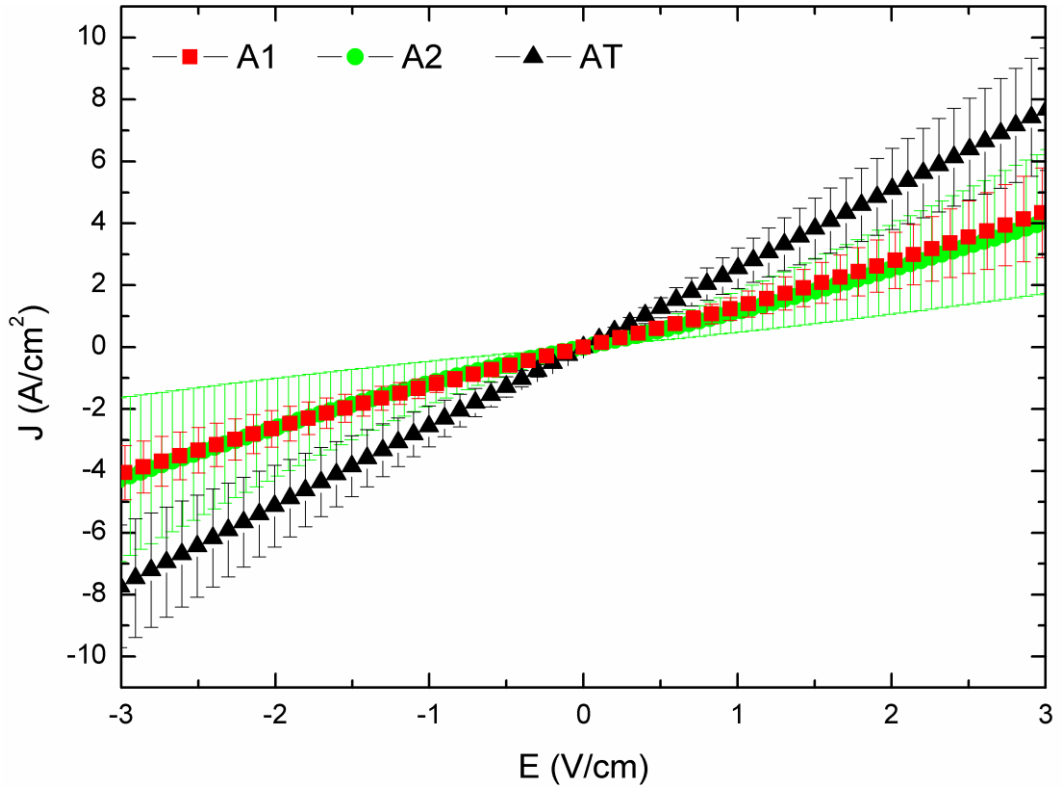

Figure 4.21 Dependence of current density on the electric field for along 1, 2, and T directions of sample A

Another way of demonstrating the anisotropic electrical conductivity in the sample A is to cut a disc shaped slab from a radial plane, and measure elelctrical conductivity as a function of rotation angle by two probes placed on its circumference. In a work dated back to 1975 by Greenwood *et al.* the angle dependent electrical resistivity of a carbon fiber reinforced polymer (CFRP) disc, is measured as a function of rotation angle [68]. In that work the resistivity as a function of angle is described with a theoretical hyperbolic trigonometric function whose parameters are the main conductivities in directions parallel and perpendicular to the fiber orientation, slab thickness and diameter, probe diameter and the rotation angle. They observed an almost linear change between 90 degrees rotation. This has to be caused by the perfect orientation of carbon fibers. On the contrary, the texture in the samples reported here is far from being perfect.

Therefore, a more gradually changing curve is expected in this case. To describe the expected behavior it is not possible to utilize the function described in [68]. Therefore, an empirical sine function is utilized to describe the effect of texture on electrical anisotropy.

In order to demonstrate the anisotropy, a disc is carved out from the A2 surface with an ultrasonic cutter. Then the current passing from the disc is measured as a function of angle under constant voltage (1 V). Copper cones with fine tips were employed as probes. Initial measurement is made in direction parallel to axis 1 (perpendicular to axis T). The measurements were carried out at 30° intervals. As the disc slab is rotated so that the measurement direction coincides with the T direction (c-axis oriented direction) the current increases which means that resistivity decreases (See Figure 4.22). When the rotation continues to 180°, again there is a reduction in current passing since the resistivity increases. This is in perfect agreement with the current density measurements described above. What is not so perfect, is the variation of the current in certain angles and also serious deviation from the fit curve. The reason is believed to be the lack of metalized contacts on the circumference of the disc. It was not possible to deposit the Au-Pd alloy on the circumference with required intervals since the disc is only 6 mm in diameter and ~1 mm in thickness. It is known that the metal to semiconductor contacts can build Schottky barriers which cause the material to behave non-Ohmic. In order to avoid this there should be a very well defined and clean interface between the suitable metal contact and the semiconductor. Apparently the interface between the Cu probes and the specimen is non-Ohmic. This cause a deviation in the measured values and a time dependent behavior in the samples reported here (not shown). Therefore, if better contacts can be fabricated on the circumference of the samples better, more defined results can be obtained. Nevertheless, the parameters of the fit function, especially amplitude A, have to be dependent on the texture degree. More experiments on sample with varying texture degrees have to be carried out in order to demonstrate this relationship. What is expected is a decrease in amplitude of the function when texture degree decreases, until the value starts to fluctuate around y0 (which should be around the conductivity of a random sample) for a random sample. It is

worth repeating that the key point is the fabricating Ohmic contacts on the disc with well defined intervals.

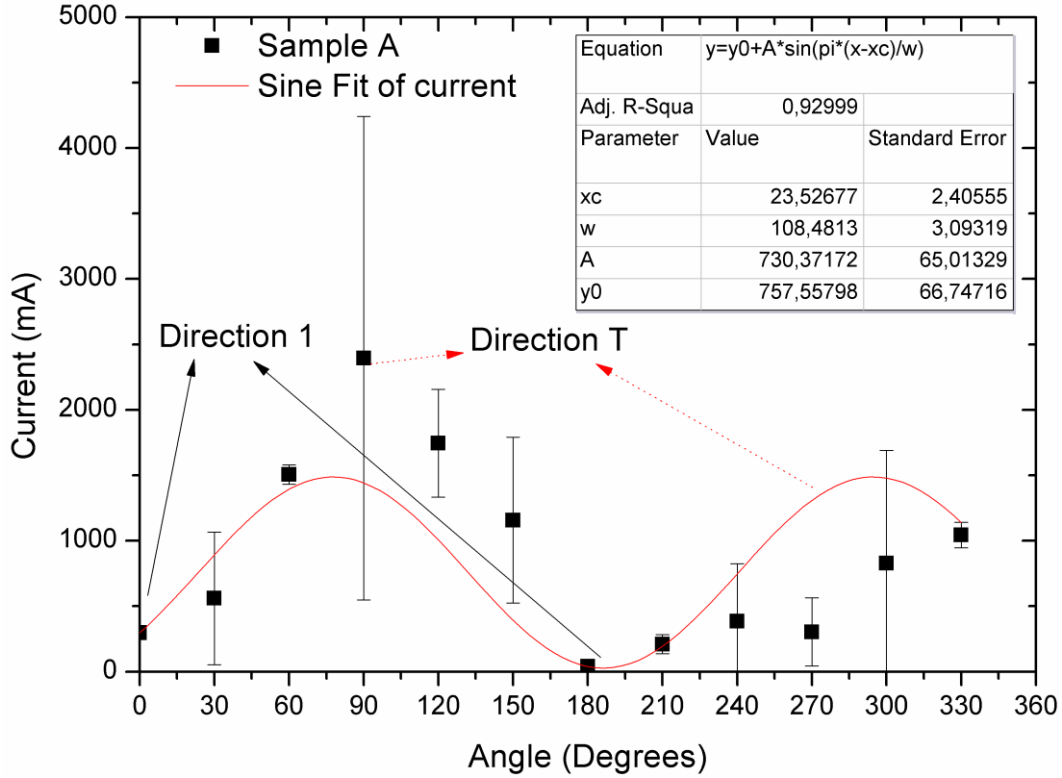

Figure 4.22 Angle dependent current measurement on a disk shaped specimen at 1 V

The highest current density in sample B occurs along the direction B1 (Figure 4.23) which is has the highest c-axis orientation for this sample but considerably less than that of the sample AT. Therefore, the conductivity of the B1 is slightly less than AT. Interestingly current density in direction BT which also has c-axis texture is not similar to the B1. Instead, it is very close to that of the B2 surface which has completely different orientation character. The explanation to this is the weak c-axis orientation along the BT direction as discussed previously. It seems that when the texture strength decreases below a certain value than the microstructure starts to play a more important role in the determination of the electrical conductivity value. Since the microstructures of the T and 2 surfaces are not so different and the texture is not so strong, it can be well expected for them to have similar conductivities. Sample C showed the current density values far lower than the textured samples and there is no agreement with different directions of this sample (Figure 4.24). This supports that the larger misorientation leads to lower conductivities.

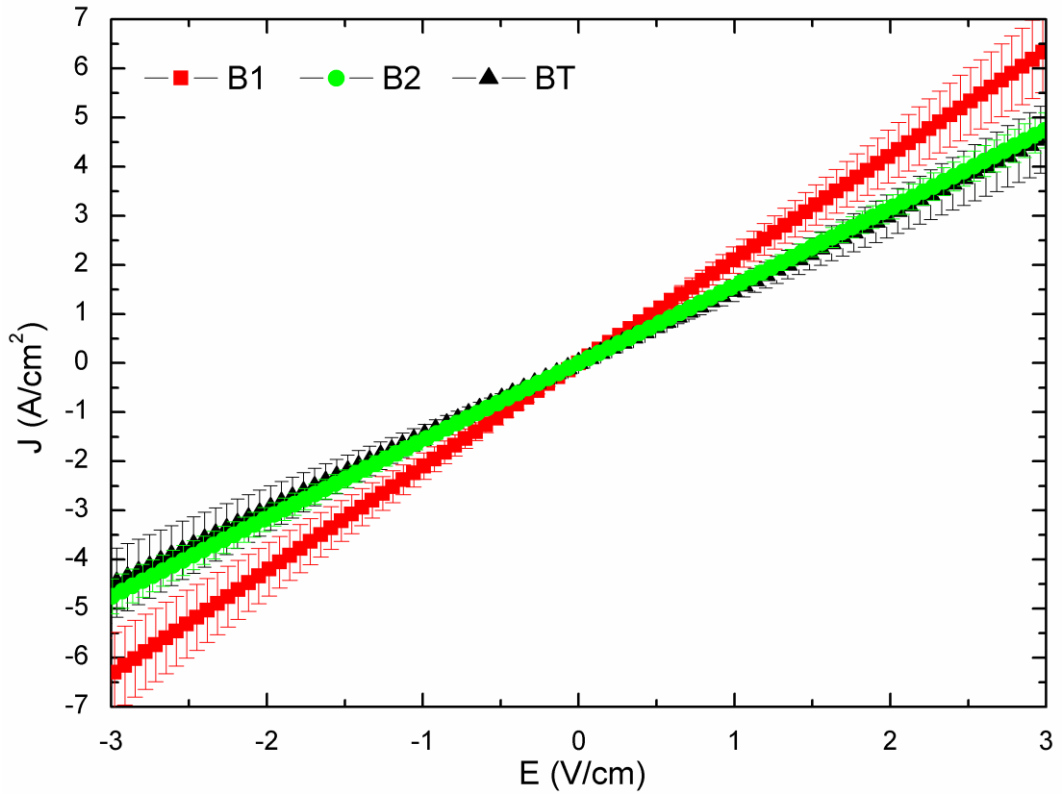

Figure 4.23 Dependence of current density for 1, 2 and T directions of sample B, on electric field

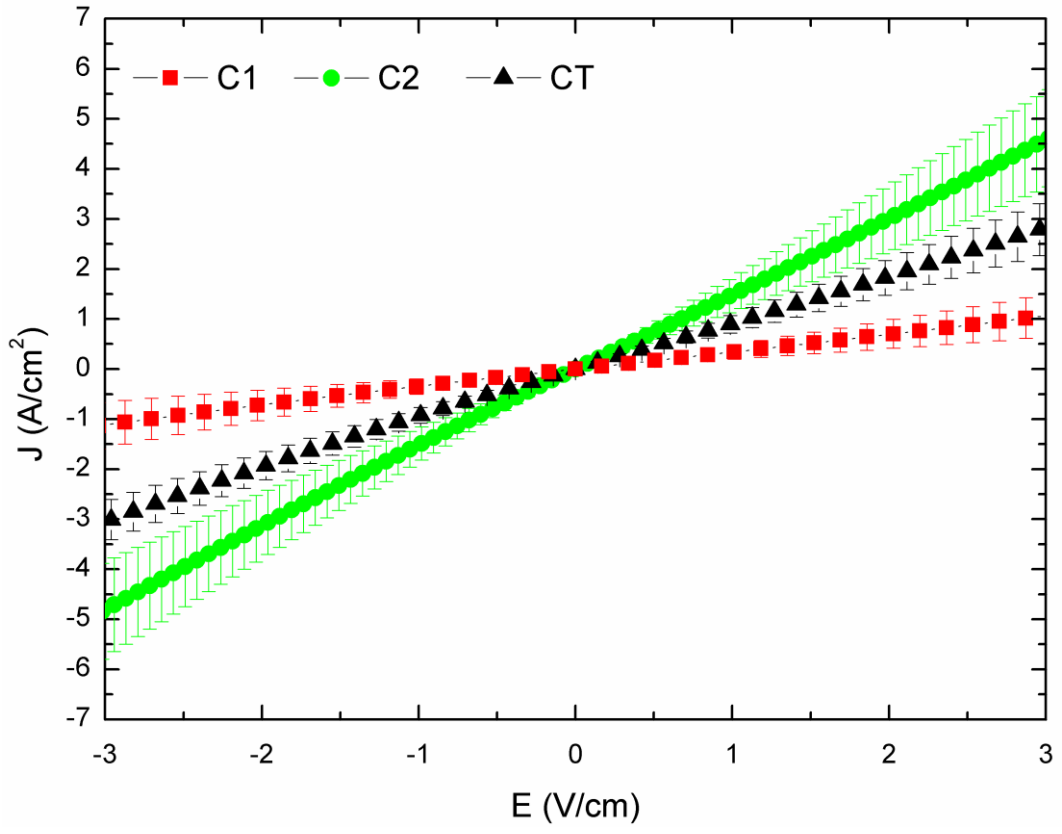

Figure 4.24 Dependence of current density of sample C in directions 1, 2, and T, on electric field

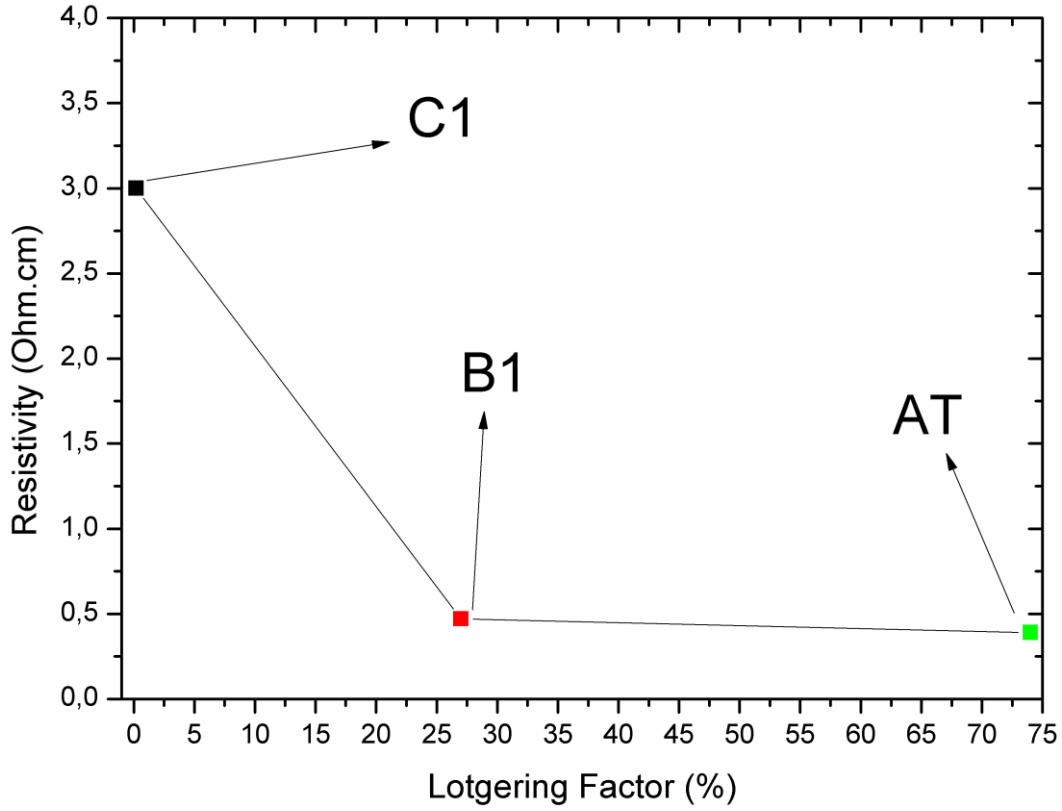

Figure 4.25 Dependenct of resistivity of polycrystalline ZnO on texture which is defined as Lotgering factor.

In order to see how the electrical resistivity changes with changing texture degree, electrical resistivity values of sample C1, B1 and AT were plotted against the corresponding Lotgering factors (Figure 4.25). It was seen that even a moderate texture has critical impact on the electrical conductivity in bulk ZnO. The sample C1 which is mostly random has a resistivity of 3 Ohm.cm while the sample B1 has 0.5 Ohm.cm with a Lotgering factor of ~27 %. Further increase in Lotgering factor does not affect resistivity significantly.

It was shown in this part that; i) electrical conductivity adopts the anisotropic symmetry of the applied process only when the texture degree is high enough and ii) electrical conductivity is critically dependent on texture degree. Also, the effect of orientation on electrical conductivity is described by an empirical sine function whose parameters are expected to depend on texture strength. Thus, it is suggested that a future work should focus on the deep investigation of the angle dependent measurement of electrical conductivity.

4.2.4. Thermal conductivity

Thermal conductivity is a very important engineering property which has significant effects on the design of a product. Among many important material properties affected by thermal conductivity, thermal shock resistance, and thermoelectricity can be counted. By controlling thermal conductivity materials can be optimized for different service conditions. For example, a good thermal conductivity is required for obtaining a better thermal shock resistant material whereas it has to be as low as possible for thermoelectric applications. The thermal conductivity of a material is can be controlled by manipulating different microstructural features. One can change chemical composition, introduce or eliminate secondary phases, play with the grain size and shape, and induce texture in order to control the thermal conductivity. It can be desirable to control the thermal conductivity without changing the composition of a material. Then, the texture induction can be a very good choice in order to engineer the thermal conductivity.

Thermal conductivity of a pure phase material is proportional to its thermal diffusivity. Therefore, by measuring the thermal diffusivity one can comment on the changes on the thermal conductivity. So, in order to find out how the thermal diffusivity is affected by texture, samples with wide surfaces A1, A2, AT and C1 were analyzed with a laser flash thermal diffusivity measurement instrument at temperature ranging from room temperature up to 1000°C by 100°C intervals (Figure 4.26).

It was observed that, when the thermal diffusivity is measured at room temperature, along c-axis oriented T direction, it was ~18.5 mm^2/s, while it was ~16.5 mm^2/s as an average in the radial direction. This slight difference in the thermal conductivities of two directions, with different texture characteristics, decreases more and more as the temperature increases until they are virtually same at 1000°C. The thermal diffusivity value of sample C1 was in between those of basal (AT) and prismatic (A1, A2) plane oriented materials. This is in accordance with expectations since the property values of a random materials are expected to be an average of the values in different directions. Thermal diffusivity of the sample C, has the same trend as other samples; as temperature increases the thermal diffusivity decreases.

Basically, there are three features of the graph shown in Figure 4.26; i) decrease of thermal diffusivity as temperature increases, ii) decrease of anisotropy in the thermal diffusivity values in different directions, and iii) the very small initial anisotropy in the thermal diffusivities of AT and A radial, despite the great difference in crystallographic texture.

The first feature is in very good agreement with the well understood behavior of dense, single phase solid materials. The thermal diffusivity of a dense solid material is expected to fall as temperature increases due to increase in phonon-phonon, phonon-electron, and electron-electron scattering, if there is no significant change in the mechanism of heat transport (such as radiation or convection transport becoming dominant). The amplitude of vibration of atoms around their equilibrium positions becomes larger and larger with increasing temperature which causes scattering of both the phonons and electrons. Another change in the ionic materials is the increase in the number of point defects in the crystal lattice. In fact the numbers of Schottky and Frenkel defects are directly related with temperature of the system. The formation of point defects has a negative effect on the thermal conductivity since they act like scattering centers for phonons and electrons. The materials characterized here are no exception to the above mentioned processes occurring during heating.

The decrease in the anisotropy of thermal diffusivity is again attributed to the increased scattering of phonons and electrons due to formation of defects in the crystal lattice and increased vibration of atoms. Presence of the crystallographic texture becomes insignificant as the temperature increases. The already small anisotropy in the thermal diffusivity decreases to a mere nothing at elevated temperatures suggesting that the scattering processes are much more dominant at these elevated temperatures.

This brings the question ‘Why is the anisotropy in the thermal diffusivity is small in the first place?’ into the stage. To understand this we need to check the microstructure of the materials. It is well known that the thermal diffusvity of a ceramic material is greatly affected by its microstructure. For example, a decrease in the grain size means and increase in the number of grain boundaries, each acting as a two dimensional scattering barrier for phonons and electrons. Therefore, a decrease in grain size will decrease the thermal conductivity of a

given ceramic material. So, with the knowledge of the effect of grain boundaries on the thermal conductivity, we can now comment on the effect of texture on thermal conductivity. If the morphological texture in the microstructure is induced by a crystallographic texture, this effectively means that the number of grain boundaries is different along two axes of the sample. This, in turn would mean a difference in the number of scattering sites in the path of phonons and/or electrons. It can be expected that, in the direction where the longer axes of the anisometric grains aligned, one should measure higher thermal conductivity. With the light of above discussion the situation observed here can be explained. First of all, the crystallographic texture is not accompanied with the morphological texture in the samples analyzed here. Therefore, the microstructures of the different faces of the sample A are quite similar (See Figure 4.4). This means that the number of scattering sites, i.e. grain boundaries, in each direction is almost same. So the anisotropy in the thermal diffusivity of sample A at room temperature is attributed completely to the crystallographic texture. Since, there is no significant morphological texture in the microstructure the anisotropy was limited and disappeared rapidly at elevated temperatures.

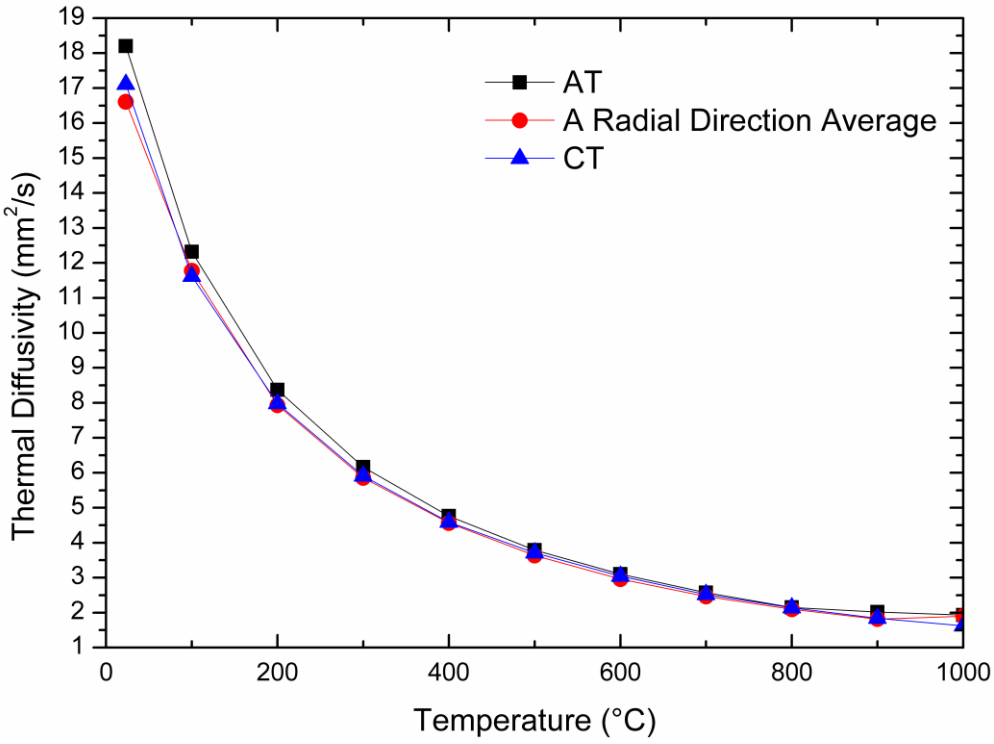

Figure 4.26 Change of thermal conductivity as a function of texture and temperature

4.3. Conclusions

The effects of magnetic field type utilized during production of ZnO compacts on microstructure and texture development were investigated by detailed microstructural analyses and x-ray and electron backscatter diffraction methods. It was found that the rotating magnetic field (sample A) causes a sharp c-axis oriented fiber texture perpendicular to the applied magnetic field. Static magnetic field (sample B) results in a weaker texture but this time, two surfaces (whose normals were perpendicular to magnetic field of the sample) has c-axis texture. One of these surfaces has a relatively higher preferred orientation due to the suction force rotating particles in this direction. Expectedly random sample (sample C), was not random at all due to suction causing the particles to rotate. This effect is most pronounced in the vicinity of mold-colloid interface.

The hardness of the textured samples was highly anisotropic and sharply reflects the symmetry of the texture. Highest hardness was obtained in the sample surface which is oriented in x-axis (AT surface). The hardness of this surface is almost half of the reported hardness of (0001) plane. This is attributed to the presence of porosity (thus relatively lower density) in the microstructure of the textured samples. Also it was found that the hardness of polycrystalline ZnO changes linearly with texture degree. Electrical conductivity of the ZnO increases with increasing texture in c-axis. Especially sample A's electrical conductivity follows the symmetry of the fiber texture (cylindrical symmetry). Anisotropy in the electrical conductivity of sample A, was successfully demonstrated by measuring the variation of current passing through a disk shaped ZnO slab, at constant voltage as a function of rotation angle. When the texture degree decreases the microstructural features become more effective (sample B). The electrical conductivity of the sample C is such that no prediction can be made due to randomly varying preferred orientation due to suction. The electrical conductivity was found to be quite sensitive to texture; a small increase in texture results in significant change in resistivity. Anisotropy in the thermal conductivity of sample A was found to be relatively small due to lack of morphological texture. This weak initial anisotropy decreases even further until it vanishes at elevated temperatures. As a conclusion, it was shown that the properties of a pure phase ZnO material can be controlled merely by controlling the texture.

5. GROWTH OF NANOSTRUCTURED ZnO

Out of the several technologically important functional materials, ZnO may be the one that is most widely investigated. Papers on the properties, processing and applications of ZnO are being increasing over the past few decades due to its potential for a range of applications. This special interest resulted in manufacture of wide variety of ZnO nanostructures [69]. Among these nanostructures, one dimensional ones such as nanowires (NWs) or nanorods (NRs) are of prime importance from an application point of view, due to their high surface area [70], piezoelectric [71] and luminescence properties [72] and also their ease of manufacture on ceramic, glass and polymeric substrates. There are two main production methods for NWs and NRs; i) gas phase and ii) solution based. In both methods, generally a coating layer composed of a catalyst or seed layer that is composed of ZnO nano particles, are required to initiate the growth of nanowires. Currently solution based methods are preferred due to fairly low processing temperatures (75-90°C). In these methods a seed layer of ZnO nanoparticles is chosen for initiating nanowire growth. The nanoparticles can be fabricated in a separate step and coated onto the surface or formed directly on the surface. When particles are pre-fabricated and dip or spin coated onto a surface, their orientation becomes random whereas if they are crystallized and grown, directly on the smooth surface of a substrate, they tend to align their c-axis normal to surface creating a strongly textured film. [73]. This substrate with a textured film, then, initiates growth of nanowires when it is put in growth medium. If a textured film can be used for aligned growth of nanowires, it may also be possible to use textured polycrystalline substrates to obtain continuous films of ZnO nanowires without any additional seed layer or catalyst. Therefore, aim of this study was to test the feasibility of this idea which turned out to be a quite interesting experiment.

Previously polycrystalline alumina substrates with random grain orientation were utilized in Au catalyzed growth which resulted in random orientation of nanowires [74], but when a thick ZnO microrod film was deposited on polycrystalline alumina substrate, then ZnO nanowires tended primarily to grow on the well faceted (0001) planes of the microrods, in the presence of a tin

catalyst [75]. Consequently, the question was, is it possible to control orientation of the NW/NRs if texture of the substrate can be better controlled?

In order to test this hypothesis, textured polycrystalline (T-PC) ZnO substrates were prepared via slip casting under a 12 T magnetic field. Nanowire growth solution and conditions were similar to those described previously in the literature [70], [76-79]. Details concerning the experimental procedure are given below.

5.1 Experimental Procedure

Green compacts were cold isostatically pressed at 392 MPa for 10 minutes and sintered at 1200°C for 4 hours. Sintered ceramic was cut into 5x5 mm pieces with wide surfaces normal to c-axis orientation direction, using a diamond wire saw. To be prepared as substrates, pieces were lapped and the surface on which the synthesis will be carried out, was polished down to colloidal silica. Then the substrates were thermally etched at 1100°C for 20 min. also un-etched c-axis oriented substrates were used for control experiments. Growth solution was prepared according to the procedure previously described in the literature [70], [76-79]. 5 mM of zinc nitrate hexahydrate solution is prepared in a 250 mL of ultra pure water with equimolar hexamethylenetetramine. The substrates were ultrasonicated in IPA, EtOH and ultra pure water successively for 5 min. and dried in oven after each step, prior to synthesis. Substrates were placed upside down in an open beaker which contained the growth solution. Synthesis was carried out at 75 - 95°C for 7.5 hours in an oven with air circulation. After synthesis substrates were briefly ultrasonicated then rinsed with ultra pure water in order to avoid any surface contamination. Nanostructures, grown over the surface were examined with scanning electron microscopy installed with a field emission gun (Supra 50 VP, ZEISS, Germany). Individual grain orientations were analyzed using an electron backscatter diffraction (EBSD) detector (HKL, Oxford Instruments, United Kingdom) installed on the microscope. Also syntheses were carried out using single crystal ZnO substrates with different orientations ([0001], $[10\bar{1}0]$ and $[11\bar{2}0]$ to correlate different nanostructures observed on textured substrates with grain orientation in conjunction with EBSD results. Single crystal

substrates were etched and prepared in the same way as textured ceramic substrates unless otherwise is stated.

5.2 Results and Discussion

Un-etched substrates yielded (75°C, 7.5 h) fine grained columnar structured films over the grains (Figure 5.1 a and b) failing to promote growth of individual NWs or NRs. The reason is believed to be the rough surface of the substrate after polishing with colloidal silica (Figure 5.2). The topography of the surface is quite random after polishing with colloidal silica. This irregularity probably results in an energetic surface and this leads to formation of many nucleation sites in close proximity. Large number of nucleation sites induces a fine grained columnar structure on the coated grains, as those shown in Figure 5.1 a and b. Another important point is that the surfaces of some grains were not covered at all suggesting that the deposition can only be achieved, selectively, on certain grains (Figure 5.1. a)).

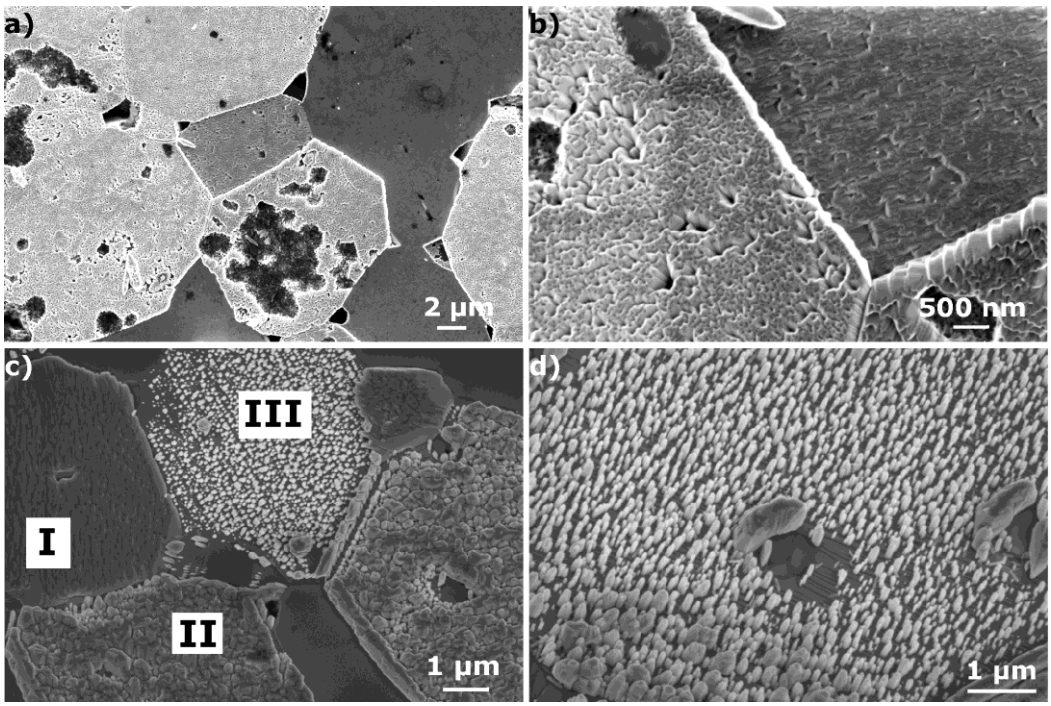

Figure 5.1 SEM images of un-etched (a), b)) and thermally etched (c), d)) substrate surfaces after growth at 75°C for 7.5 h.

Several kinds of nanostructures which were deposited on the thermally etched textured substrates can be seen in Figure 5.1 c) and d). These nanostructures can basically be classified into three major groups; i) relatively denser fine structured films, ii) moderately dense coarse grained columnar films, and iii) aligned NR films. Individual growth of NRs and coarse grained films are attributed to the step formation on the surface of grains during annealing at 1100°C for 20 min. (Figure 5.2). The step formation creates a relatively ordered surface morphology and amount of nucleation sites decreases. This leads to growth of either individually oriented NRs (Figure 5.1 d and Figure 5.2 c) or coarse grained films (Figure 5.1 c). Coarse grained films appear to be coalesced NRs. Fine grained films which are similar to those found in un-etched sample are attributed to the orientation of the grains which deviate strongly from the c-axis direction.

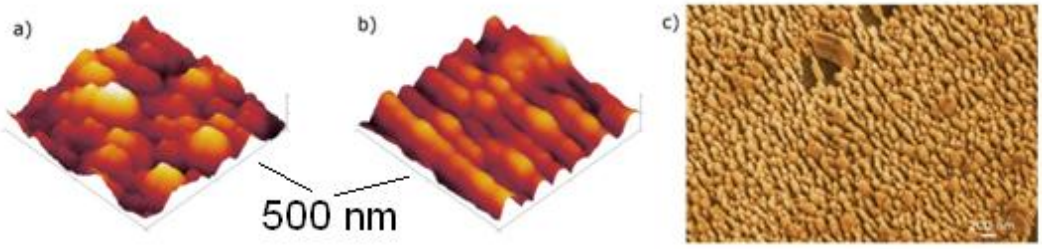

Figure 5.2 AFM images pf polished surfaces before a), and after b) annealing at 1100°C for 20 min. Step formation can be seen in b). SEM image of a grain after growth of ZnO at 75°C for 7.5 hours. SEM image is contrast enhanced and colored for enhanced visibility.

Generally, the alignment of the nanostructures on a grain is homogenous, suggesting that a particular grain can yield only a particular orientation for a nanostructure (Figure 5.1 d). In addition, the orientation of film on a single grain is constant across the whole grain (Figure 5.1 c)).

These observations suggest a strong correlation of the film structure with the orientation of the grain underneath. EBSD analyses were carried out on polycrystalline samples after growth to investigate this correlation (Figure 5.3). EBSD results are compared with detailed secondary electron (SE) images (Figure 5.4) in order to find out which crystallographic orientation leads to which type of growth morphology.It should be noted that, in some cases EBSD data can come

solely from the grown nanostructures. Therefore an assumption is made such that the orientation of the grains and the grown nanostructures are same. It is well known that fastest growth direction of ZnO single crystals is the [0001][39], so it was expected that grains with orientations close to [0001] (red colored grains in the EBSD maps) should yield nanostructures but as can be seen from Figure 5.4 a and d some of the grains whose orientations are close to c-axis ([0001]), yielded a small number of nanostructure in the best cases, whereas some other red colored grains yielded well faceted NR arrays. This may be attributed to the polarity of the ZnO crystals which is caused by the oppositely charged (+c) and (-c) surfaces which are mainly composed of Zn^{2+} and O^{2-} ions respectively. +c direction exhibits the fastest growth rate, pyramidal face normals come second followed by prismatic face normals and –c direction has the lowest growth rate of all [39]. So it was expected that the nano structures selectively form on +c surface. Therefore red colored grains with little or no NR films can be ocygen terminated surfaces (-c) or some higher index surface close to the oxygen surface From the comparison between the EBSD maps and the SEM images it is also seen that brown colored grains generally tend to yield fine grained relatively dense films with columnar structures. Single crystal experiments fall short to completely resolve this issue as will be discussed later. From the comparison between EBSD maps and SEM images it is also seen that brown colored grains generally tend to yield fine grained relatively dense films with columnar structures (Figure 5.4 a-d and b-e) which are similar to those obtained on un-etched substrates. Grains with colors green-violet-rose (Figure 5.4 c-f) generally tend to yield individually grown NR films (Figure 5.4 a-d and b-e) which are similar to those obtained on un-ethced substrates. Grains with colors green-violet-red (Figure 5.4 c-f), generally tend to yield individually grown NR films.

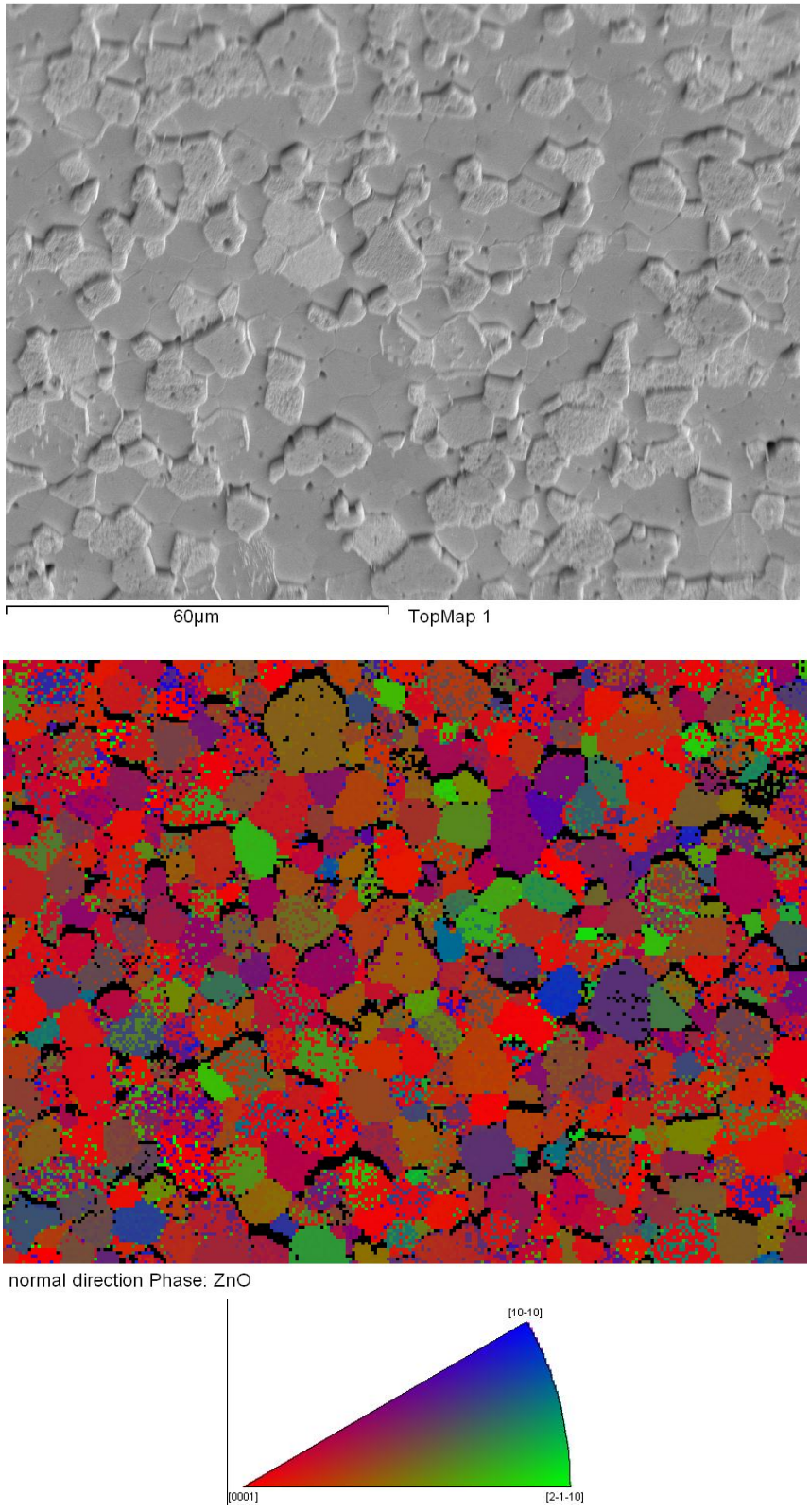

Figure 5.3 SEM image (top) and EBSD map (middle) of the corresponding area. Bottom – Color code for EBSD map.

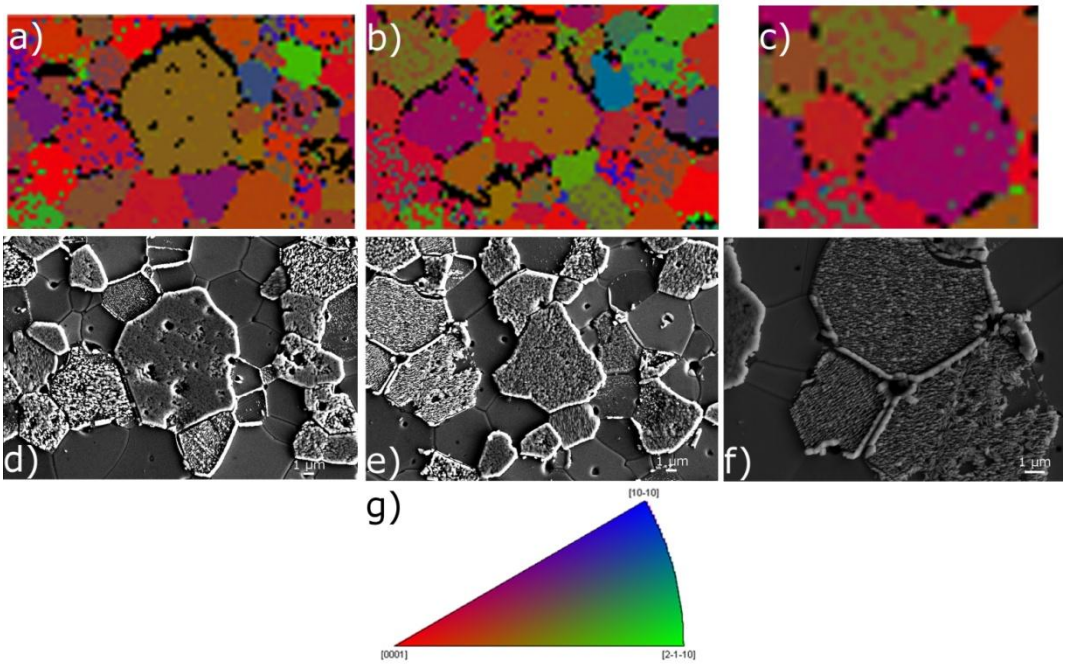

Figure 5.4 EBSD maps of the substrate after growth (a, b, and c) and SEM images of the same areas (d, e, and f). g) is the color code for EBSD map

Experiments with single crystals were carried out in order to facilitate a better understanding. Zn face of the [0001] crystal yielded individually grown, well faceted NRs (Figure 5.5 a) which are similar to those found on certain grains of the T-PC substrate (Figure 5.5. d). Oxygen terminated face resulted in a relatively dense columnar film with occasional individually grown NRs. This result seems to contradict with previous results when evaluated in conjunction with EBSD of polycrystalline substrate, but the conditions of the Oxygen face

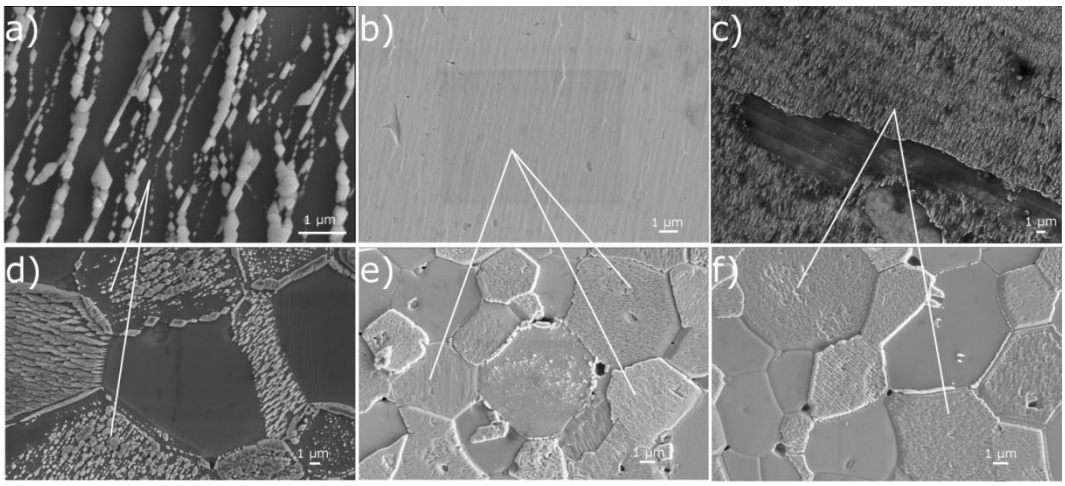

Figure 5.5 Grown ZnO structures on a) Zn face, b) on [$10\bar{1}0$], c) on [$11\bar{2}0$], d) on top surface of textured substrate, e) and f) on side surface of the textured substrate

single crystal experiment were not exactly same with polycrystalline; in the experiment with O face single crystal there were no alternatives other than homogeneous nucleation to the growth of nanostructures on O face but in the polycrystalline substrate there were virtually infinitely many alternative grains with continuous distribution of orientation in a certain range (range is limited though, due to strong crystallographic texture). The prismatic, [$10\bar{1}0$] cut crystal (first type prismatic) resulted in a dense film with occasional defects (Figure 5.5 b). This type of growth was not common in T-PC substrate but when growth is carried out on the side surface of the substrate it was observed that this type of growth is quite common (Figure 5.5 e). This is an expected result since T-PC substrates' side surfaces are prismatic plane oriented. [$11\bar{2}0$] cut single crystal (second type prismatic) was covered with fine grained columnar film (Figure 5.5 c). This direction is equivalent of [$2\bar{1}\bar{1}0$] direction which is the green color on the EBSD color code. Therefore, this type of structure again is not common in T-PC substrate but can be found on side surface (Figure 5.5 f).

5.3. Conclusions

It was possible to grow well aligned NR arrays on certain crystallographic planes, after step formation via thermal etching. However, uttermost control of texture is required for a homogenous coverage of the surface of a polycrystalline substrate, which is extremely difficult in practical terms. Therefore, homogeneity of the film structure was found to be confined to single grains in this study. Further research must be conducted in order to explain several points; what are the exact growth directions of the NRs on grains with orientations deviating strongly from c-axis (such as those seen in Figure 5.4 c-f)? Only NRs on c-axis oriented grains grew normal to substrate surface. On other occasions, the NR films made an acute angle with the substrate surface. This can be resolved by investigating samples from radial direction with HRTEM. Especially, the NR substrate interface must be looked into. Textured, polycrystalline substrates were utilized for the growth of ZnO NRs, as opposed to the other substrates coated with an additional thin ZnO films. Moreover, the structure of the films was associated with their alignment by utilizing EBSD and SEM. It was found that only certain crystallographic planes let grow of individually grown aligned NR films.

6. GENERAL SUMMARY

In this thesis, ZnO materials were studied from macro to nano level. The objective of utilizing a colloidal processed bulk ZnO ceramic as a substrate for growth of ZnO nanostructures was realized. In the path to realization of the main research objective the processing parameters required to obtain a dense, textured ZnO ceramic, were optimized.

Anisotropic sintering shrinkage, which is a common problem for most of the texture inducing techniques, is investigated in depth. It was found that the incorporation of a defective template in a critical volume amount results in suppression of anisotropic sintering shrinkage and enhanced densification.

The hardness, electrical conductivity, and thermal conductivity of the textured samples fabricated under different magnetic field conditions were measured. It was found that the dependence of the property on texture is property specific. Some properties such as thermal diffusivity is more critically dependent on microstructure while some properties show a clear dependence on texture such as hardness. Electrical conductivity showed a behavior in between two ends of the spectrum.

The highly textured ZnO materials were utilized as substrates for growth of ZnO nanostructures without use of an additional seed or catalyst layer. The growth type was highly dependent on surface morphology. The step formation upon thermal annealing resulted in sharply defined growth of individual oriented nano rod arrays on grains with certain orientations. It was found that crystallographic planes such as pyramidal and basal planes, let growth of individual, aligned nano rod arrays while prismatic planes result in fine grained dense thin films.

As a conclusion, the polycrystalline ZnO materials were fabricated in controllable texture. Process parameters were optimized in accordance with this target. This texture is often reflected by properties of the final product. It was also shown that the textured ceramics can be utilized for growth of aligned 1 dimensional nano structures, should the texture ultimately controlled.

7. FUTURE WORK

- The defect structure of the ZnO template particles is worth investigating. An in depth analysis via high resolution transmission electron microscopy would reveal the nature of the defects present in this interesting micro structures.

- The decrease in texture strength after extended sintering durations is an interesting phenomenon. The investigation of this can be made via diffusion experiments utilizing radioactive zinc atoms. The understanding of the underlying mechanism will pave the way to obtain materials with more well defined textures.

- The angle dependent resistivity measurements must be investigated in further depth. In addition to the scientific value of such a pursuit, there are several possibilities for practical applications such as characterization of texture degree by electrical conductivity measurement or use of the textured materials as a transducer.

- Interface between the ZnO nanorods and substrate must be investigated via high resolution transmission electron microscopy to reveal possibly different growth directions of ZnO nanorods.

8. REFERENCES

[1] H. J. Bunge, "Textures in Ceramics", *Texture, Stress, and Microstructure*, [24], 1, 1-12, 1995.

[2] G. L. Messing, "Textured Ceramics", in *Encyclopedia of Materials Science and Technology*, Elsevier Science, Ltd, 2001.

[3] Guenter Wassermann, *Texturen metallischer Werkstoffe.*, 808th ed. (Berlin): Springer, 1962.

[4] W. Skrotzki, K. Kegler, R. Tamm, and C. G. Oertel, "Grain structure and texture of cast iron aluminides", *Crystal Research and Technology*, [40], 1, 90-94, 2005.

[5] M. Pötschke, U. Gaitzsch, S. Roth, B. Rellinghaus, and L. Schultz, "Preparation of melt textured Ni–Mn–Ga", *Journal of Magnetism and Magnetic Materials*, [316], 2, 383-385, 2007.

[6] J. Pei, J. T. Li, G. H. Liu, and K. X. Chen, "Fabrication of bulk Al2O3 by combustion synthesis melt-casting under ultra-high gravity", *Journal of Alloys and Compounds*, 2009.

[7] S. Jin et al., "Melt-textured growth of polycrystalline YBa2Cu3O7- delta with high transport Jc at 77 K", *Physical Review B*, [37], 13, 7850, May. 1988.

[8] M. Holmes, R. E. Newnham, and L. E. Cross, "Grain-oriented ferroelectric ceramics", *AM. CERAM. SOC. BULL. Am. Ceram. Soc. Bull.*, [58], 9, 872, 1979.

[9] K. Okazaki, H. Igarashl, K. Nagata, T. Yamamoto, and S. Tashiro, "Processing, Microstructure and Properties of Grain-Oriented Ferroelectric Ceramics", in *Applications of Ferroelectrics. 1986 Sixth IEEE International Symposium on*, 328-337, 1986.

[10] K. Okazaki, "Grain oriented technology of ferroelectric ceramics", in *Applications of Ferroelectrics, 1996. ISAF \uc0\u821796., Proceedings of the Tenth IEEE International Symposium on*, 779-782 [2], 1996.

[11] M. M. Seabaugh, M. D. Vaudin, J. Cline, and G. L. Messing, "Comparison of Texture Analysis Techniques for Highly Oriented Al2O3", *Journal of the American Ceramic Society*, [83], 8, 2049-2054, 2000.

[12] E. Suvaci and G. L. Messing, "Critical Factors in the Templated Grain

Growth of Textured Reaction-Bonded Alumina", *Journal of the American Ceramic Society*, [83], 8, 2041-2048, 2000.

[13] E. Suvaci and I. Ö. Özer, "Processing of textured zinc oxide varistors via templated grain growth", *Journal of the European Ceramic Society*, [25], 9, 1663-1673, Jun. 2005.

[14] H. Itahara and T. Tani, "Highly-Textured Thermoelectric Oxide Polycrystals Synthesized by the Reactive-Templated Grain Growth (RTGG) Method", *R&D Review of Toyota CRDL*, [39], 1, 63-70, 2004.

[15] T. Kimura, Y. Sakuma, and M. Murata, "Texture development in piezoelectric ceramics by templated grain growth using heterotemplates", *Journal of the European Ceramic Society*, [25], 12, 2227-2230, 2005.

[16] T. Kimura, "Application of Texture Engineering to Piezoelectric Ceramics-A Review-", *Journal of the Ceramic Society of Japan*, [114], 1325, 15-25, 2006.

[17] C. Uyeda, R. Takashima, and K. Tanaka, "Magneto-rotation of nonmagnetic micro-crystals caused by diamagnetic anisotropy", *Applied Physics Letters*, [86], 9, 094103-3, Feb. 2005.

[18] T. Kimura, "Study on the Effect of Magnetic Fields on Polymeric Materials and Its Application", *Polym J*, [35], 11, 823-843, 2003.

[19] T. S. Suzuki and Y. Sakka, "Control of Texture in ZnO by Slip Casting in a Strong Magnetic Field and Heating", *Chemistry Letters*, [31], 12, 1204-1205, 2002.

[20] S. Tanaka, A. Makiya, Z. Kato, N. Uchida, T. Kimura, and K. Uematsu, "Fabrication of c-axis oriented polycrystalline ZnO by using a rotating magnetic field and following sintering", *Journal of Materials Research*, [21], 703-707, Mar. 2006.

[21] H. Kaga et al., "Fabrication of c-axis Oriented Zn0. 98Al0.02O by a High-Magnetic-Field via Gelcasting and its Thermoelectric Properties", *Journal of the Ceramic Society of Japan*, [114], 1335, 1085-1088, 2006.

[22] T. S. Suzuki, T. Uchikoshi, H. Okuyama, Y. Sakka, and K. Hiraga, "Mechanical properties of textured, multilayered alumina produced using electrophoretic deposition in a strong magnetic field", *Journal of the European Ceramic Society*, [26], 4, 661-665, 2006.

[23] Y. Sakka and T. S. Suzuki, "Textured Development of Feeble Magnetic Ceramics by Colloidal Processing Under High Magnetic Field", *Journal of the Ceramic Society of Japan*, [113], 1313, 26-36, 2005.

[24] S. W. Sofie and F. Dogan, "Freeze Casting of Aqueous Alumina Slurries with Glycerol", *Journal of the American Ceramic Society*, [84], 7, 1459-1464, 2004.

[25] L. Wang, C. Tiu, and T.-J. Liu, "Effects of nonionic surfactant and associative thickener on the rheology of polyacrylamide in aqueous glycerol solutions", *Colloid & Polymer Science*, [274], 2, 138-144, 1996.

[26] H. Kaga et al., "Orientation dependence of transport property and microstructural characterization of Al-doped ZnO ceramics", *Acta Materialia*, [55], 14, 4753-4757, Aug. 2007.

[27] Y. Sakka, T. S. Suzuki, N. Tanabe, S. Asai, and K. Kitazawa, "Alignment of titania whisker by colloidal filtration in a high magnetic field", *Japanese journal of applied physics*, [41], 12, 1416–1418, 2002.

[28] M. Raj, A. Odulena, and W. R. Cannon, "Anisotropic shrinkage during sintering of particle-oriented systems—numerical simulation and experimental studies", *Acta Materialia*, [50], 10, 2559–2570, 2002.

[29] I. O. Ozer, E. Suvaci, B. Karademir, J. M. Missiaen, C. Carry, and D. Bouvard, "Anisotropic sintering shrinkage in alumina ceramics containing oriented platelets", *Journal of the American Ceramic Society*, [89], 6, 1972–1976, 2006.

[30] A. R. Boccaccini and E. A. Olevsky, "Processing of platelet-reinforced glass matrix composites: effect of inclusions on sintering anisotropy", *Journal of Materials Processing Technology*, [96], 1, 92–101, 2000.

[31] A. Zavaliangos, J. M. Missiaen, D. Bouvard, and C. Carry, *Crystallographic Texture as Potential Origin of Anisotropy in Sintering of Magnetic Materials. Sintering 03*. 2003.

[32] A. Shui, Z. Lingke, Liu, X. Cheng, and K. Uematsu, "Anisotropic Sintering Shrinkage of Spherical Alumina Particle Compact Aligned in High Magnetic Field", *Journal of the Ceramic Society of Japan*, [114], 1327, 290-292, 2006.

[33] A. Wonisch, O. Guillon, T. Kraft, M. Moseler, H. Riedel, and J. Rodel,

"Stress-induced anisotropy of sintering alumina: Discrete element modelling and experiments", *ACTA MATERIALIA*, [55], 15, 5187-5199, Se 2007.

[34] H. N. Ch'ng and J. Pan, "Modelling microstructural evolution of porous polycrystalline materials and a numerical study of anisotropic sintering", *Journal of Computational Physics*, [204], 2, 430-461, Apr. 2005.

[35] S. Tanaka, Y. Tomita, R. Furushima, H. Shimizu, Y. Doshida, and K. Uematsu, "Fabrication of crystal-oriented barium-bismuth titanate ceramics in high magnetic field and subsequent reaction sintering", *Science and Technology of Advanced Materials*, [10], 014602, 2009.

[36] X. W. Zhu, Y. Sakka, T. S. Suzuki, T. Uchikoshi, and S. Kikkawa, "The c-axis texturing of seeded Si3N4 with [beta]-Si3N4 whiskers by slip casting in a rotating magnetic field", *Acta Materialia*, [58], 1, 146-161, 2010.

[37] U. Ozgur et al., "A comprehensive review of ZnO materials and devices", *Journal of Applied Physics*, [98], 4, 041301-103, 2005.

[38] C. Klingshirn, "ZnO: From basics towards applications", *physica status solidi (b)*, [244], 9, 3027-3073, 2007.

[39] L. N. Demianets, D. V. Kostomarov, I. Kuz'mina, and S. V. Pushko, "Mechanism of growth of ZnO single crystals from hydrothermal alkali solutions", *Crystallography Reports*, [47], 86-98, 2002.

[40] K. Maeda, M. Sato, I. Niikura, and T. Fukuda, "Growth of 2 inch ZnO bulk single crystal by the hydrothermal method", *Semiconductor Science and Technology*, [20], 4, 49, 2005.

[41] D. C. Reynolds et al., "High-quality, melt-grown ZnO single crystals", *Journal of applied physics*, [95], 4802, 2004.

[42] C. H. Lu and C. H. Yeh, "Influence of hydrothermal conditions on the morphology and particle size of zinc oxide powder", *Ceramics International*, [26], 4, 351–357, 2000.

[43] W. A. Dollase, "Correction of intensities for preferred orientation in powder diffractometry: application of the March model", *Journal of Applied Crystallography*, [19], 4, 267-272, 1986.

[44] S. TANAKA, "Design of Packing Structures through Direct Characterization of Ceramics Green Bodies", *Journal of the Ceramic Society of Japan*, [114], 1326, 141-146, 2006.

[45] W. Chen, Y. Hotta, T. Tamura, K. Miwa, and K. Watari, “Effect of suction force and starting powders on microstructure of Bi4Ti3O12 ceramics prepared by magnetic alignment via slip casting”, *Scripta Materialia*, [54], 12, 2063-2068, Jun. 2006.

[46] H. M. Rietveld, “A profile refinement method for nuclear and magnetic structures”, *Journal of Applied Crystallography*, [2], 2, 65-71, 1969.

[47] B. D. Cullity and S. R. Stock, *Elements of X-ray Diffraction*. Addison-Wesley Reading, MA, 1978.

[48] N. C. Popa and D. Balzar, “Elastic strain and stress determination by Rietveld refinement: generalized treatment for textured polycrystals for all Laue classes”, *Journal of Applied Crystallography*, [34], 2, 187-195, 2001.

[49] F. K. Lotgering, “Topotactical reactions with ferrimagnetic oxides having hexagonal crystal structures–I”, *Journal of Inorganic and Nuclear Chemistry*, [9], 2, 113–123, 1959.

[50] J. Xu, Q. Pan, Y. Shun, and Z. Tian, “Grain size control and gas sensing properties of ZnO gas sensor”, *Sensors and Actuators B: Chemical*, [66], 1, 277-279, Jul. 2000.

[51] Q. Wan et al., “Fabrication and ethanol sensing characteristics of ZnO nanowire gas sensors”, *Applied Physics Letters*, [84], 3654, 2004.

[52] A. Dogan, E. Suvaci, G. Gunkaya, and E. Uzgur, “Electrophoretic deposition of ZnO”, *EURO CERAMICS VIII, PTS 1-3*, [264], 269-272, 2004.

[53] V. A. Karpina et al., “Zinc oxide - analogue of GaN with new perspective possibilities”, *Crystal Research and Technology*, [39], 11, 980-992, 2004.

[54] C. R. Gorla et al., “Structural, optical, and surface acoustic wave properties of epitaxial ZnO films grown on (01-12) sapphire by metalorganic chemical vapor deposition”, *Journal of Applied Physics*, [85], 5, 2595-2602, Mar. 1999.

[55] J.-B. Lee, M.-H. Lee, C.-K. Park, and J.-S. Park, “Effects of lattice mismatches in ZnO/substrate structures on the orientations of ZnO films and characteristics of SAW devices”, *Thin Solid Films*, [447], 296-301, 2004.

[56] W.-C. Shih, M.-J. Wang, and I. N. Lin, “Characteristics of ZnO thin film surface acoustic wave devices fabricated using nanocrystalline diamond film on silicon substrates”, *Diamond and Related Materials*, [17], 3, 390-395,

Mar. 2008.

[57] J. L. Ning, D. M. Jiang, K. H. Kim, and K. B. Shim, "Influence of texture on electrical properties of ZnO ceramics prepared by extrusion and spark plasma sintering", *Ceramics International*, [33], 1, 107-114, 2007.

[58] K. Hisashi et al., "Preparation and Thermoelectric Property of Highly Oriented Al-Doped ZnO Ceramics by a High Magnetic Field", *Jpn J Appl Phys Part 2*, [45], 42, L1212-L1214, 2006.

[59] B. J. Lokhande, S. Patil, and M. D. Uplane, "Studies on structural, optical and electrical properties of boron doped zinc oxide films prepared by spray pyrolysis technique", *Physica B: Condensed Matter*, [302], 59-63, 2001.

[60] R. E. Newnham, *Properties of materials: anisotropy, symmetry, structure*. Oxford University Press, USA, 2005.

[61] T. K. Gupta and R. L. Coble, "Sintering of ZnO: II, Density Decrease and Pore Growth During the Final Stage of the Process*", *Journal of the American Ceramic Society*, [51], 9, 525-528, 1968.

[62] L. N. Demyanets, N. L. Sizova, and L. E. Li, "Zinc oxide single crystals: Influence of temperature and orientation of crystals on their mechanical properties", *Crystallography Reports*, [50], 4, 646-653, 2005.

[63] N. Bansal and J. Singh, *Processing and Properties of Advanced Ceramics and Composites: Ceramic Transactions*. John Wiley and Sons, 2009.

[64] S. F. Li, H. Izui, M. Okano, W. H. Zhang, and T. Watanabe, "Spark Plasma Sintered Alumina-Zirconia Nano-Composites by Addition of Hydroxyapatite" in *Processing and Properties of Advanced Ceramics and Composites* (eds N. Bansal and J. Singh), John Wiley & Sons, Inc., Hoboken, NJ.

[65] D. B. Sirdeshmukh, G. Krishna, and K. G. Subhadra, "Systematic hardness measurements on single crystals and polycrystalline blanks of cesium halides", *Bulletin of Materials Science*, [25], 3, 203-207, 2002.

[66] L. Mezeix and D. J. Green, "Comparison of the Mechanical Properties of Single Crystal and Polycrystalline Yttrium Aluminum Garnet", *International Journal of Applied Ceramic Technology*, [3], 2, 166-176, 2006.

[67] U. Ozgur et al., "A comprehensive review of ZnO materials and devices", *Journal of Applied Physics*, [98], 4, 041301-103, 2005.

[68] J. H. Greenwood, S. Lebeda, and J. Bernasconi, “The anisotropic electrical resistivity of a carbon fibre reinforced plastic disc and its use as a transducer”, *Journal of Physics E: Scientific Instruments*, [8], 369, 1975.

[69] Z. L. Wang, “Nanostructures of zinc oxide”, *Materials Today*, [7], 6, 26–33, 2004.

[70] L. E. Greene et al., “Low-temperature wafer-scale production of ZnO nanowire arrays”, *Angewandte Chemie*, [115], 26, 3139–3142, 2003.

[71] Z. L. Wang and J. Song, “Piezoelectric nanogenerators based on zinc oxide nanowire arrays”, *Science*, [312], 5771, 242, 2006.

[72] J. Bao, M. A. Zimmler, F. Capasso, X. Wang, and Z. F. Ren, “Broadband ZnO single-nanowire light-emitting diode”, *Nano Lett*, [6], 8, 1719–1722, 2006.

[73] L. E. Greene et al., “General Route to Vertical ZnO Nanowire Arrays Using Textured ZnO Seeds”, *Nano Letters*, [5], 7, 1231-1236, Jul. 2005.

[74] Z. L. Wang, “Zinc oxide nanostructures: growth, properties and applications”, *Journal of Physics: Condensed Matter*, [16], 25, R829-R858, 2004.

[75] X. Gao, Y. Ding, and Z. L. Wang, “Crystallographic Orientation-Aligned ZnO Nanorods Grown by a Tin Catalyst”, *Nano Letters*, [3], 9, 1315-1320, 2003.

[76] S. Xu et al., “Patterned Growth of Vertically Aligned ZnO Nanowire Arrays on Inorganic Substrates at Low Temperature without Catalyst”, *Journal of the American Chemical Society*, [130], 45, 14958-14959, Nov. 2008.

[77] S. Xu, C. Lao, B. Weintraub, and Z. L. Wang, “Density-controlled growth of aligned ZnO nanowire arrays by seedless chemical approach on smooth surfaces”, *Journal of Materials Research*, [23], 8, 2072-2077, 2008.

[78] M. Wang, C.-H. Ye, Y. Zhang, H.-X. Wang, X.-Y. Zeng, and L.-D. Zhang, “Seed-layer controlled synthesis of well-aligned ZnO nanowire arrays via a low temperature aqueous solution method”, *Journal of Materials Science: Materials in Electronics*, [19], 3, 211-216, Mar. 2008.

[79] L. Vayssieres, K. Keis, A. Hagfeldt, and S.-E. Lindquist, “Three-Dimensional Array of Highly Oriented Crystalline ZnO Microtubes”, *Chemistry of Materials*, [13], 12, 4395-4398, Dec. 2001.